An Investigation of Conical Roof Edge Vortices

Richard Marwood

Lincoln College

University of Oxford

Trinity Term 1996

An Investigation of Conical Roof Edge Vortices

Richard Marwood

Lincoln College, University of Oxford

Abstract of thesis submitted for the degree of Doctor of Philosophy

Trinity Term 1996

This thesis describes experiments carried out using laser Doppler anemometry (LDA) to measure velocities within conical roof edge vortices. These roof edge vortices produce high surface suctions and are a primary cause of damage to roofs, and therefore warrant investigation. Time averaged mean velocities in the vortex are initially considered and in later work instantaneous velocity events are related to maximum and minimum suctions exerted on the roof under the vortex.

The work relating surface pressures to velocity events was made possible by the development of a simultaneous pressure-velocity measuring technique and a conditional statistical technique to analyse the resulting data. The conditional sampling technique has allowed a point measurement technique (LDA) to be used to determine pressure-conditional instantaneous velocity events over an entire 2-D flow field.

In addition, the relationship between velocity vectors in the flow upstream of the building and the suctions on the model roof is assessed. These results have been used to show that quasi-steady theory is a good basis for the prediction of conical vortex induced loading. Quasi-steady theory predicts that instantaneous flow patterns, and hence surface pressures, produced by short duration wind gusts are the same as those produced by a time averaged mean flows with the same magnitude and direction.

Acknowledgements

The research that went into producing this thesis would not have been possible without the help of a number of people, whom I would like to thank:

Colin Wood, my supervisor, who encouraged me when my enthusiasm flagged and who tempered my haste when enthusiasm threatened to get the better of scientific rigour! Rex Belcher, for helping to develop the simultaneous measurement system that made much of this work possible and for his help using the wind tunnel facilities and computer network. Andrew Minson, for all his help in my first year at Oxford which allowed me to make a good start with my research.

In addition to their practical help I would like to thank Colin, Rex and Andrew and also Bryan Marshall, for their friendship and good humour which has made the Wind Engineering Research Group such a pleasant environment to work in.

This project has involved collaboration with a number of academics whose comments, discussion and suggestions have proved extremely useful. I am grateful to Dr Chris Baker of Nottingham University, Professor Hirosama Kawai of Tokyo Denki University, Japan, and Dr Chris Letchford of The University of Queensland, Australia.

My time at Oxford has been funded by a studentship from The Engineering and Physical Science Research Council (Award Ref. 93311696). I am grateful for this financial support and the opportunity it has given me.

I would like to thank Eva and Iain for their time and effort in helping to proof read this thesis.

Finally, I would like to thank my Mum and Dad for their constant help and support throughout my time at university, both at Sheffield and at Oxford. It is to them that I would like to dedicate this work.

Richard Marwood

'The art of drawing conclusions from experiments and observations consists of evaluating probabilities and in estimating whether they are sufficiently great and numerous enough to constitute proofs. This kind of calculation is more complicated and more difficult than it is commonly thought to be... '

Antoine Lavoisier

'...sow the wind and reap the whirlwind.'

Hosea, Chapter 8, Verse 7

List of Figures

List of Tables

1. Introduction

Vortices are formed when flow encounters a sharp edge on a structure and separates. When the flow is other than perpendicular to the sharp edge, a three dimensional vortex structure is formed. This structure is a conical vortex.

Conical vortices were first observed on the swept-back leading edges of aeroplane wings, at high angles of attack. It was not until later (Salter[1958]) that these vortices were recognised on the roof edges of buildings in oblique onset wind flows.

Conical vortices produce high suctions. On aircraft wings these large suctions are beneficial as they increase lift (Rediniotis, Hoang and Telionis[1991]). In contrast, high suctions on building roofs are detrimental as they can lead to structural damage. The roof loading produced by conical vortices typically acts over a small proportion of the total roof area and so does not affect overall loads significantly. However, roof cladding may be damaged in roof edge regions and this damage may spread.

A diagram of a conical roof edge vortex and the typical mean pressures caused beneath it appears below in Fig 1-1. Figs 1-2 and 1-3 show a conical vortex made visible by smoke.

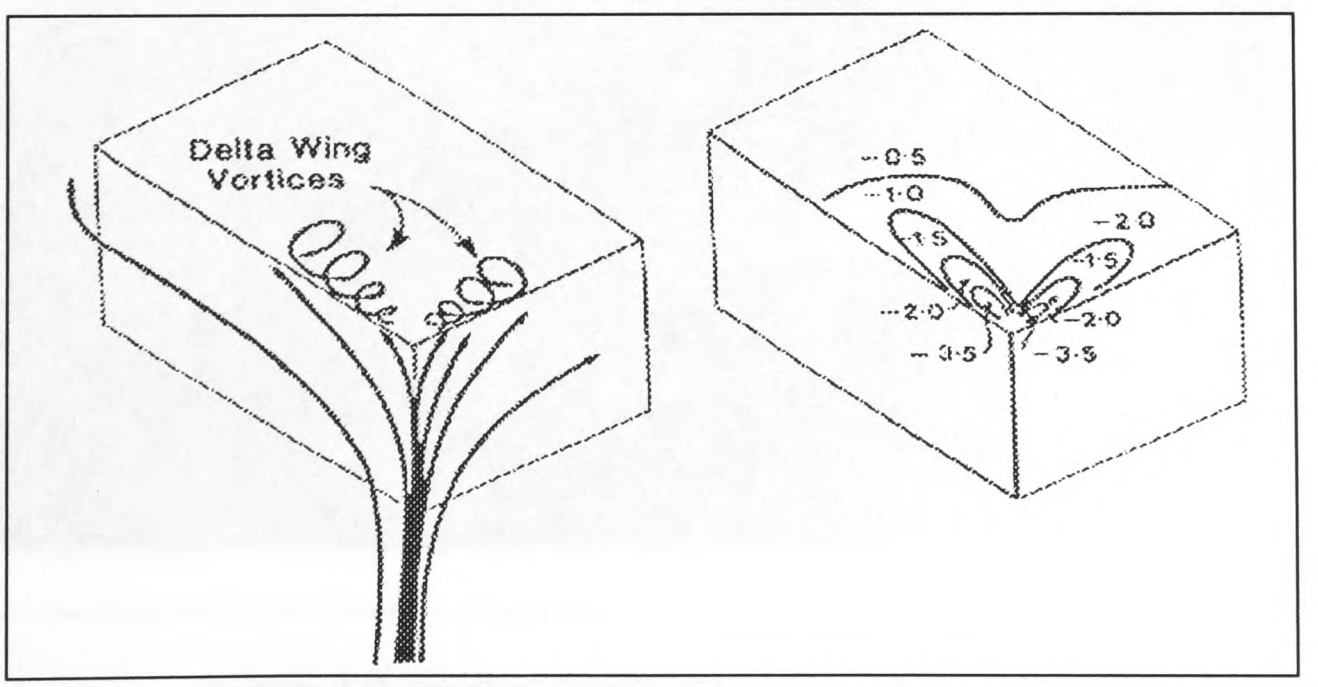

Figure 1-1 Diagram of delta wing vortices and resulting mean pressure coefficients

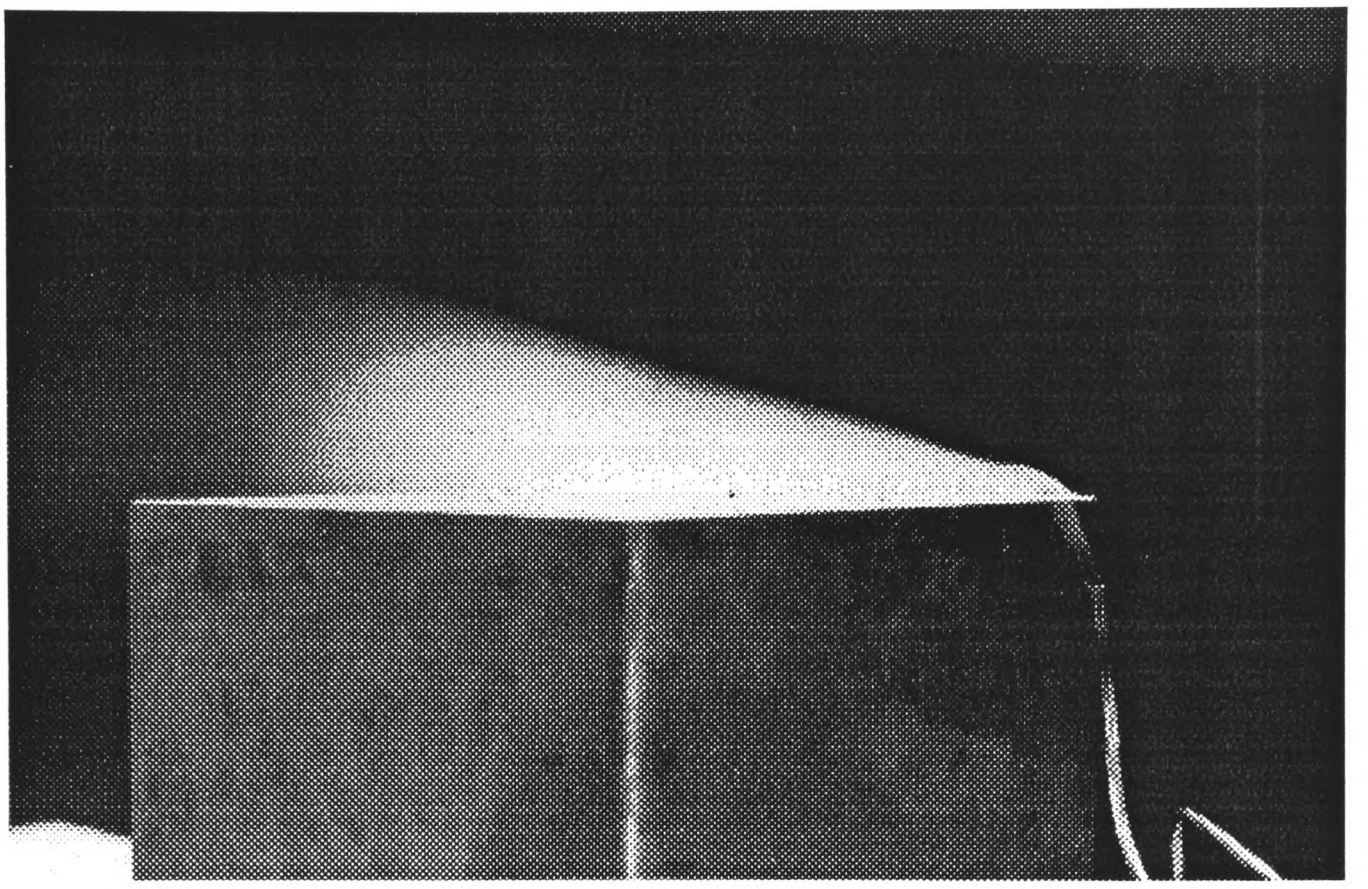

Figure 1-2 Smoke visualisation of a conical vortex

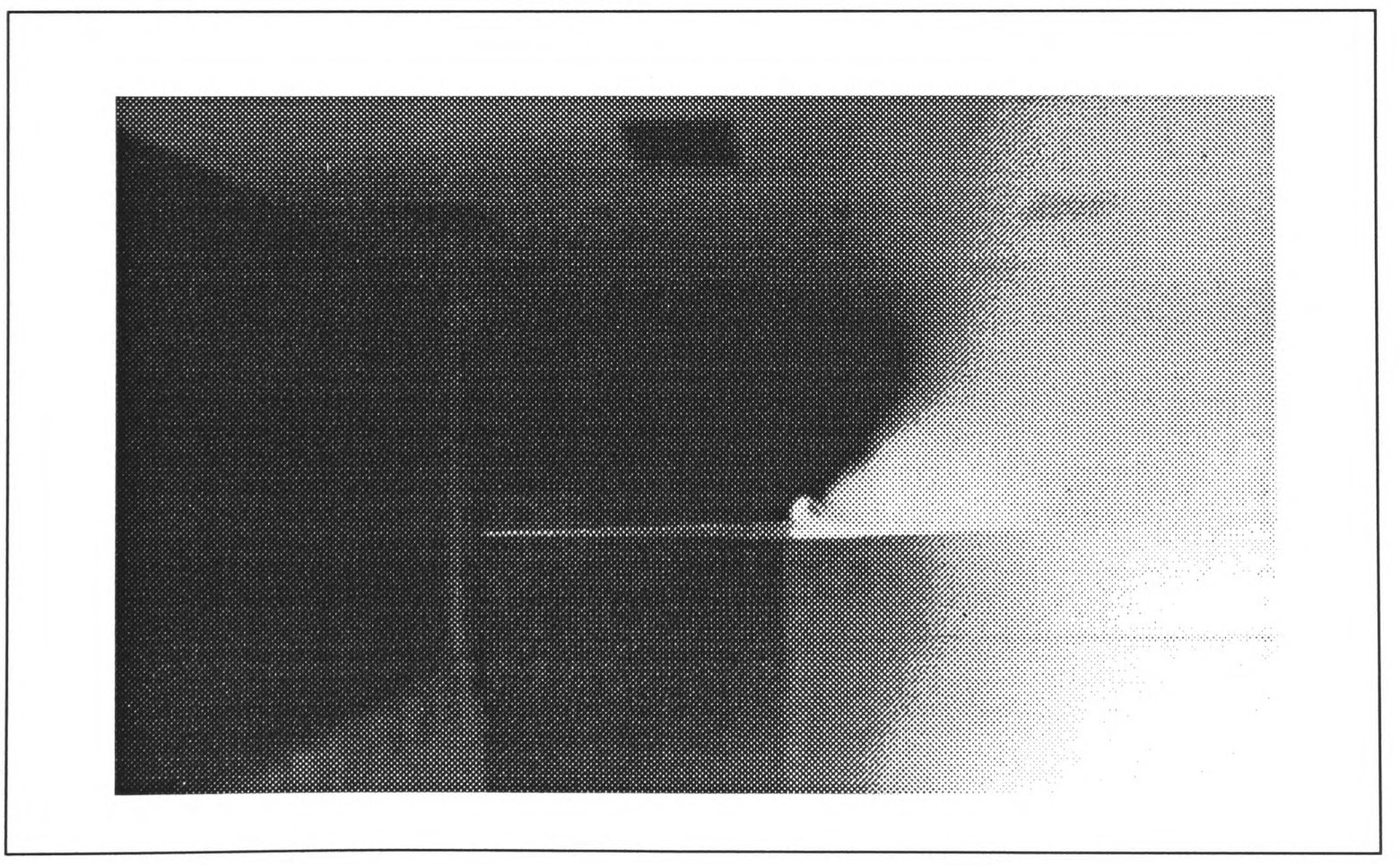

Figure 1-3 Smoke visualisation of a conical vortex

Thesis outline

The work described in this thesis extends the Oxford study of conical roof edge vortices. The principal achievement of the work is the development of a conditional sampling technique which facilitates the measurement of the instantaneous vortex flow field associated with a specified fluctuating pressure value on the underlying surface. This study reveals how the position, size and strength of the vortex affect the roof edge pressure. Finally, the applicability of quasi-steady theory to vortex effects is investigated.

Chapter 2 reviews studies already made of conical vortices.

Chapter 3 describes the experimental facilities used in this study. This covers the wind tunnel used to achieve accurate wind simulations and also the instrumentation used to make velocity and pressure measurements.

Chapter 4 presents extensive mean velocity data from measurements made in the vortex. Some mean pressure measurement data is also presented.

Chapter 5 describes the measurement technique developed to achieve simultaneous pressure-velocity measurements. The conditional statistical technique devised to analyse the simultaneous pressure-velocity data is also discussed. Additionally, results from some simultaneous pressure- velocity measurements are presented. These results give a detailed insight into variations in vortex strength.

Chapter 6 looks at the vortex intermittency that has been observed in smoke visualisations.

Chapter 7 investigates the variations in instantaneous size and position of the vortex, their relationship to onset turbulence and the effect of such variations instantaneous surface pressures under the vortex.

Chapter 8 investigates the applicability of quasi-steady theory to predict roof pressures in the light of the results presented in this thesis.

Chapter 9 presents the conclusions drawn from these experiments.

Having determined the nature of the vortex, Appendix A goes on to assess what can be done to minimise the roof damage which it causes.

Appendix B outlines the technique of Particle Image Velocity (PIV) which would be an ideal measurement tool in future studies of conical vortex flows.

2. Literature Survey

The earliest research into edge vortices in oblique flows was connected with the design of aircraft with highly swept back wings. For this reason the name 'Delta-wing vortex' has become common.

Early investigations of conical vortices involved visualisation of the flow structure (Werlé[1953], Roy[1957], Ostrowski[1960]). The earliest description of these vortices occurring on buildings is Salter[1958] who observed steady edge vortices on roofs. The first suggestion of a connection between roof edge vortices and high wind loads was made by Ostrowski and Golebiewski[1958] who measured high suctions near the edge of a model gymnasium roof. A possible link between high loads and conical vortices was also suggested by Marshall and Cermak[1966] from their model studies for the Bank of America headquarters.

In early studies of pressures on building surfaces researchers expressed concern about the poor agreement between wind tunnel pressure measurements and the pressures found at full scale. This problem was discovered when Rathbun[1940] made full scale measurements of pressures on the face of the Empire State Building in New York (at the time the tallest building in the world). Rathbun's full scale data was compared to model scale measurements made by Dryden and Hill in 1933 and the agreement between the two sets of data was very poor. With hindsight it is easy to see that the poor wind tunnel results were due primarily to the fact that the wind tunnel flows used by Dryden and Hill were uniform, with no significant boundary layer shear or turbulence. Although this is reasonable for aircraft studies, it is not valid for buildings, since a building can be much larger than a typical turbulent eddy and the mean flow velocity increases with height. This problem of

velocity gradient was soon recognised and reported by Bailey and Vincent[1943]. Over the following ten years, modelling techniques were refined and this development culminated in the modelling laws of Jensen[1954] which heralded the development of wind tunnels designed specifically for investigating the aerodynamics of buildings.

The new kind of research facility was the environmental wind tunnel. These wind tunnels use upstream roughness elements to produce good simulations of the velocity profile, turbulence intensity profile and gust spectrum of real wind. Descriptions of these facilities are extensively reported (Cook[1975], Sykes[1977], Wood[1977], Blessman[1982], Hertig[1984], Parkinson[1984], Stathopoulos[1984], Kramer, Gerhardt and Regenscheit[1984], Hansen and Sorenen[1985]).

The development of the boundary layer environmental wind tunnel has greatly improved the quality of flow simulation, but by no means perfected it.

Surry[1991], Richardson and Surry[1991], Cochran and Cermak[1992] and Okada and Ha[1992] all compared full scale data from the Texas Tech (USA) research project with measurements made in wind tunnel simulations. The model studies all produce mean pressure data which agrees well with the full scale results. However, fluctuating (root-mean-squared, RMS) and peak pressures measured at model scale significantly underestimate those found at full scale in roof edge regions. Milford, Goliger and Waldeck[1992] encountered a similar discrepancy between model and full scale peak pressures for the Jan Smuts project in South Africa.

Tieleman[1993] has shown that peak pressures can be reproduced more reliably at model scale by carefully modelling the lateral and small scale turbulence found in full scale flows. Although Tieleman's work has improved the agreement between model and full scale

measurements, there is still room for improvement and boundary layer wind tunnel modelling has yet to be perfected.

The following sections review five areas of conical vortex study: pressure measurement, flow visualisation, failure testing, velocity measurement and computational fluid dynamic (CFD) modelling.

2.1 Pressure measurement

Of the five types of study, pressure measurements have been by far the most frequently reported. Kind[1986] presents a good review of some of the pressure measurements made up to the early 1980's. Large suctions were found on roof surfaces near the upwind corners with oblique onset flows but the magnitudes of these suctions, both mean and peak, varied widely from author to author. For example, Stathopoulos, Surry and Davenport[1978a, 1978b and 1980] gave minimum mean and peak suction coefficients of -1 and -5 respectively, while Kind and Wardlaw[1982] reported -3 and -7. Later work, such as Kramer and Gerhardt[1990 and 1991], Ginger and Letchford[1992 and 1993] and Tieleman, Surry and Lin[1992] have all shown that a minimum mean pressure coefficient of around -3 is realistic for regions close to the corners of low buildings.

While mean pressure measurements agree well from study to study, a wide spread of peak pressures has still been reported. The largest reported peak suction coefficient is -18 by Tieleman et al[1992]. Tieleman showed that peak pressures are strongly influenced by turbulence intensities, with larger turbulence intensities leading to larger suction peaks. Variations in the turbulence in simulations, the pressure measurement instrumentation and the exact pressure tap position from author to author are likely to be responsible for the wide variation in measured peak suctions.

In early pressure measurement studies it was assumed that the strongest suctions were produced by an onset wind angle of 45^0 to the edge of the model producing the separation. This has since been disproved. Ginger and Letchford[1992], Tieleman et al[1992] and many others have shown that the strongest suctions occur when the onset flow angle is 30^0 from perpendicular to the separation edge.

2.2 Flow visualisation

In an extensive wind tunnel study Payne, Ng, Nelson and Schiff[1988] used smoke visualisation to examine leading edge vortices on wing models in a smooth onset flow. The vortices produced in these studies were steady. However, in a similar smoke visualisation study in a turbulent boundary layer, Minson and Wood[1992] noted that roof edge vortices on a building model appeared to exist only intermittently.

Kramer and Gerhardt used oil[1991] and loose sand[1992] to examine surface shear stress patterns on the flat roof of a building model in oblique flow. These patterns show rays diverging from the leading corner and thus indicate the presence of conical vortices.

2.3 Failure testing

A good example of model failure testing is given by Okabe[1991] who studied the displacement of roof cladding tiles. The failure patterns confirmed that cladding loads are highest near the edge of the roof and at the upwind corner. These results correspond closely to observations of damage on full scale buildings.

2.4 Velocity Measurement

The majority of measurements of velocities in a conical vortex have been in aeronautical studies. Payne, Ng and Nelson[1989], Rediniotis, Hoang and Telionis[1991] and Visser and

Nelson[1993] are the best examples, but all these measurements were made in low turbulence wind tunnels.

Velocities have been measured in roof edge vortices, in a simulated turbulent boundary layer, by Minson and Wood[1992] and Marwood, Belcher, Minson and Wood [1994]. These studies measured mean velocity components near a cuboidal building model using a two component laser Doppler anemometer.

Kawai[1995] has also made velocity measurements in a roof edge vortex using a X-wire hot wire probe. Kawai's measurements were made near a model of a low rise building in both smooth and turbulent flow.

When comparing the wing vortices studied in aeronautical wind tunnels and roof edge vortices measured in simulated turbulent boundary layers, two major differences are apparent.

Firstly, velocity vector plots show that the steady wing vortices have approximately circular flow patterns, whereas the roof edge vortices have mean flow patterns with a distinctly elliptical appearance.

Secondly, mean axial velocities in the cores of roof edge vortices are approximately equal to the mean undisturbed flow speed, whereas the cores of wing leading edge vortices may travel axially at up to three times the free stream speed.

2.5 Computational Fluid Dynamic (CFD) modelling

Computational Fluid Dynamics has evolved very quickly over the last ten years. This rapid growth is primarily due to the advances in computer technology which have lead to computers that can handle the extremely large numbers of iterative calculations typical in

CFD. Murakami[1990] and Laurence and Mattei[1993] present reviews of the state of the art of computational wind engineering at their respective times of writing.

The flow around a building immersed in a turbulent boundary layer is extremely complex and difficult to model numerically. This is especially the case in separated flows, such as a conical vortex.

Area averaged pressure data which agrees well with full and model scale measurements has been produced by CFD (Selvam[1992], Richards and Hoxey[1992], Selvam and Konduru[1993], Stathopoulos and Zhou[1993], Mochida, Murakami, Shoji and Ishida[1993]). However, predicting roof edge pressures in oblique flows (i.e. loading induced by conical vortices) has proved problematic, with CFD consistently underestimating suctions.

CFD modelling has become increasingly important in wind engineering in the last decade, but it is unlikely in the immediate future to overtake wind tunnel modelling as the primary method used to predict full scale loading. However, with suitable collaboration between researchers working in full scale measurement, wind tunnel modelling and CFD modelling, and the continued advance of computing technology, it is likely that CFD data will eventually become as reliable as wind tunnel measurements.

3. Experimental Facilities

3.1 Wind tunnel

3.1.1 Boundary layer simulation

The experiments described in this thesis were carried out in the 4m x 2m environmental wind tunnel at the University of Oxford. A detailed description of the design of the tunnel is given by Wood[1977].

The wind tunnel is not sufficiently long to develop the required rough-surface boundary layer flows naturally and so model scale simulations of the natural wind boundary layers are achieved using empirically selected turbulence grids and upstream roughness elements. By varying the turbulence grid and upstream roughness elements it is possible to generate realistic boundary layer flows representing the wind over terrain types ranging from open sea to city centres, at scales from 1:75 to 1:2000. The largest model scales that the tunnel can accommodate with accurate boundary layer modelling is limited to 1:75. At scales larger than 1:75, generating the lower frequencies in the spectrum is impossible because the required eddies are physically larger than the tunnel cross section.

A diagram of the upstream roughness pattern used in the experiments carried out for this thesis is shown in Fig 3-1.

The characteristics of full scale boundary layers are extensively documented by ESDU items 82026, 83045, 84011 and 85020 and are characterised by a single parameter z_0. z_0 is the intercept on the height (z) axis of a straight line plot of mean wind speed against the logarithm of height. Particular values of z_0 are associated with well defined terrain types (see table 3-1), provided that the same terrain extends over a nominally infinite, level fetch

upwind.

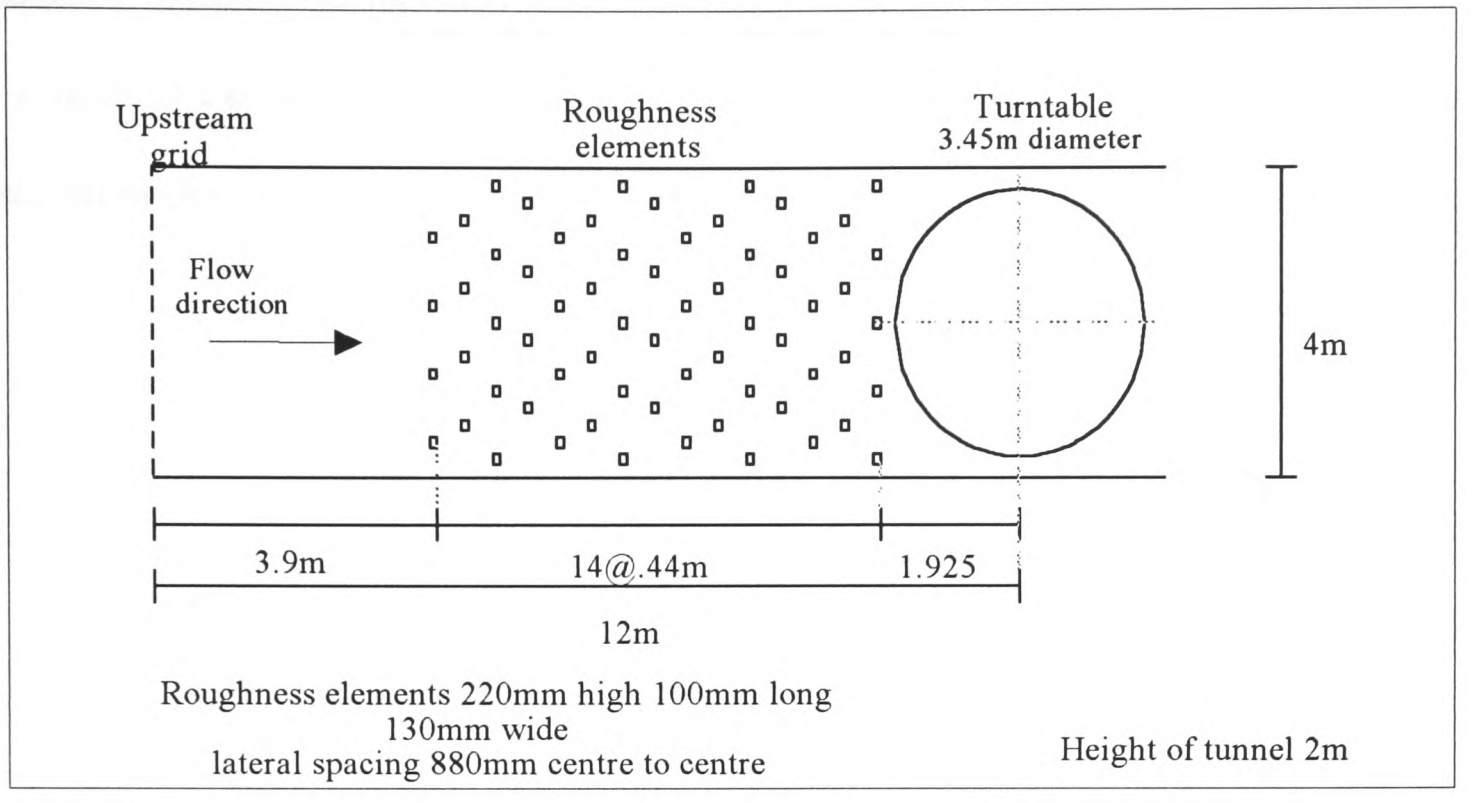

Figure 3-1 Upwind roughness elements in wind tunnel.

z_0 (m)	Description of terrain
0.003	Large expanses of water, mudflats, snow covered farmland.
0.01	Flat grassland, parkland or bare soil. Very few isolated obstructions.
0.03	Typical UK farmland. Nearly flat fields with crops, fences and low boundary hedges.
0.1	Farmland with frequent boundary hedges. Occasional houses and trees.
0.3	Dense woodland or built up domestic housing area.
0.8	Heavily built up city centre.

Table 3-1 Terrain roughness parameters

Figs 3-2, 3-3 and 3-4 show mean velocity and turbulence intensity profiles and a gust frequency spectrum for the wind tunnel simulation used in this study. The height (h) is given as a ratio of the height of the building model, 200mm. The ESDU target, which is well matched by this simulation, is a z_0 of 0.25m (built up suburban terrain) at a scale of 1:75.

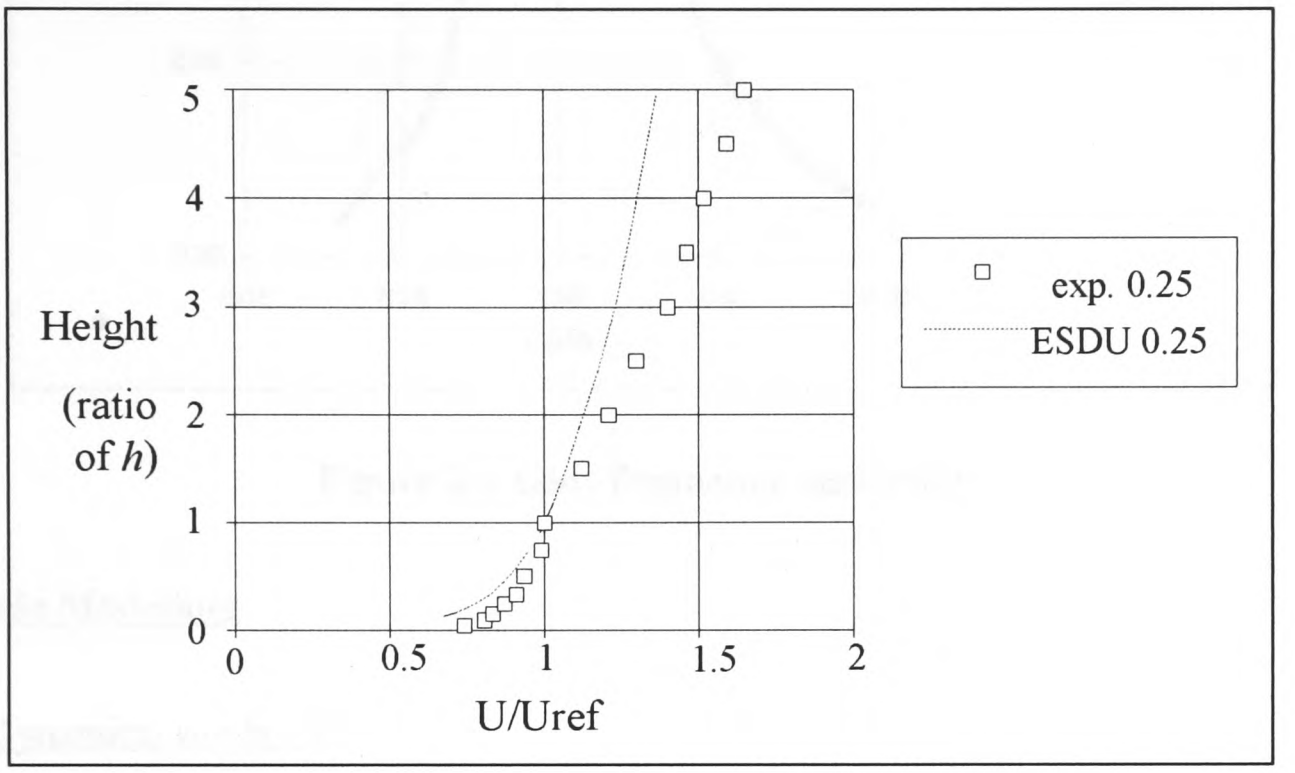

Figure 3-2 Velocity profile

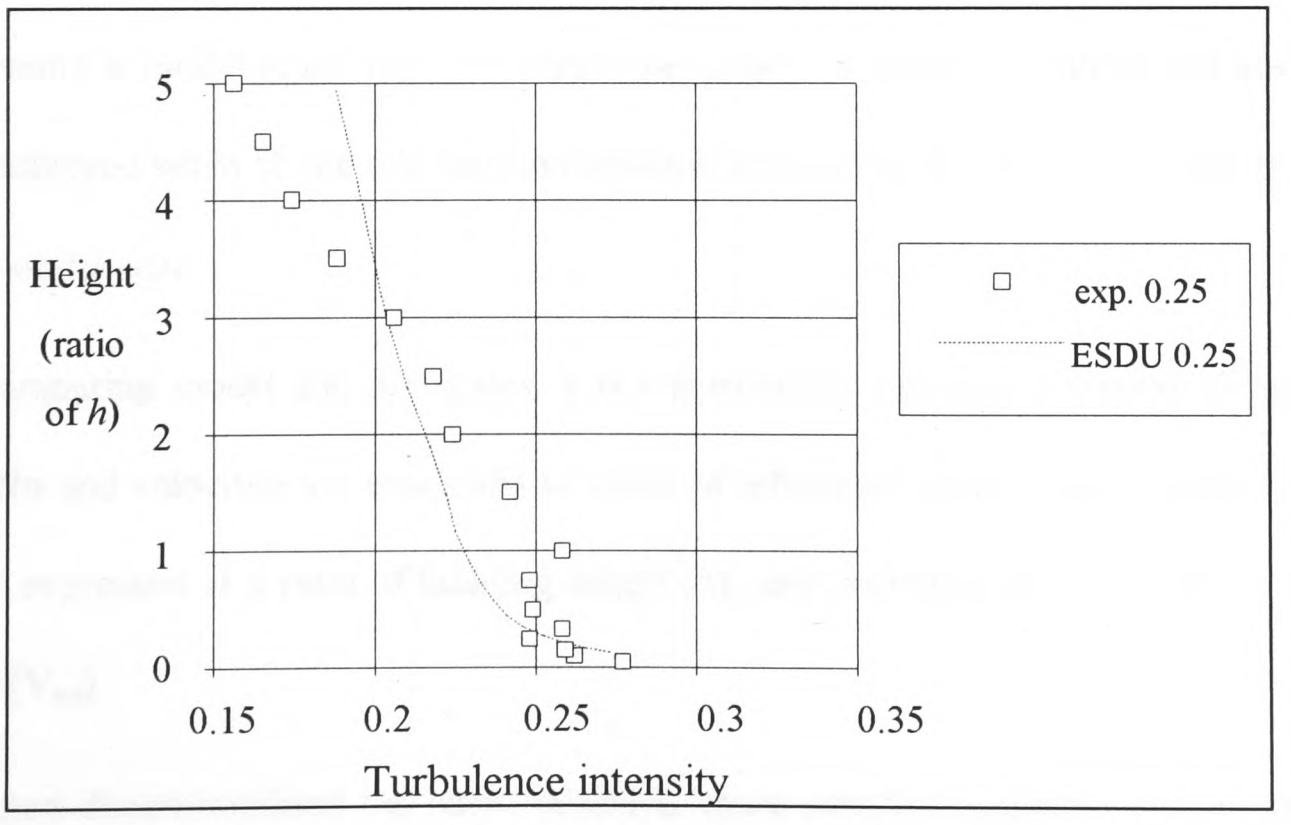

Figure 3-3 Turbulence intensity profile

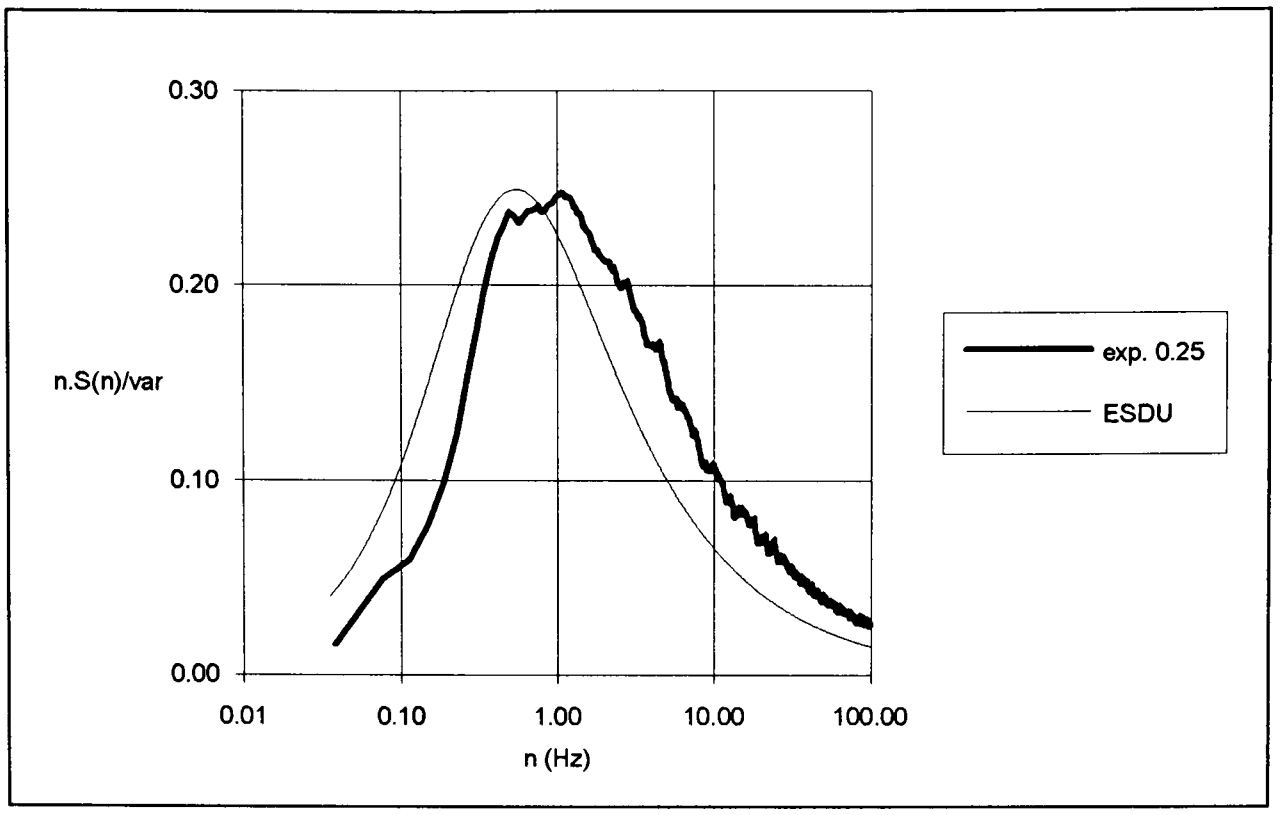

Figure 3-4 Gust frequency spectrum

3.2 Scale Modelling

3.2.1 Dynamical similarity

When carrying out experiments at model scale, the aim is to try to achieve dynamical similarity between events at full and model scale. Dynamical similarity is an ideal state where events at model scale occur in exactly the same way as they would at full scale. This state is achieved when all the relevant non-dimensional parameters have equal values in both full and model scale.

When comparing model and full scales, it is important to non-dimensionalise all variables. All lengths and velocities are expressed as ratios of reference values. Length dimensions are typically expressed as a ratio of building height (h), and velocities as a ratio of a reference velocity (V_{ref}).

Having non-dimensionalised the basic variables, more complex similarity relationships can then be considered. For a static structure, such as the one studied in this thesis, the three

most important non-dimensional parameters are Jensen number (Je) Strouhal number (St) and Reynolds number (Re).

3.2.2 Jensen number

$$Je = \frac{h}{z_0} \tag{3.1}$$

Jensen[1954] was the first to apply dynamical similarity to the aerodynamic modelling of buildings. He showed that the most important dimensionless parameter that must be matched to full scale at model scale, when modelling flow around structure in the Earth's boundary layer, is the ratio of the structure's height (h) to the aerodynamic roughness of the ground (z_0). It was not until several decades after his work that Jensen was honoured by the eponymous naming of the Jensen number (Cook[1986].)

Matching Jensen number at full and model scale means that the scale model is subject to a realistic increase in mean velocity with increased height (velocity gradient.) Fig 3-2 shows that this was achieved for the experiments described in this thesis.

3.2.3 Strouhal number

$$St = \frac{nh}{V} \tag{3.2}$$

n is frequency

V is velocity.

The Strouhal number was originally derived to define the characteristic frequency (n_s) of vortex shedding. However, since frequency is the reciprocal of time, the Strouhal number is generally interpreted as being the formal definition that velocity is length divided by time.

Since the velocity scale is a function of length and time scales, selecting values for any two of the three scales dictates the value of the third.

The length scale of the $z_0 = 0.25$m simulation used for the experiments in this thesis is 1:75. Since modelling of a realistic wind speed is crucial, the velocity scale is the other fixed scale.

The hourly mean wind speed, for a reference height of 15m, with a probability of exceedance of 1%, for much of inland England is approximately 13 m/s. The wind tunnel produces a velocity of around 4.5 m/s at the model height, 200mm, with the $z_0 = 0.25$m simulation in place. Therefore, if we assume that the 200mm cube represents a 15m high building subject to the hourly mean speed then the velocity scale is 1:(13/4.5) = 1:2.9. This, along with the length scale of 1:75, dictates a time scale of 1:26.

Therefore, 2 minutes 18 seconds of tunnel running time simulates one of the 88 most windy hours that would be expected in an inland region of the UK in a typical year.

The hourly wind speed varies around the country and so velocity and time scales vary depending on the site being modelled. For example, if a site in the Orkney Islands (where the hourly mean wind speed is approximately 19 m/s) were modelled then the velocity and time scales would be 1:4.2 and 1:18 respectively.

3.2.4 Reynolds number

$$Re = \frac{\rho h V}{\mu} \tag{3.3}$$

ρ is fluid density

μ is fluid viscosity

The Reynolds number is the ratio between inertial and viscous forces in the flow. Typically

in wind engineering flows the Reynolds number is high and viscous forces are negligible compared to inertia forces. However, in flows near a surface, viscosity becomes significant as it controls flow separation and re-attachment. Separation around curved structures is particularly sensitive to Reynolds number, and must be modelled carefully. In contrast, boundary layer flow around a sharp edged structure, such as the one used in this study, is unaffected by Reynolds number. This is fortunate because producing realistic Reynolds numbers at model scale is difficult. Velocities and lengths are typically much smaller at model scale than those they represent at full scale, leading to much smaller values of Reynolds number. If we consider the model described in this chapter and the full scale scenario it represents, $Re_{model} = 6 \times 10^5$ and $Re_{full} = 13 \times 10^6$.

3.3 Velocity measurement

3.3.1 Background

Prior to the development of easily positioned laser anemometers, with flexible fibre optic cables, the standard instrument for measuring fluctuating velocities was the hot wire anemometer. However, the flow around buildings is highly turbulent and there are large changes in flow direction as well as speed. In these flows the hot-wire anemometer does not give useful measurements because it cannot distinguish flow direction. In addition to this directional ambiguity, hot-wire probes are delicate and easily damaged and great care is required when using them close to surfaces.

The Laser Doppler Anemometer (LDA) has been developed over the last 25 years and is now a powerful measurement tool. The underlying theory behind LDA operation is the Doppler principle which states that a wave reflected back from a moving particle has a different frequency from the incident wave. The change in frequency, known as the Doppler

shift, is a linear function of the particle velocity. This intrinsic link between velocity and frequency means that measurement systems based on this theory suffer no drift and so, unlike hot-wire anemometer systems, never need calibration.

In typical LDA technique, two laser beams are focused at a point to form an interference pattern at the measuring volume (see Fig 3-5). This technique is commonly called the dual beam method. The component of velocity measured is in the plane of the two beams and normal to the line bisecting the two laser beams, as shown in Fig 3-5.

The light scattered by particles passing though the interference pattern is modulated at a frequency dependent upon the particle velocity. The light scattered from the measuring volume is collected and analysed to determine the modulation frequency and hence the velocity of the particle. Typically, velocity data from many particles is analysed to give a time series of the velocity component from which time averaged statistics can be calculated. It is possible to measure more than one component at a time by introducing additional pairs of laser beams.

The mode of operation described above would leave a directional ambiguity for each component since particles passing through an interference pattern in opposite directions with the same speed will scatter light at the same frequency. To overcome this problem the frequency of one beam is shifted to produce moving fringes in the measuring volume. If the fringes move faster in the negative direction than any one particle, then all particles will seem to be moving in the positive direction and thus will be associated with a unique frequency of scattered light. The effect of this frequency shift is removed during signal processing and the correct sign allocated to the velocity of each particle.

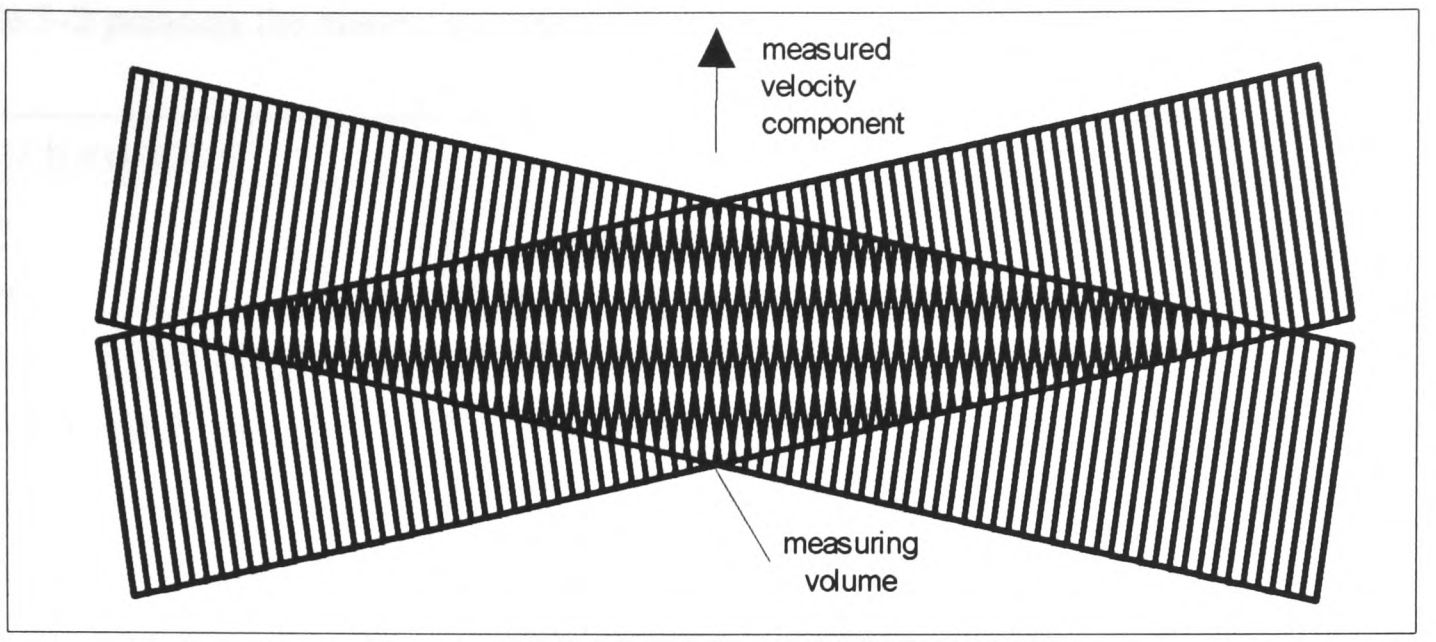

Figure 3-5 Measuring volume of Laser Doppler Anemometer

3.3.2 LDA system description

A diagram of the DANTEC LDA system used in this work is shown in Fig 3-6.

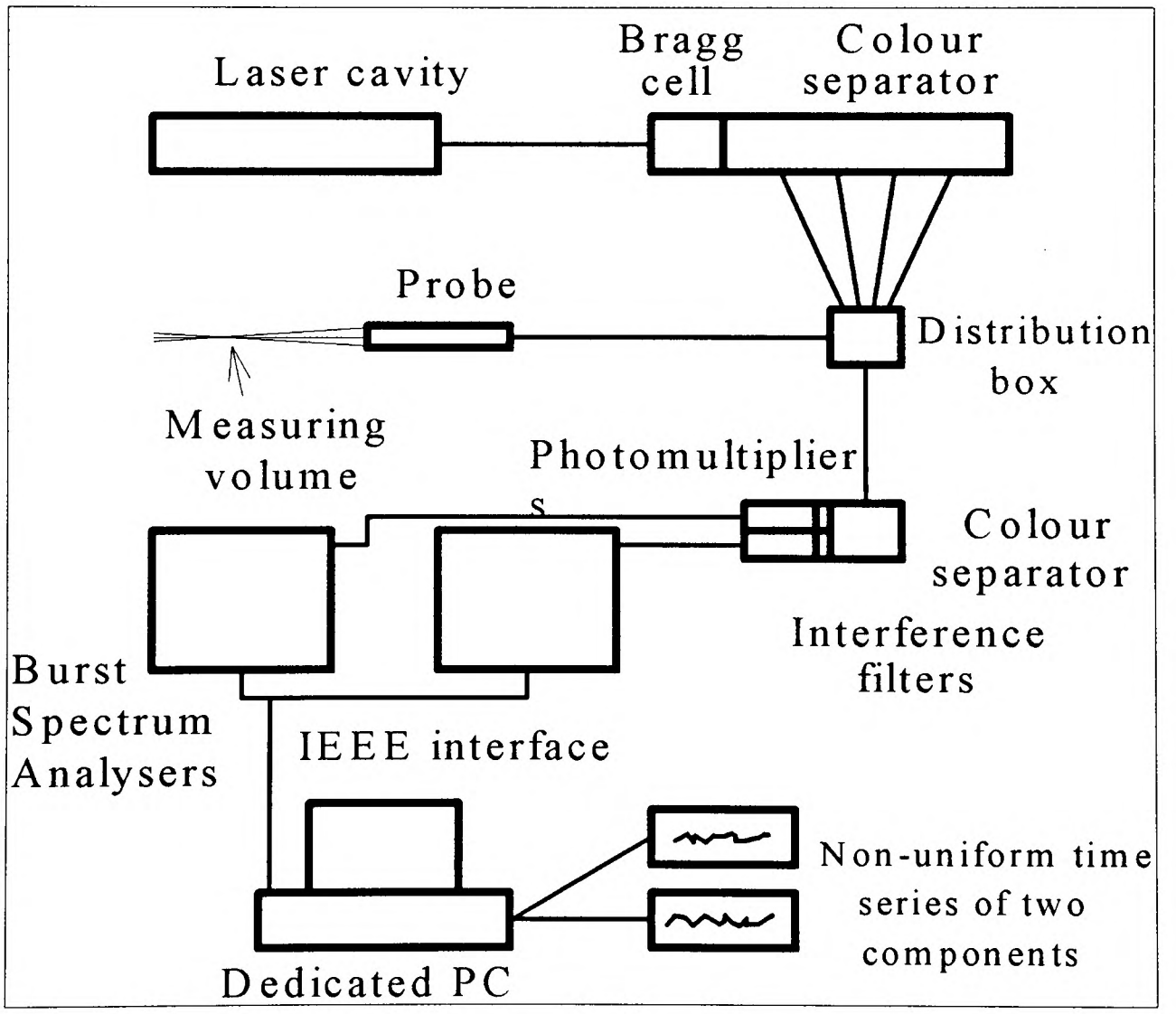

Figure 3-6 Diagram of LDA system

Table 3-2 presents the system specifications.

LASER/OPTICS		
Type	Argon-ion	
Power	300mW	
Bragg Cell Frequency	40MHz	
Beams Transmitted	488.0nm	
	488.0nm Bragg Cell shifted	
	514.5nm	
	514.5nm Bragg Cell shifted	
PROBE		
Type	Back-Scatter	
Length	105mm	
Diameter	14mm	
Weight	0.1kg	
Focal Length	50mm	
Beam Separation	8mm	
Receiving Aperture	11mm	
Working Distance	46.3mm	
MEASURING VOLUME		
Beam wavelength	488.0nm	514.5nm
Length	1.44mm	1.52mm
Width	0.115mm	0.122mm
No. of fringes	37	37
SEEDING		
Generator type	TSI Model 9306 Atomiser	
Material	Water/Glycerine Ratio 5:1	
Mean Aerodynamic Diameter	Approximately 1μm	
PROCESSORS		
Type	Burst Spectrum Analyser	
Manufacturer/Model	DANTEC 57N14	
Peak Data Rate	1.5MHz	
Capacity	16384 bursts	

Table 3-2 LDA system specification

The laser source in the DANTEC laser anemometer system used at Oxford is a 300mW Argon-ion laser. This produces two dominant light wavelengths, 488nm (blue) and 514.5nm (green) which are split to form two beams by a Bragg cell. The laser beams are transmitted along fibre optic cables to the measurement probe, where they are focused by a lens onto the measuring volume.

The LDA system is a back scatter system, which means that the probe transmitting the laser light is also the receiver for the light scattered from the seeding particles. Unlike forward scatter systems, back scatter systems do not require the separate alignment of transmitting and receiving optics.

When seeding a flow for LDA measurement, it is necessary to compromise between having particles sufficiently large to scatter enough light and the particles being small enough to follow the flow accurately. In the Oxford tunnel, the seeding is produced by two TSI Model 9306 atomisers, using a solution of 1 part glycerine to 5 parts water. These particles have an average diameter in the order of 1 micrometer (1×10^{-6} m). Durst, Melling and Whitelaw[1976] showed that particles up to 10μm could still follow frequencies up to 700 Hz with an accuracy of 99%. The highest frequency flow structures occurring in the Oxford tunnel are approximately 100 Hz so the 1μm particles can be assumed to accurately follow small scale turbulence patterns in the flow.

The Oxford environmental wind tunnel is open circuit and exhausts into the laboratory building. The seeding therefore additionally needs to be both non-toxic and non-corrosive. Both of these criteria are satisfied by the water-glycerine particles.

The light scattered from the seeding particles is focused onto the end of an optical fibre within the measuring probe. This fibre transmits the received light to a colour separator.

This separated light is then directed onto a photomultiplier, via an interference filter for the appropriate wavelength. The photomultiplier converts the scattered light into an electrical signal. This signal is termed a burst and can comprise of 8, 16, 32 or 64 individual samples.

The signal processing is carried out by two DANTEC Model 57N10 Burst Spectrum Analysers (BSA), one for each velocity component. The BSA use a hard wired fast Fourier transform to determine the frequency spectrum for each burst. The peak of the frequency spectrum is the Doppler frequency. The largest spectral peak must be four times greater than any other peak in the spectrum, otherwise the measurement is rejected.

The BSA output is a listing of particle velocities and their occurrence times. Since a velocity is only measured when a particle passes through the measuring volume the time series is non-uniform.

If the mean velocity is calculated by averaging all the particle velocities, the non-uniformity in the time series can result in a bias away from the true mean. If the flow is uniformly seeded then more particles will pass through the measuring volume when high velocities occur and so the mean velocity will be overestimated. This biasing is corrected out by a technique known as 'time interval weighting' or 'sample and hold.'

A true mean velocity can be determined from the integral of a smooth curve fitted through the non-uniformly spaced data points. Fig 3-7 shows an example of measured data points, a full time series and a sample and hold reconstructed time series.

If the data points are separated by a non-uniform time interval, Δt, then the mean velocity from the sample and hold technique is given by equation (3.4).

$$\text{Sample and hold mean} = \frac{\sum \text{Particle velocity} \times \Delta t}{\sum \Delta t} \qquad (3.4)$$

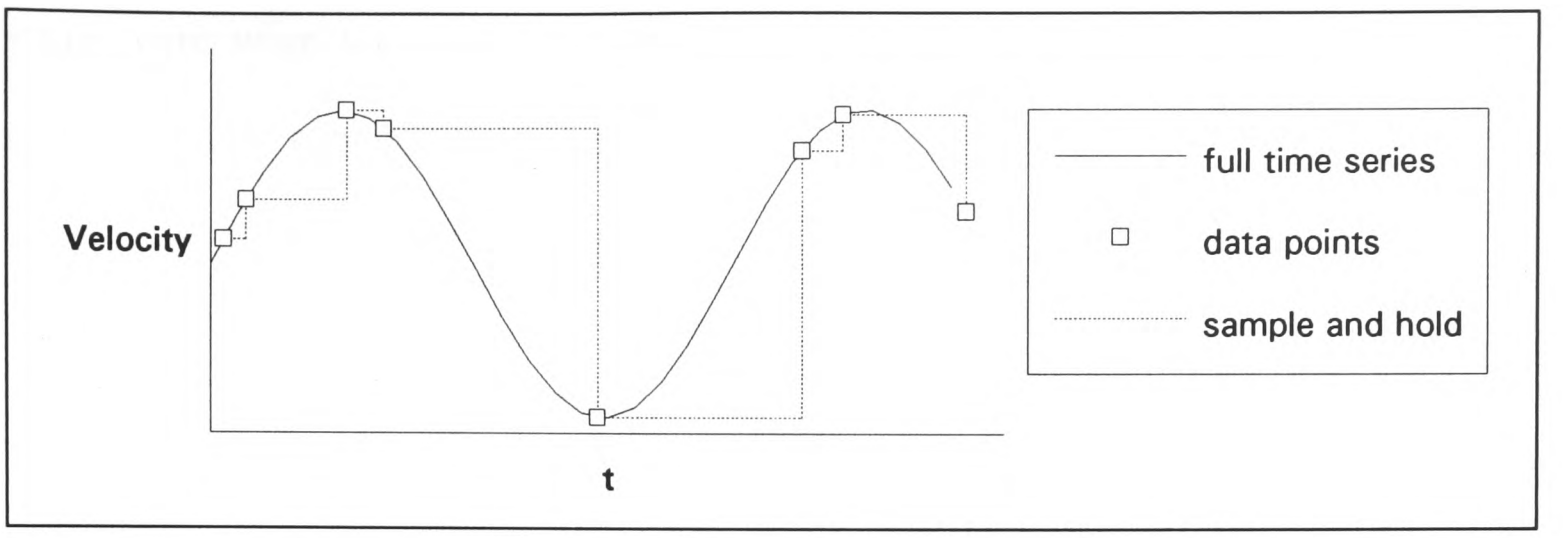

Figure 3-7 Sample and hold time series

3.4 Pressure Measurement

Pressure measurements were made by drilling tapping points in the models and connecting these taps to a Setra 237 pressure transducer via a Scanivalve pressure-scanning switch and tubing network.

The pressure transducer converts pressure measurements into an electrical signal. The transducer has an output range of 0-5 volts, with a calibration factor of 270 Pascals/Volt, giving a range of 1350 Pa and a resolution of approximately 4Pa.

The Scanivalve is a computer controlled switching device which allows up to 44 taps to be connected in turn to a single pressure transducer.

3.4.1 Location of pressure tappings

The purpose of these measurements was specifically to examine the pressure field immediately beneath the conical vortex. Therefore, before choosing locations for the pressure tappings, the position of the vortex was estimated from the mean velocity measurements described in Chapter 4. The drilling pattern shown in Fig 3-8 was devised from these results. Tappings number 1-4 (on the 16^0 ray) lie under the mean position of the

vortex core when the model is orientated at 45^0 to the onset flow. Tappings 5-8 are positioned to lie approximately at the vortex reattachment points.

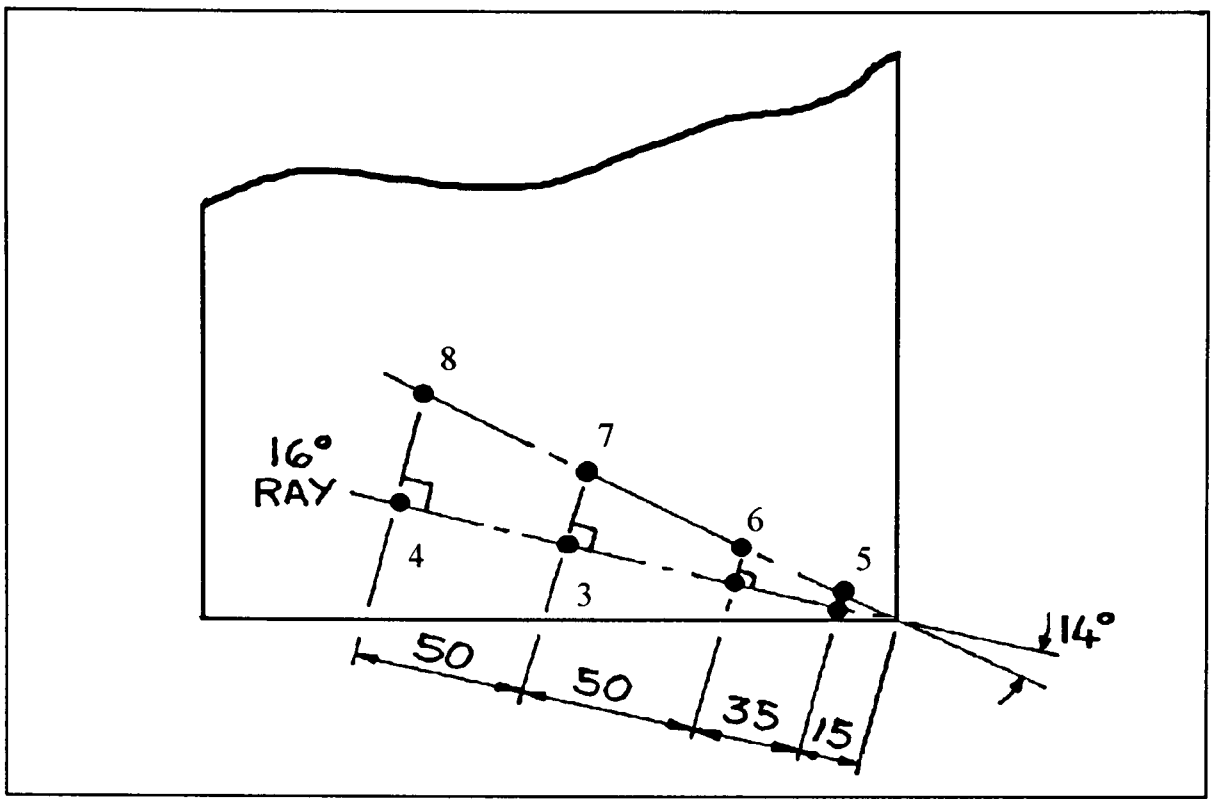

Figure 3-8 Pressure tap locations

3.4.2 Tube connections to the pressure transducer

When measuring fluctuating pressures with a remote transducer, it is essential to avoid amplitude and phase distortion caused by acoustic resonance in the connecting tube.

Irwin et al [1979] and Surry and Stathopoulos[1977] showed that restricting the flow area at points along the tube connecting the tapping and transducer can alleviate acoustic resonance problems. The size and position of the restrictions can be varied to achieve the desired acoustic damping. The aim of the damping is to make the amplitude of the pressure signal at the transducer equal to that at the tap, and to make the phase lag between the signals vary linearly with frequency. These criteria need to be met throughout the frequency range in which measurements are going to be made. With correct damping the signal seen at the transducer is identical to that at the pressure tap, albeit subject to a time delay.

In most pressure measurements, it is sufficient to establish that the transfer function of the tubing has a unity gain and linear phase shift so that the input pressure is transmitted to the transducer without distortion. The fact that there is a finite time lag is of no interest. In contrast, the current study intends to examine simultaneous records of surface pressure and local velocity. Therefore, it is necessary to know the magnitude of, and take into account, any time lag in the pressure tubing.

A linear relationship for phase lag causes a uniform time lag between actual and measured signals since phase lag (φ) equals a constant (k) multiplied by frequency (n). Therefore:

$$\text{Time lag} = \frac{\varphi}{n} = \frac{kn}{n} = k \tag{3.5}$$

Early research used experimentation to determine the optimum configuration of tubing networks, but this was later superseded by the work of Gumley[1981], who solved the problem analytically. The outcome of Gumley's work was a design methodology for pneumatic tubing systems (Gumley[1982]). His computer programmes, subsequently enhanced by Letchford[1987], were used to design the connecting tubes used in this study. The frequency response plots are shown in Figs 3-9 and 3-10.

In this study, the frequencies of interest are up to 100Hz. Fig 3-9 shows that the amplitude response is unity up to 100 Hz, and hence meets the damping criterion. Fig 3-10 shows that the phase response is linear up to approximately 160Hz, and thus is also acceptable. The time lag in the pressure signal was evaluated by calculating the slope of the frequency-phase plot from 0-100Hz. Accounting for the time lag is discussed in section 5.2.2.

$$\Delta T = \frac{d\varphi}{dn} = 11.6\text{ms} \tag{3.6}$$

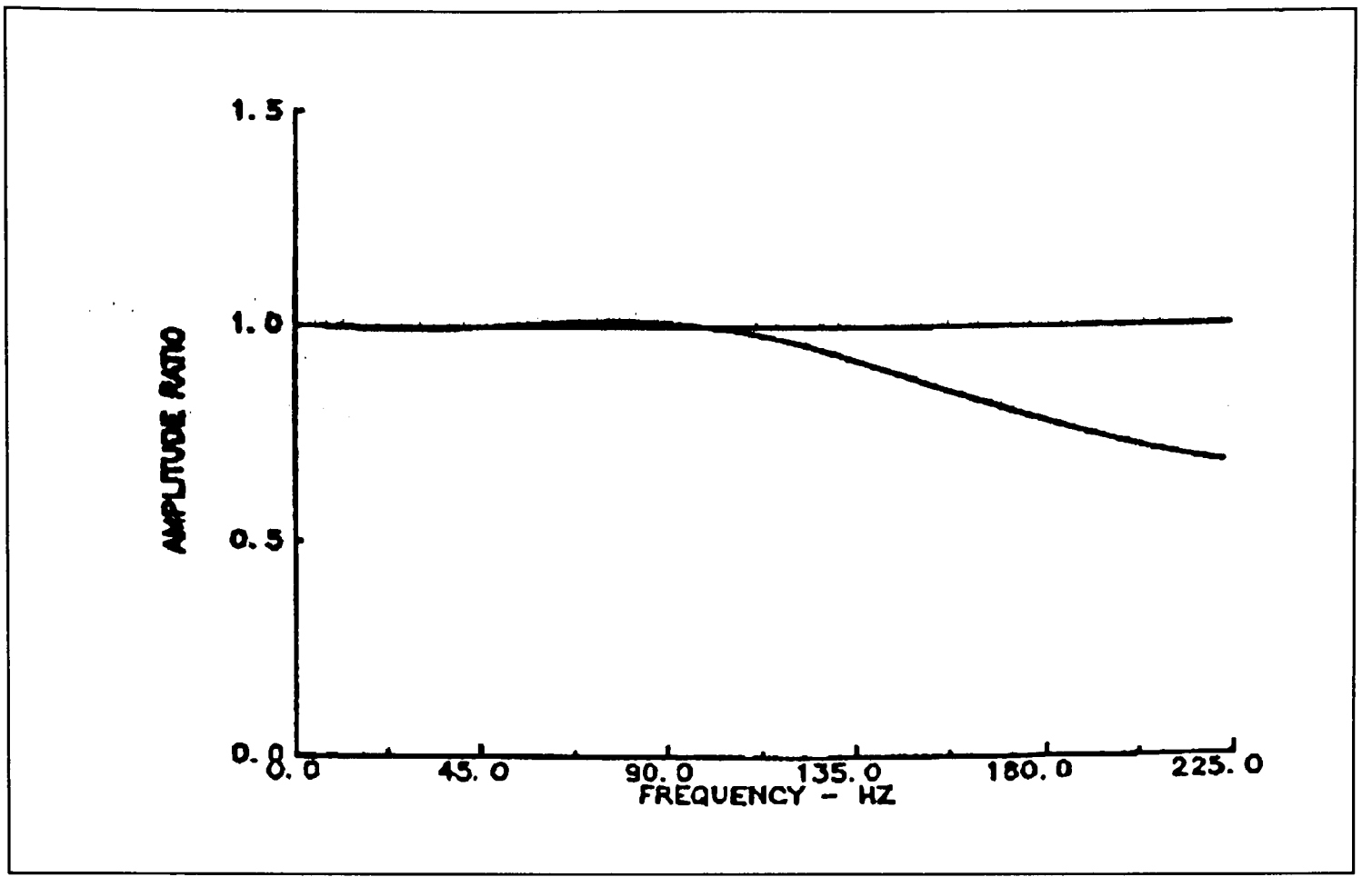

Figure 3-9 Amplitude frequency response of pressure tubing.

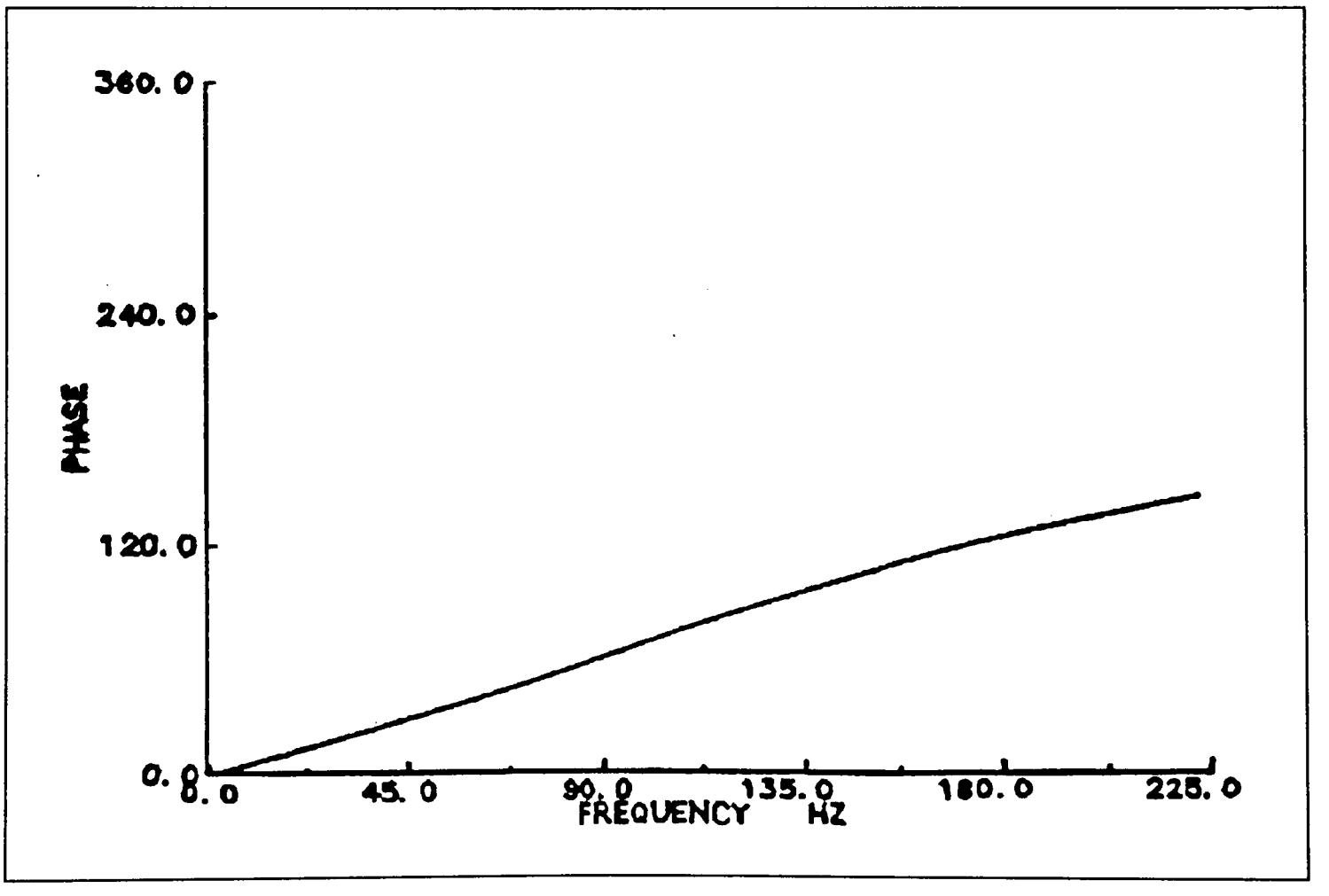

Figure 3-10 Phase frequency response of pressure tubing.

3.4.3 Reference Dynamic Pressure

In order to produce a dimensionless pressure coefficient, the pressure measured at a tapping is divided by a reference dynamic pressure. The reference value used is the dynamic pressure of the undisturbed flow measured at the centre of the wind tunnel turntable, at the height of the model (200mm) without the model in place. Obviously, this cannot be measured when the model is in place. To overcome this difficulty the tunnel is calibrated with the model removed. The velocity, V_{tun}, is measured with a pitot static tube at a secondary reference location away from the model and the velocity at the turntable centre, at the height of the model (V_{ref}) measured with a hot-wire anemometer. The reference dynamic pressure can then be calculated from equation (3.7).

$$\text{Reference dynamic pressure} = \tfrac{1}{2}\rho V_{ref}^2 = \tfrac{1}{2}\rho V_{tun}^2 \left(\frac{V_{ref}}{V_{tun}}\right)^2 \qquad (3.7)$$

For the tunnel configuration used in this study $\frac{V_{ref}}{V_{tun}} = 0.484$. Therefore, the reference dynamic pressure is that measured by the pitot tube at the secondary location multiplied by 0.484^2.

A pressure occurring on the model (p) is non-dimensionalised into a pressure coefficient (Cp) using the equation (3.8).

$$Cp = \frac{p - p_{back}}{\frac{1}{2}\rho V_{ref}^2} \qquad (3.8)$$

$p - p_{back}$ is the pressure measured by the pressure transducer (see section 3.4.4).

3.4.4 Transducer Backing Pressure

The pressure transducer determines pressures by measuring the deflection of a diaphragm.

The input pressure (p) is applied to one side of the diaphragm and a back pressure (p_{back}) is applied to the other side. Hence, the pressure that the transducer measures is $p - p_{back}$.

The back pressure used in this study is an arbitrary tunnel static pressure. This pressure is made steady by a large volume in the tubing connecting the tapping to the transducer.

At the start of each pressure measurement run it is customary to establish a zero datum for the pressure transducer. This is done by connecting the back pressure to both sides of the transducer diaphragm.

In this study it is not the absolute values of pressure that are of interest. Rather, it is the pressure values considered either in comparison to other pressure values in the same measurement sample or values measured at other tappings on the model. Pressures within the same measurement sample can be compared since the back pressure is steady and pressure measurements made at different tappings on the model can be compared since the same back pressure was used for all measurements.

4. Mean Velocities in the Vortex and Resulting Surface Pressures

4.1 The mean velocity field

Many researchers have measured roof-edge pressures under conical vortices (see section 2.1) but, as section 2.4 shows, measurements of the velocity field in the vortex have been very scarce. At the time of writing, the work presented in this chapter, and that of Minson and Wood[1992] and Kawai[1995] are the only sets of velocity data for a conical vortex in a turbulent simulated atmospheric boundary layer.

Tieleman et al[1992] deduced the location of roof-edge vortices by mapping surface pressure fields and assuming that the locus of minimum pressure was directly beneath the mean axis of the vortex. Tieleman's work showed, that with the leading edge of the model at 45^0 to the onset flow, the vortex formed above a ray through the windward apex at an angle of 15^0 to the edge of the building.

The assumption that pressure minima occur below the axis of the vortex is supported by potential flow theory. This theory predicts vortices which are termed free vortices. In a free vortex the streamlines are in the form of a nest of concentric circles and the tangential velocity (q) at a point is inversely proportional to its distance (r) from the centre of the vortex. Since (q x r) is constant the circulation (Γ) around any circumferential path in the vortex is independent of radius. Therefore:

$$\Gamma = 2\pi rq(r) \qquad (4.1)$$

The difference in stream function (ψ) between two streamlines is equal to the volume flow between them. Thus:

$$d\Psi = q(r)\, dr = \frac{\Gamma}{2\pi r}\, dr \tag{4.2}$$

Integrating equation (4.2)

$$\Psi = \frac{\Gamma}{2\pi} \ln(r) + \text{constant} \tag{4.3}$$

If a free vortex is near a surface then the flow field can be calculated by using the image vortex technique. An image vortex, rotating in the opposite sense to the free vortex, is placed as far behind the surface as the free vortex is in front of it, as shown in Fig 4-1.

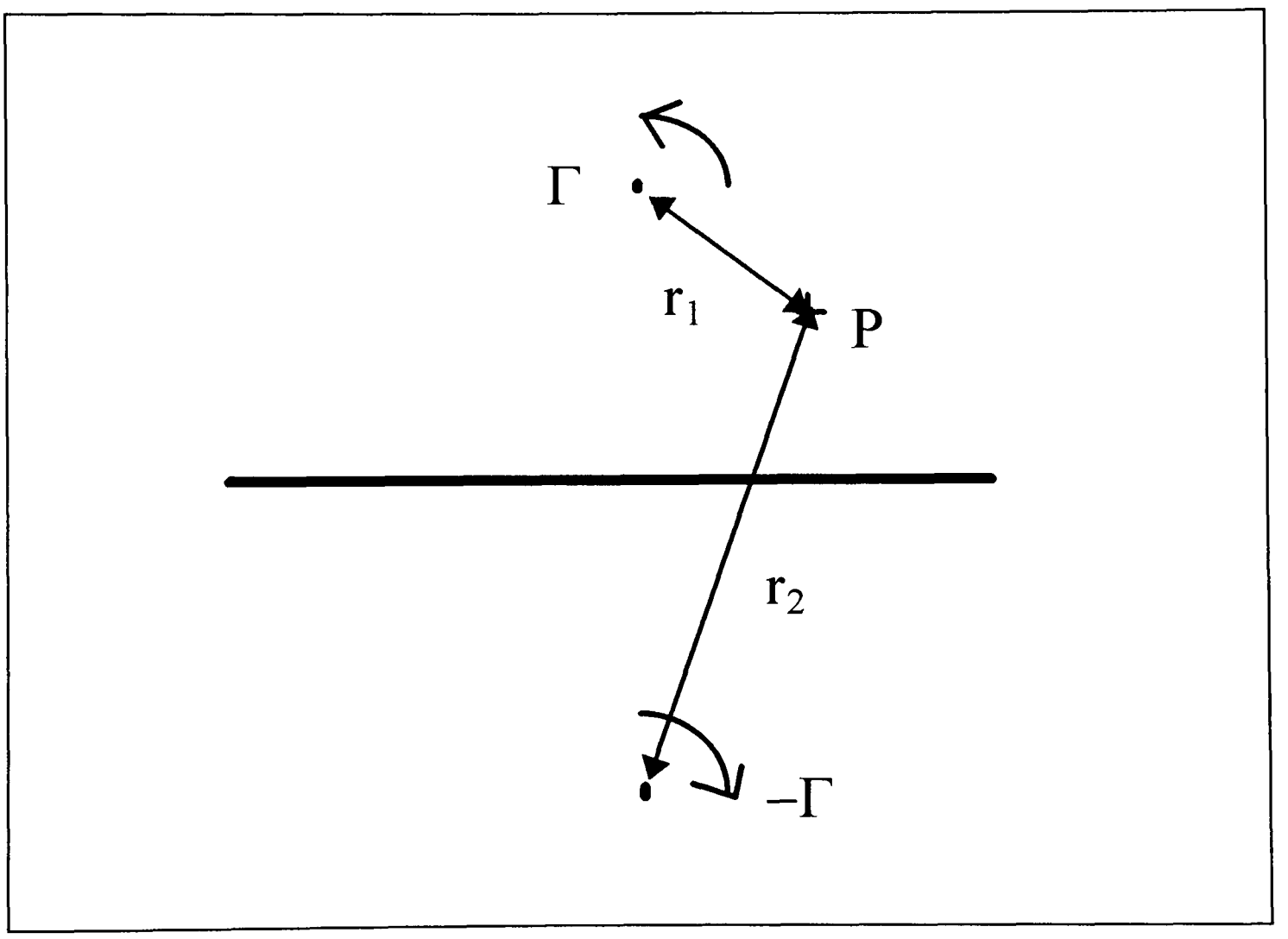

Figure 4-1 Image vortex technique

With the image vortex in place the stream function at a point, Ψ_p, is found by adding the effect of the real and the image vortices. Therefore:

$$\psi_p = \frac{\Gamma}{2\pi}(\ln(r_1) - \ln(r_2)) = \frac{\Gamma}{2\pi}\ln\frac{r_1}{r_2} \tag{4.4}$$

Having calculated the stream function field from equation (4.4) the velocity field can then also be calculated. The relationship between stream function and velocity is:

$$\frac{\partial \Psi}{\partial z} = v \quad \text{and} \quad \frac{\partial \Psi}{\partial y} = -w \tag{4.5}$$

Using Bernoulli's equation to calculate pressures from the velocity field produces a pressure distribution on the surface underlying the vortex of the form shown in equation (4.6) and Fig 4-2.

$$\frac{p}{p_{min\,ima}} = \frac{1}{\left(\left(\frac{y}{z_h}\right)^2 + 1\right)^2} \tag{4.6}$$

p is the surface pressure at a point.

p_{minima} is the peak suction.

y is the perpendicular distance from the vortex axis, parallel to the roof surface.

z_h is the height of the vortex core above the roof surface. This is predicted by equation (4.7)

$$z_h = y_{1/2}\sqrt{\sqrt{2} - 1} \tag{4.7}$$

$y_{1/2}$ is the 'half width' of the vortex, the value of y at which $(p/p_{minima}) = 0.5$.

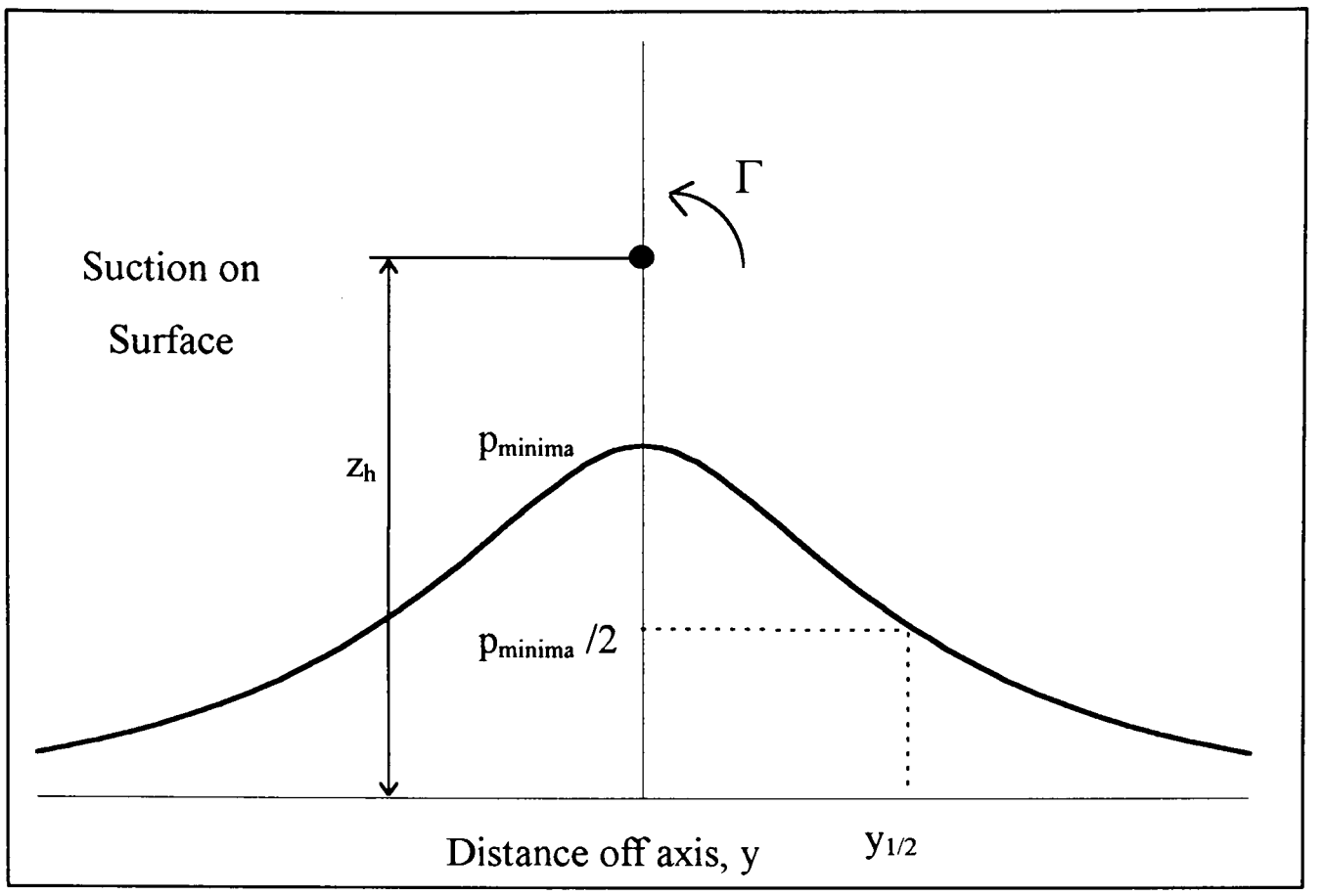

Figure 4-2 Pressure distribution under a free point vortex

Greenwell and Wood[1992] and Kawai and Nishimura[1994] measured pressure along planes perpendicular to the locus determined by Tieleman and found good agreement between measured pressures and the pressure distributions predicted by equations (4.6) and (4.7).

In order to confirm these pressure deduced vortex positions, measurements of velocity components normal and parallel to the 15^0 ray were made using LDA, with the cube placed at 45^0 to the onset flow. Guided by the findings of Tieleman, a frame of reference for these velocity measurements was defined. The axes are defined as show in fig 4-3. The velocity components are defined u in the x direction, v in the y direction and w in the z direction.

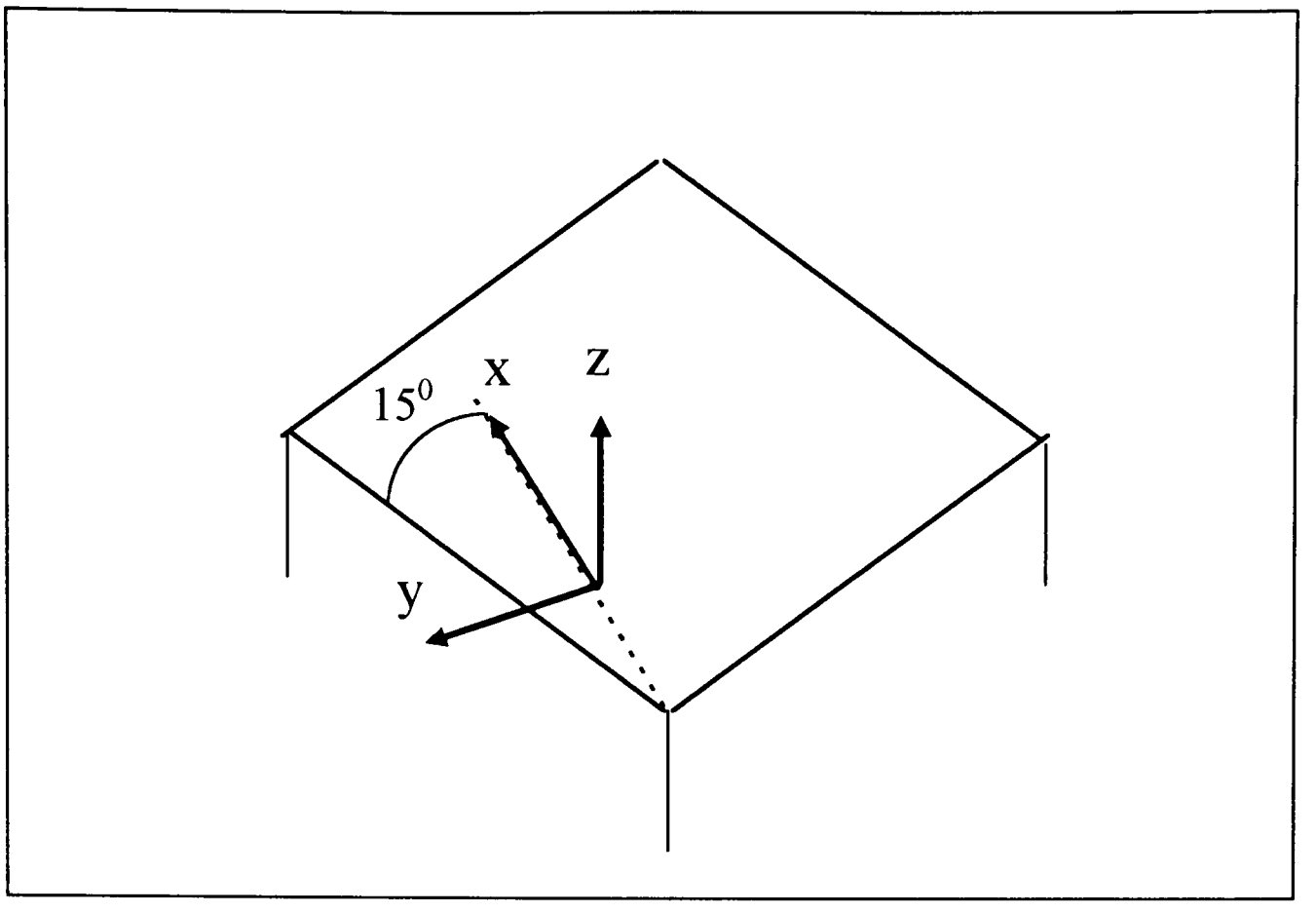

Figure 4-3 Measurement co-ordinate axes

Taking measurements in the vortex is by no means a trivial matter. Making measurements close to the surface of a model presents two major problems, reflection of the laser from the model surface and the necessity to tilt the LDA probe.

Measurements within 2mm of the model surface are difficult to make because the laser beams are reflected from the surface. This reflected light is scattered back into the light receiving optics, masking the signal produced by the light reflected back from the seeding particles.

Norman[1992] used a model with matt black surfaces, but this did not alleviate the problem of reflected light.

Improved signal discrimination is offered by DANTEC in their enhanced BSAs. Unfortunately, funds were not available for such equipment. Therefore, the measurements in this study are restricted to locations more than 2mm from the model surface.

The LDA probe is 14mm in diameter. Therefore, to measure at locations closer than 7mm

to the surface the probe must be tilted downwards. The measuring volume is 46mm away from the lens of the probe and therefore tilting the probe downwards at 9^0 ($\tan^{-1}(7/46)$) allows the measuring volume to go right down to the surface of the model. Inevitably, tilting the probe means that the nominally vertical velocity component is actually inclined by up to 9^0 from the vertical. This distortion can be corrected using a technique described by Norman[1992], and later used by Minson and Wood[1992]. This technique involves making two sets of measurements for each measurement location, with the probe orientated differently for each set. Using two sets of measurements has the drawback that only mean velocities can be considered, as the two sets of data are not simultaneous.

Measuring at one point from two LDA probe positions makes it necessary to reset the zero reference point in the x-y plane for the traversing robot between measurements. The large velocity gradients in the vortex mean that a small change in position can lead to a significant change in velocity and therefore the resetting between measurements must be done very carefully.

4.2 Flow interference by the LDA probe

Rediniotis et al[1991] measured velocities in a conical vortex above a model aircraft wing using two measuring instruments, a 7 hole probe and an LDA. The 7 hole probe determines flow velocity from the pressure on the probe surface and thus the measurement point coincides with the probe position. In contrast, the LDA measuring volume is remote from the probe, allowing the LDA probe to be mounted outside the working section of the wind tunnel. Surface pressures on the wing were also measured.

Rediniotis noted significant differences when compared the measurements made with the 7 hole probe and those made with the LDA:

- a reduction of 50% in the mean axial velocity near the core of the vortex at breakdown
- a dramatic increase in the RMS fluctuation of the vortex axial velocity
- a reduction of approximately 20% in the suctions induced under the vortex
- the velocity vectors in the core region being erratic in direction.

These differences were attributed solely to the presence of the 7 hole probe within the flow field.

The probe used by Rediniotis had a diameter of approximately 4% of the width of the vortex. This is small in comparison with the LDA probe used in the work for this thesis, which has a diameter of up to 50% of the width of the vortex which it is being used to measure. However, unlike the 7 hole probe, the measuring volume of the LDA probe is not coincident with the probe position, the LDA measuring volume being 46mm (3 probe diameters) away from the probe.

4.2.1 Investigation of flow disturbance from a probe on the vortex axis

When measuring the velocities in a plane normal to the vortex axis, which are of primary interest in this study, the probe must be pointed along the vortex axis. The effect of this LDA probe position was investigated and quantified as described below.

4.2.1.1 Effect on lateral and axial velocity components

The LDA probe was mounted inside the model, with the laser beams shining through the top of the model, to measure the axial and lateral velocities at two points above the 15^0 ray. Positioning the probe inside the model is problematic, as the wind tunnel traversing mechanism cannot be used, and so only two positions along the ray were considered; one at 50mm from the leading corner, at a height of 5.5mm from the model surface; and the

other 100mm downstream of the corner, also at a height of 5.5mm. Two sets of measurements were taken at each position. One set with a dummy probe 14mm in diameter and 105mm long mounted in the tunnel traversing mechanism and positioned parallel to the 15^0 ray, in the exact position required to measure the velocities at the points described above, and the other with no dummy probe in place.

The velocities measured at both locations, with and without the dummy probe in place, are shown in Tables 4-1 and 4-2.

As the data in the tables shows, the mean axial velocity is reduced by the presence of the probe. For both positions the probe produced a 7% reduction in axial velocity. Additionally there is an increase in the RMS of the axial velocity of approximately 2%.

The reduction in axial velocity and increase in axial RMS is far less severe than that by Rediniotis. Moreover, the erratic direction of velocity vectors in the vortex core which was reported by Rediniotis is not seen in the velocity vector plots presented later in this chapter.

There is no consistent effect of the probe on the mean or RMS of the lateral velocity.

Velocity Component	No probe in place		With Probe in place		AVERAGE OF RUNS	
	Run 1	Run 2	Run 1	Run 2	No Probe	With Probe
$Axial_{mean}$	1.08	1.06	0.99	1.00	1.07	0.995
$Axial_{RMS}$	0.37	0.38	0.39	0.38	0.375	0.385
$Lateral_{mean}$	-0.0008	0.008	-0.006	0.01	0.004	0.002
$Lateral_{RMS}$	0.23	0.21	0.23	0.22	0.22	0.23

Table 4-1 Velocities measured at 50mm back from leading corner of model (velocities shown as ratio of V_{ref})

Velocity Component	No probe in place		With Probe in place		AVERAGE OF RUNS	
	Run 1	Run 2	Run 1	Run 2	No Probe	With Probe
$Axial_{mean}$	0.94	0.93	0.87	0.88	0.935	0.875
$Axial_{RMS}$	0.42	0.41	0.43	0.41	0.415	0.42
$Lateral_{mean}$	-0.13	-0.13	-0.12	-0.12	-0.13	-0.12
$Lateral_{RMS}$	0.26	0.27	0.27	0.26	0.265	0.265

Table 4-2 Velocities measured at 100mm back from leading corner of model (velocities shown as ratio of V_{ref})

4.2.1.2 Effect of the LDA probe on surface pressure

Pressure measurements were made at tappings under the vortex, with and without the dummy LDA probe in position.

Table 4-3 show that with the probe in place the mean suctions on the roof reduced are by approximately 10%. As in the velocity measurements, the probe's effect on the surface pressures was less severe than that noted by Rediniotis.

Pressure tapping	Pressure coefficient	
	No Probe	Dummy Probe
1	-3.61	-3.18
2	-3.1	-2.70
3	-1.95	-1.77
4	-1.48	-1.37

Table 4-3 Pressure coefficients with and without LDA probe in place

When measuring velocities in a plane normal to the vortex axis there is no alternative but to point the LDA probe along the axis of the vortex, which does effect the vortex. However, as was discussed in section 3.4.3, it is not absolute values of pressure and velocity that are of primary interest in this study, but values relative to one another. Therefore, since the effect of the probe on the flow is consistent for all measurements it can be neglected.

4.3 Mean velocity results

4.3.1 Velocities in cross-axis planes

Measurements of mean velocity (averaged over 90 seconds) were made with the LDA at a large number of locations on planes perpendicular to a 15^0 ray at 50, 100 and 150mm back from the leading corner (0.25, 0.5 and 0.75h respectively). v and w velocities were measured to construct two dimensional velocity vectors.

Figs 4-4, 4-5 and 4-6 show plots of these results. On these plots the horizontal axis gives the distance relative to the 15^0 ray and the vertical axis the height above the building. The root of the velocity vector arrow denotes the measurement location.

The positions of the vortex core and the flow reattachment point were estimated and are shown on the vector plots as '**CORE**' and '**R**' respectively.

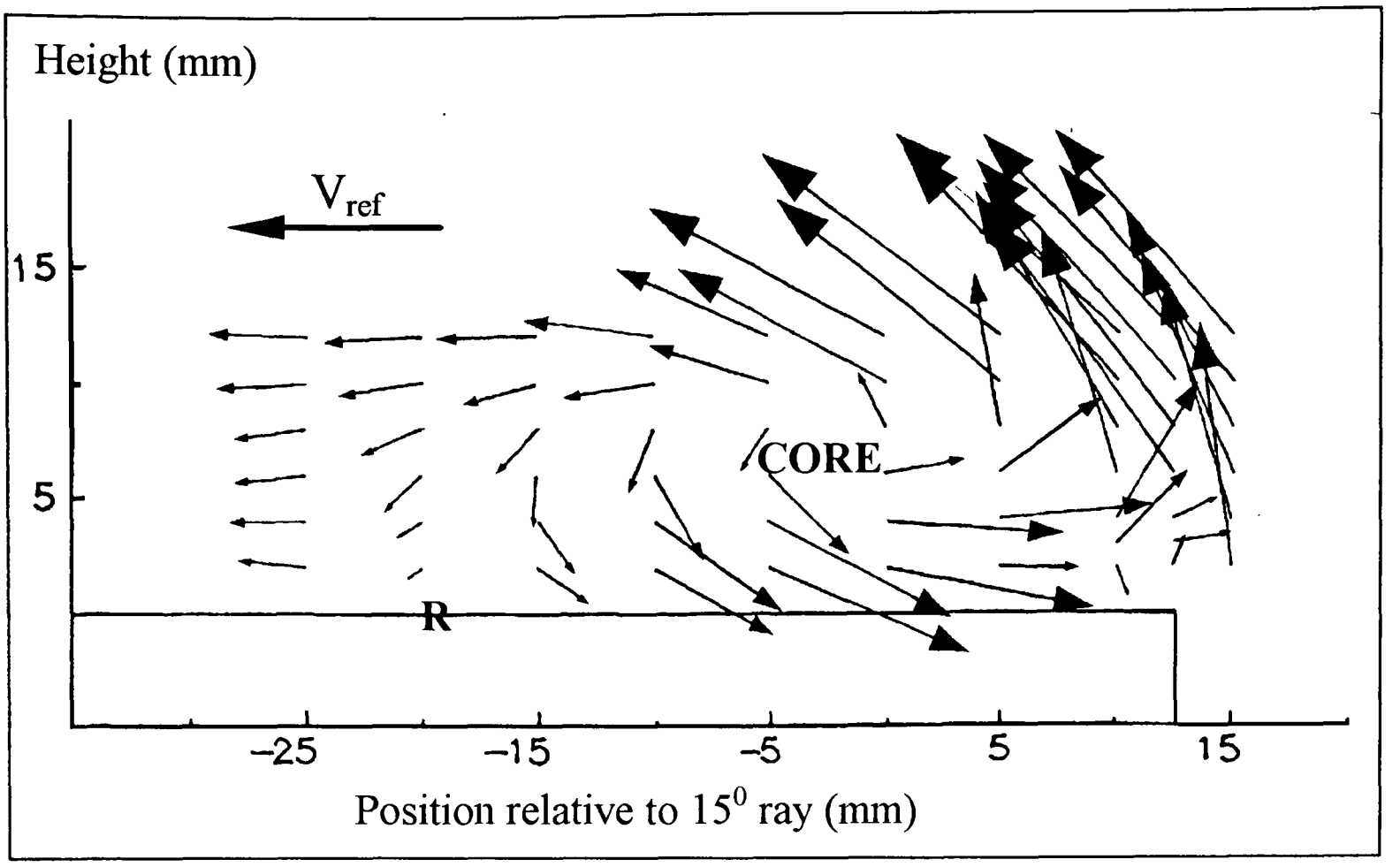

Figure 4-4 Vortex 50mm downstream from leading corner.

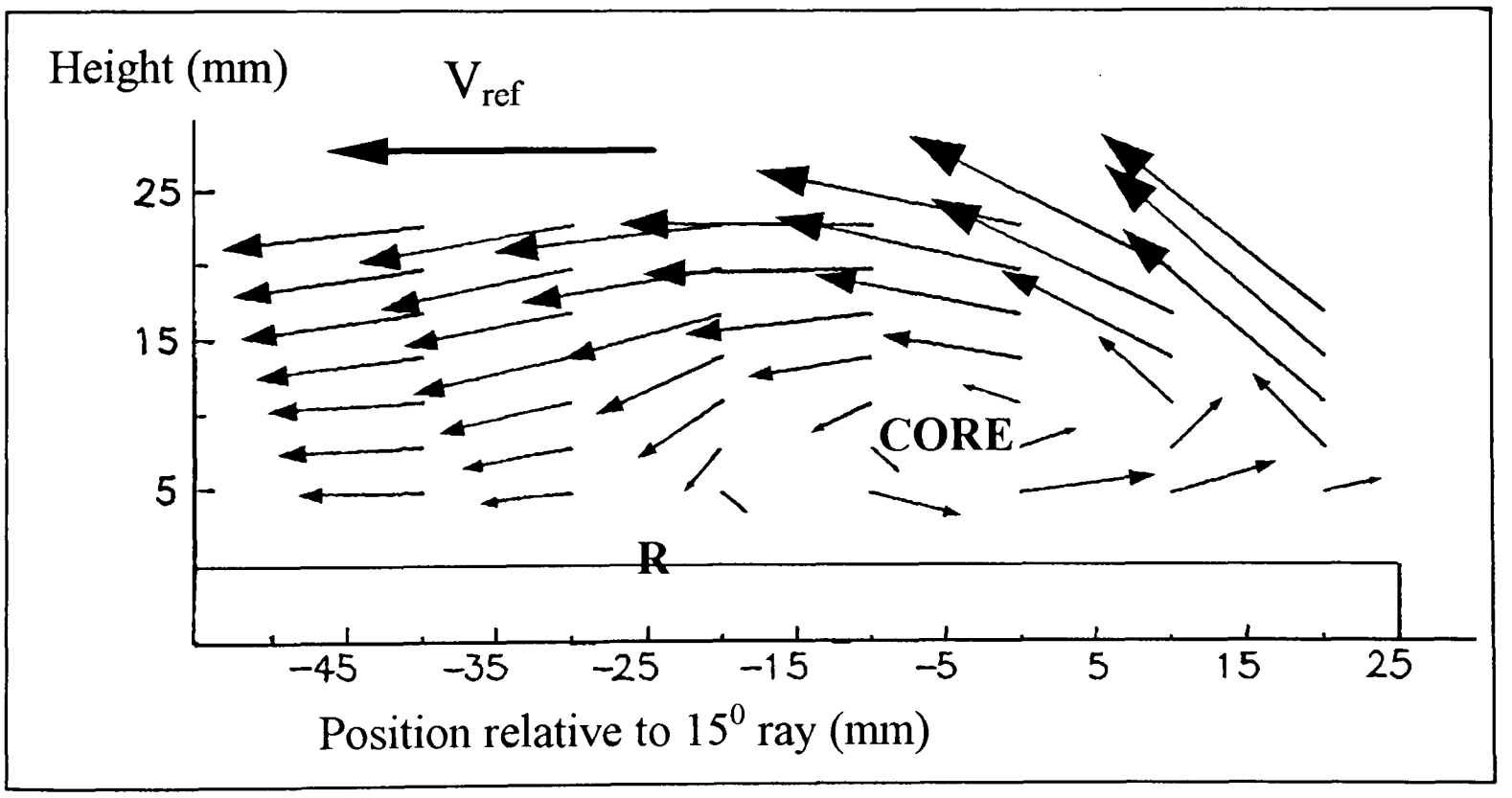

Figure 4-5 Vortex 100mm downstream from leading corner.

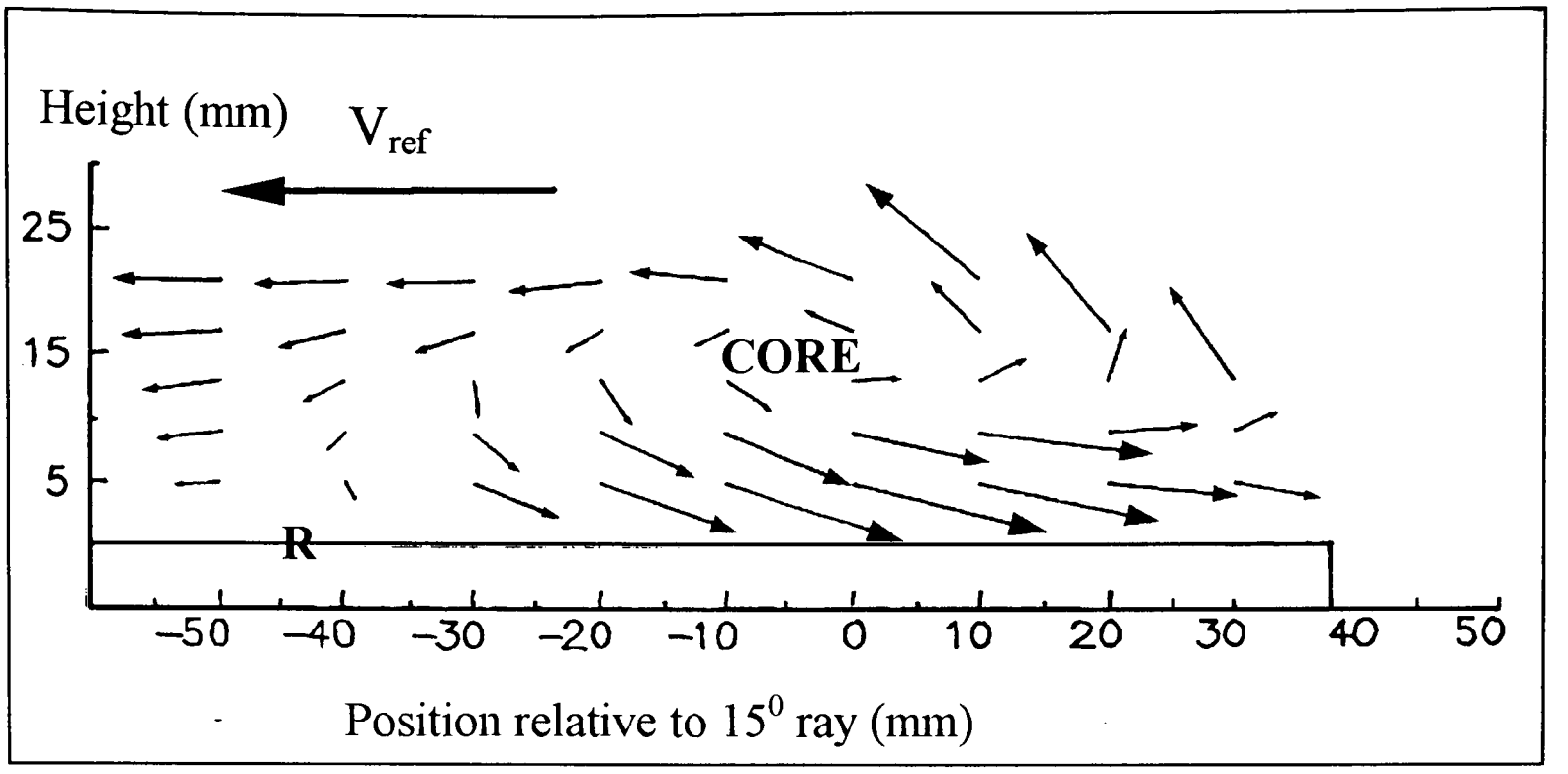

Figure 4-6 Vortex 150mm downstream from leading corner.

The mean reattachment locus is estimated to lie on a line at 30^0 to the edge of the model.

The angular position of the vortex relative to the roof edge was calculated to be 16^0 from the estimated core positions. This compares well with other published velocity data which showed angles of 15^0 (Kawai et al[1995]) and 15.5^0 (Minson and Wood[1992]).

The vortex positions estimated from the LDA results are compared to surface flow visualisation results in section 4.3.2.

The measurements taken on the planes perpendicular to the 15^0 ray were assumed to be sections perpendicular to the vortex. This assumption is not entirely valid as the results have shown that the vortex actually lies above a ray at 16^0 to the model edge. However, the error resulting from assuming the core lies on a ray at 15^0 rather than one at 16^0 is negligible (less than 1%.)

The height of the vortex core, δ, is estimated to diverge away from the model surface at 5.1^0. This again compares well with Kawai et al[1995] and Minson and Wood[1992], as

shown in Fig 4-7.

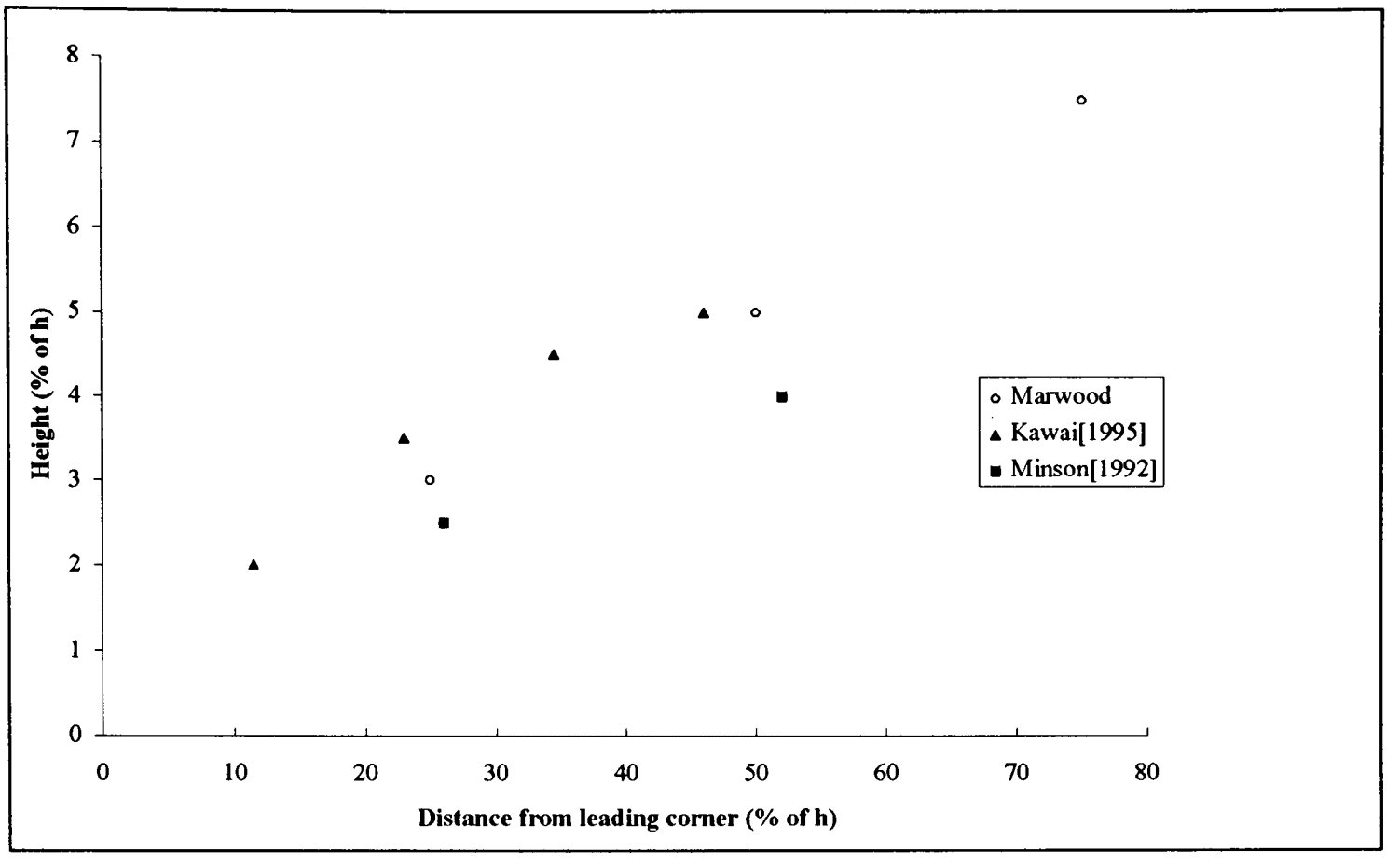

Figure 4-7 Vortex core height

Figs 4-4, 4-5 and 4-6 show that the magnitude of the velocities in the vortex reduce with respect to the reference velocity with increasing distance downstream of the leading corner. This weakening of the vortex is reflected in the surface pressures, which reduce with increasing distance from the leading apex (see Table 4-3.)

Fig 4-4 shows evidence of a small counter rotating vortex close to the roof edge. The existence of this vortex was first suggested by Kramer and Gerhardt[1991] from surface flow visualisation experiments. A similar counter rotating vortex has been measured above delta wings in aeronautical studies. Visser and Nelson[1993] measured velocities in a wing edge vortex and showed a small region of vorticity, with the opposite sign to the main vortex, near the leading edge of the wing.

4.3.2 Surface flow visualisation

In order to support the vortex position results of section 4.3.1 a surface flow visualisation experiment was performed.

A 5:1 mixture of kerosene and titanium dioxide, TiO_2, (a fine white powder) was used. The TiO_2 does not dissolve in the kerosene so a suspension is formed. When applied to the surface of the model this liquid flows under the influence of the surface shear. Gradually the kerosene evaporates leaving streaks of the white TiO_2 powder, effectively 'freezing' the surface shear pattern. The surface of the model is painted black so that these white streaks show up in sharp contrast. Since the process occurs over time it records only mean surface shear patterns.

Oil flow visualisation experiments were carried out on the on the roof of the cube model, with the cube placed at 45^0 to the onset flow. A picture of the resulting streak patterns can be seen in Fig 4-8. In this photograph the surface shear pattern produced by the conical vortices is clearly visible. Fig 4-9 shows the same picture with the vortex core and reattachment locus estimated from the LDA measurements drawn in.

Although the surface flow visualisations clearly show the shear pattern produced by the vortex, it is difficult to conclude whether the mean vortex position determined from the surface shear visualisations and that from the LDA velocity results agree well with each other.

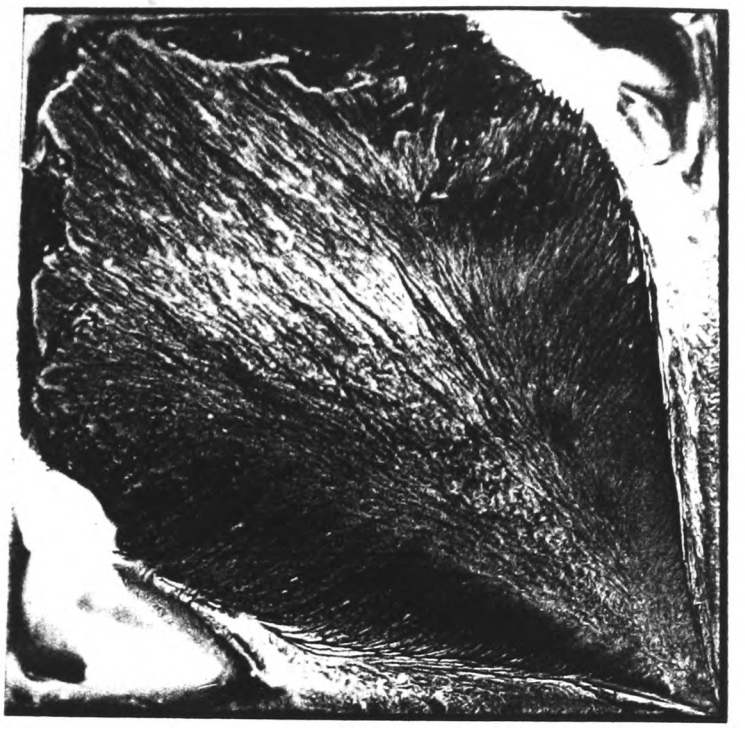

Figure 4-8 Surface flow visualisation

Figure 4-9 Surface flow visualisation with estimated vortex axis and reattachment lines

4.3.3 Axial velocities

Figs 4-10, 4-11 and 4-12 show contour plots of the dimensionless axial velocity at three sections along the vortex. The plots are made up from measurements made at the same locations as the velocity vector plots (Figs 4-4, 4-5, and 4-6).

In the axial velocity contour plots it can be seen that the axial velocity increases away from the edge of the model. Additionally, the velocities near the core of the vortex decrease with distance downstream of the leading corner.

The results presented in this thesis are the first axial velocity measurements carried out in a vortex produced by turbulent wind. All previous measurements (Payne et al[1988], Payne et al[1989], Rediniotis et al[1991] and Visser and Nelson[1993]) were made in low turbulence flows. The measurements made in this study differ dramatically from previously published measurements of axial velocities in conical vortices. In the roof edge vortices the mean axial velocity components are similar to the free stream speed, whereas the mean axial velocities in wing vortex cores reach maximum values of up to three times the free stream velocity. None of the wing vortex studies have explained the flow mechanism which produces such high mean axial velocities.

As well as the fundamental difference in onset flow between roof and wing studies it is also noteworthy that the aeronautical studies were carried out with delta wings at various non-zero angles of attack. Fig 4-13 compares published data and shows that axial velocities increase with angle of attack.

Additionally the sweep angles of the models in the aeronautical studies were less than 90^0. The results in Fig 4-13 also suggest that axial velocity reduces with increasing sweep angle.

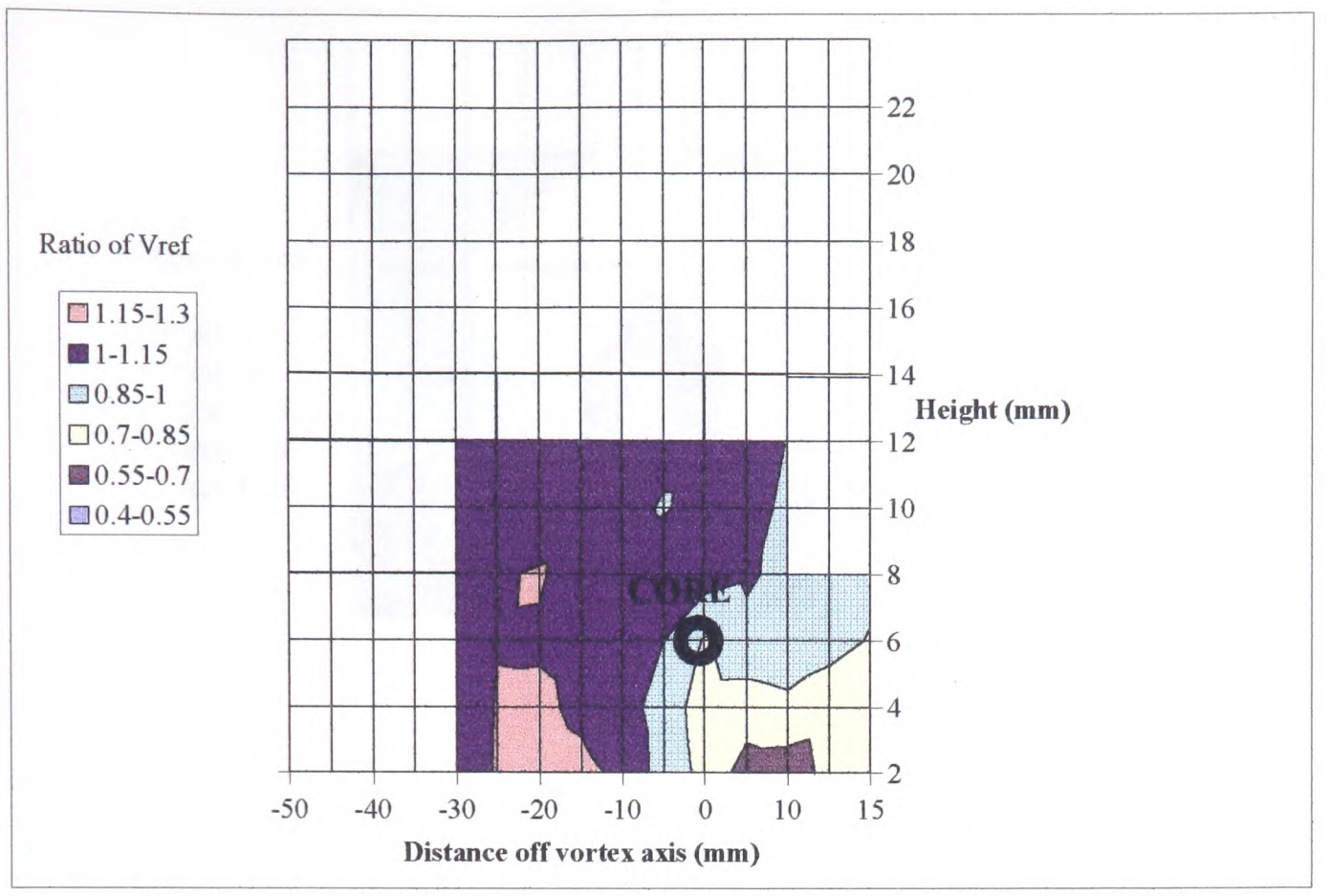

Figure 4-10 Axial velocity contours in a transverse plane 50mm downstream from leading corner of the model.

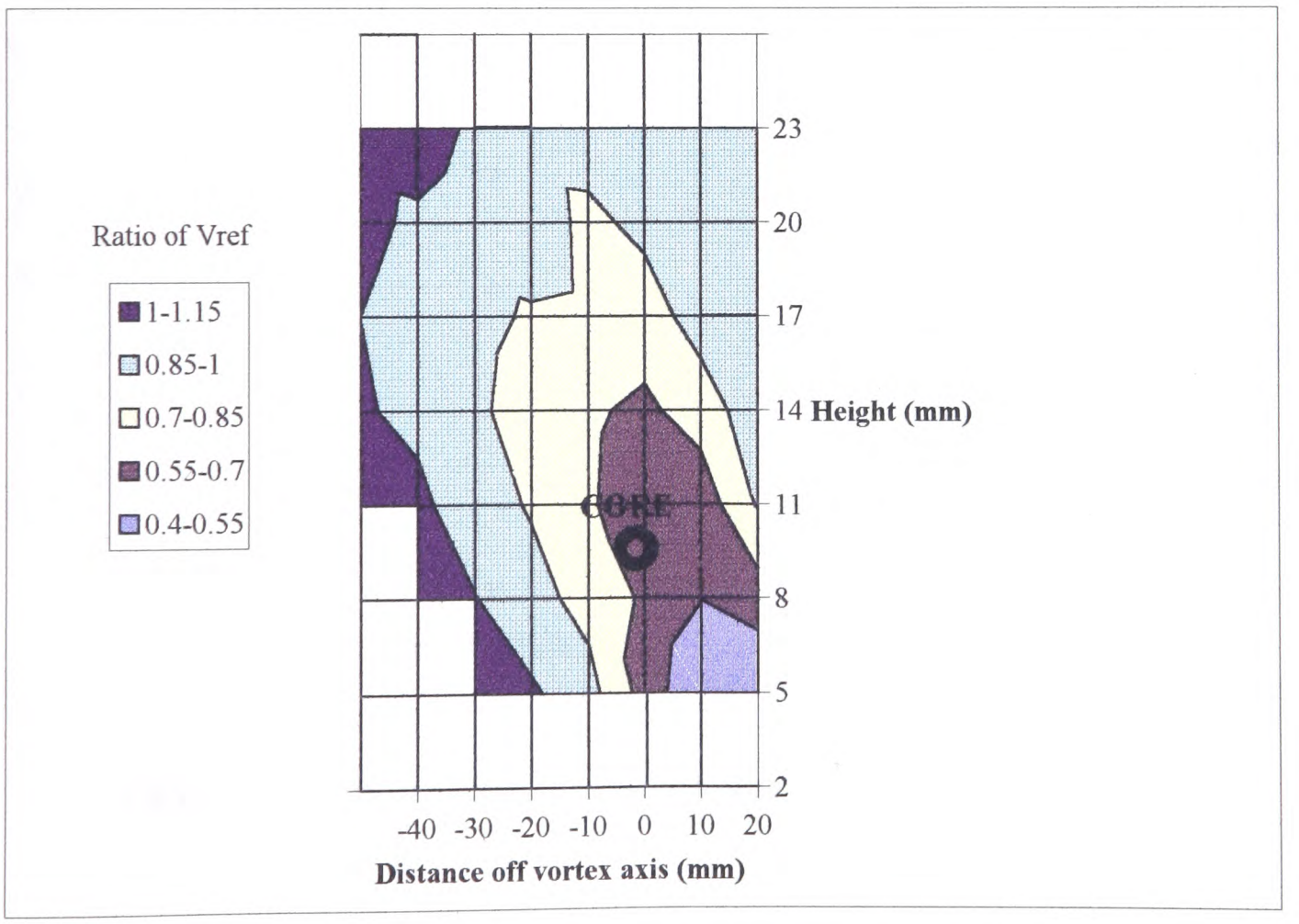

Figure 4-11 Axial velocity contours in a transverse plane 100mm downstream from leading corner of the model

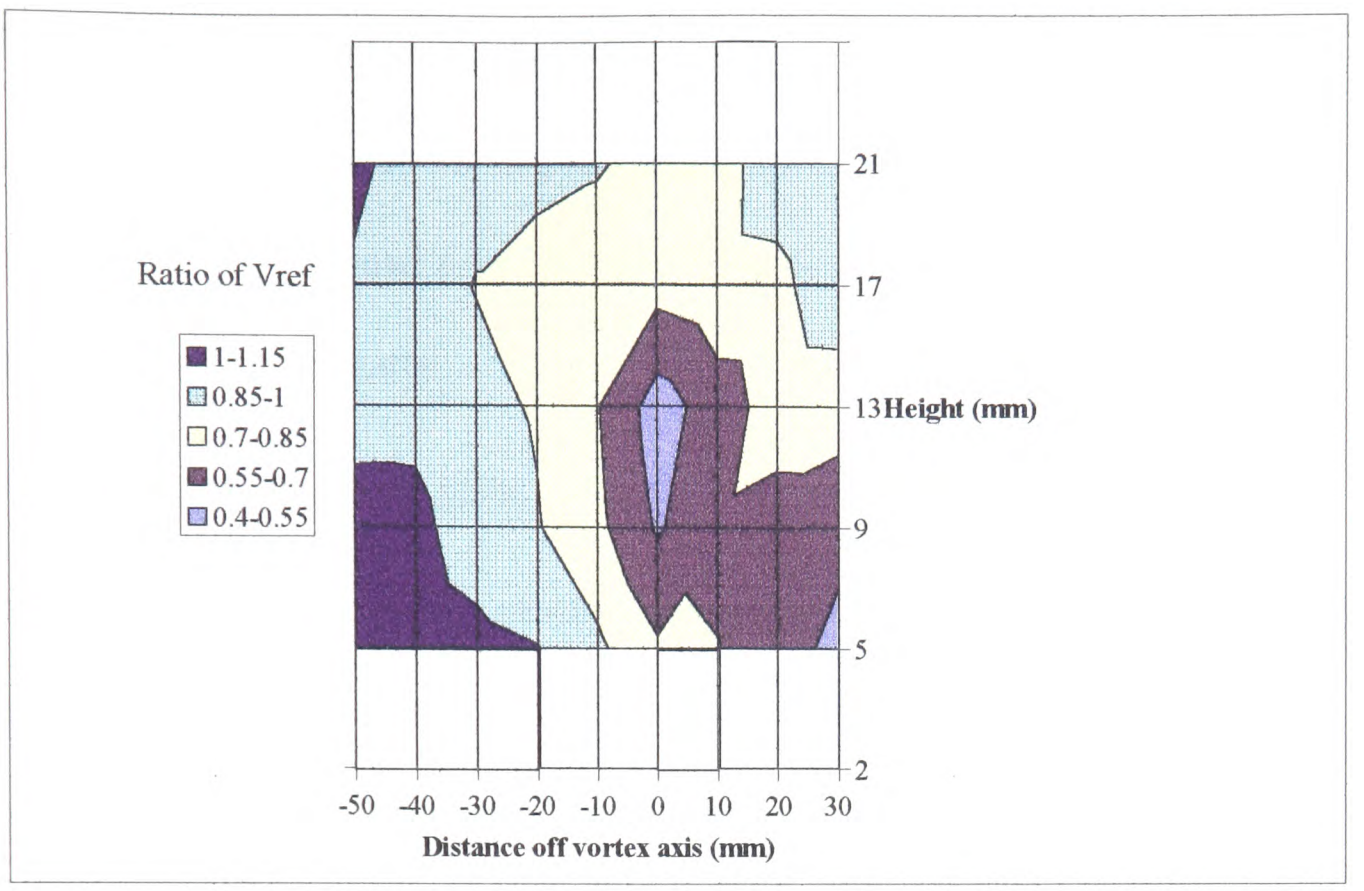

Figure 4-12 Axial velocity contours in a transverse plane 150mm downstream from leading corner of the model

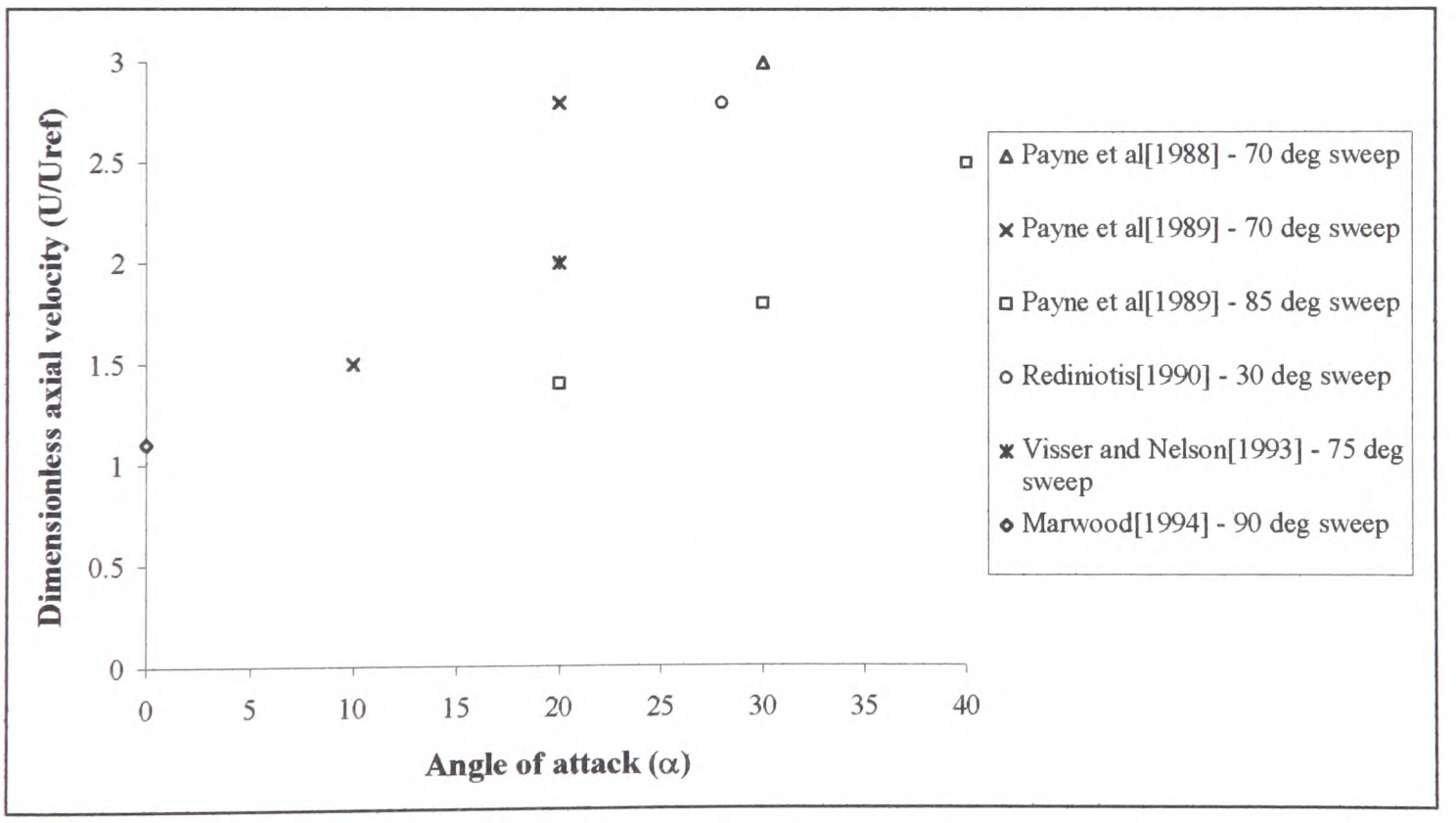

Figure 4-13 Effect of angle of attack and sweep on axial velocity

4.4 Effect of varying onset wind azimuth

The results presented so far in this chapter have been for those cases in which the cube is placed at 45^0 to the onset flow ($\beta = 45^0$ in Fig 4-14). In this section the effect of varying this onset angle is investigated.

4.4.1 Velocity in the vw plane

Figs 4-15 to 4-18 show velocity vector plots of the vortex in a transverse plane, perpendicular to a ray at 16 degrees to the eaves, 100mm downstream from the leading corner, with differing onset wind directions.

The measurement plane and angle convention is shown in Fig 4-14.

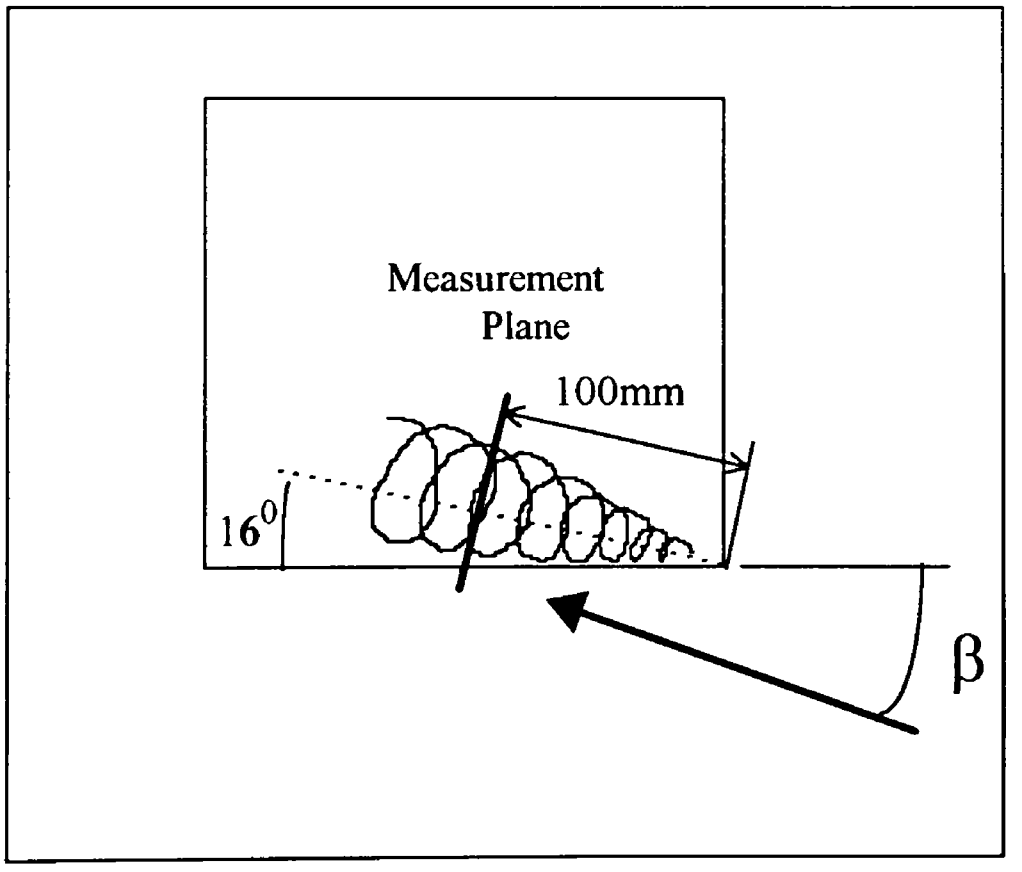

Figure 4-14 Measurement plane and onset wind angle convention

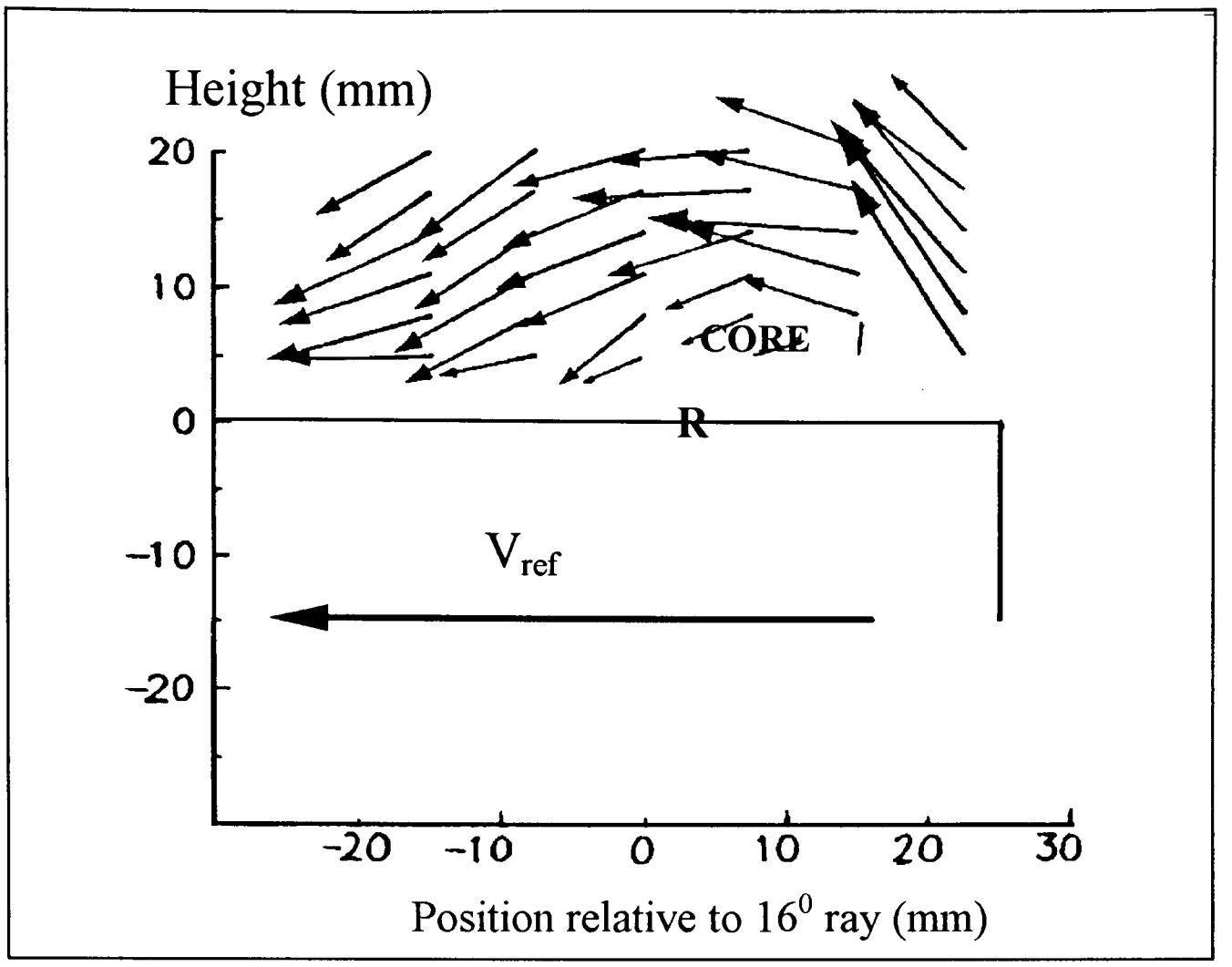

Figure 4-15 Velocity vector plot with β=15^0 100mm downstream of leading corner

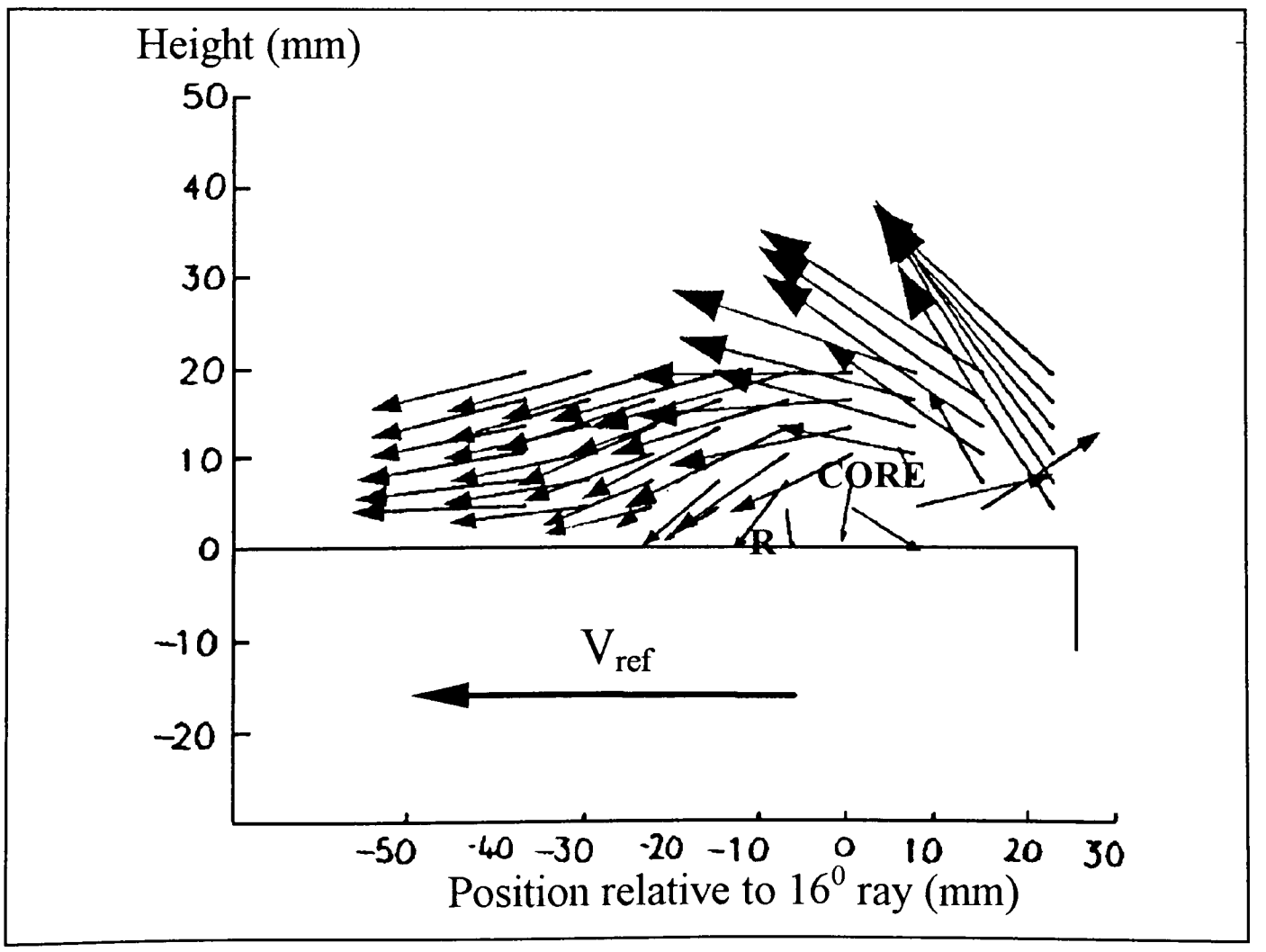

Figure 4-16 Velocity vector plot with β=30^0 100mm back from leading corner

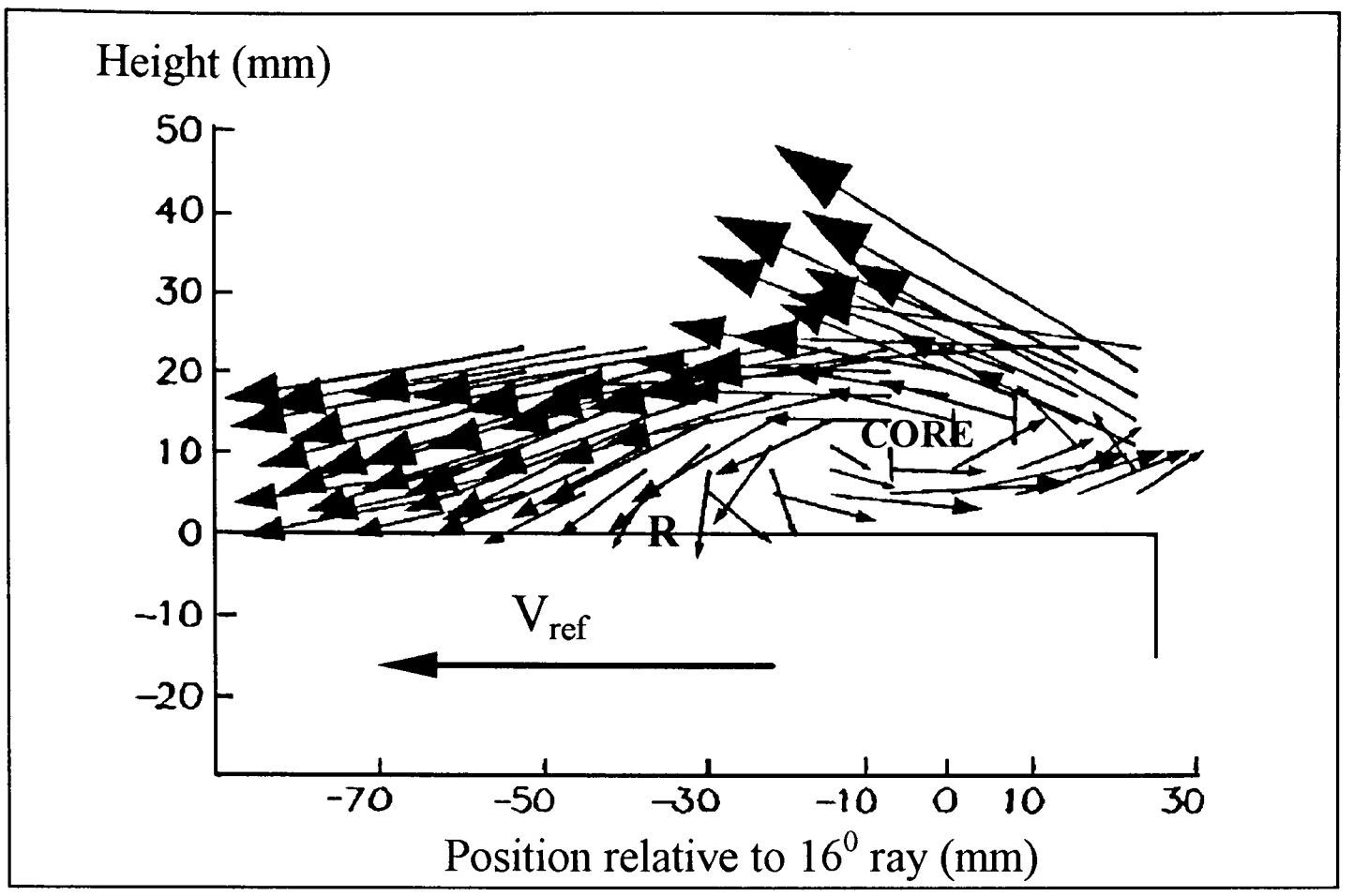

Figure 4-17 Velocity vector plot with $\beta=60^0$ 100mm back from leading corner

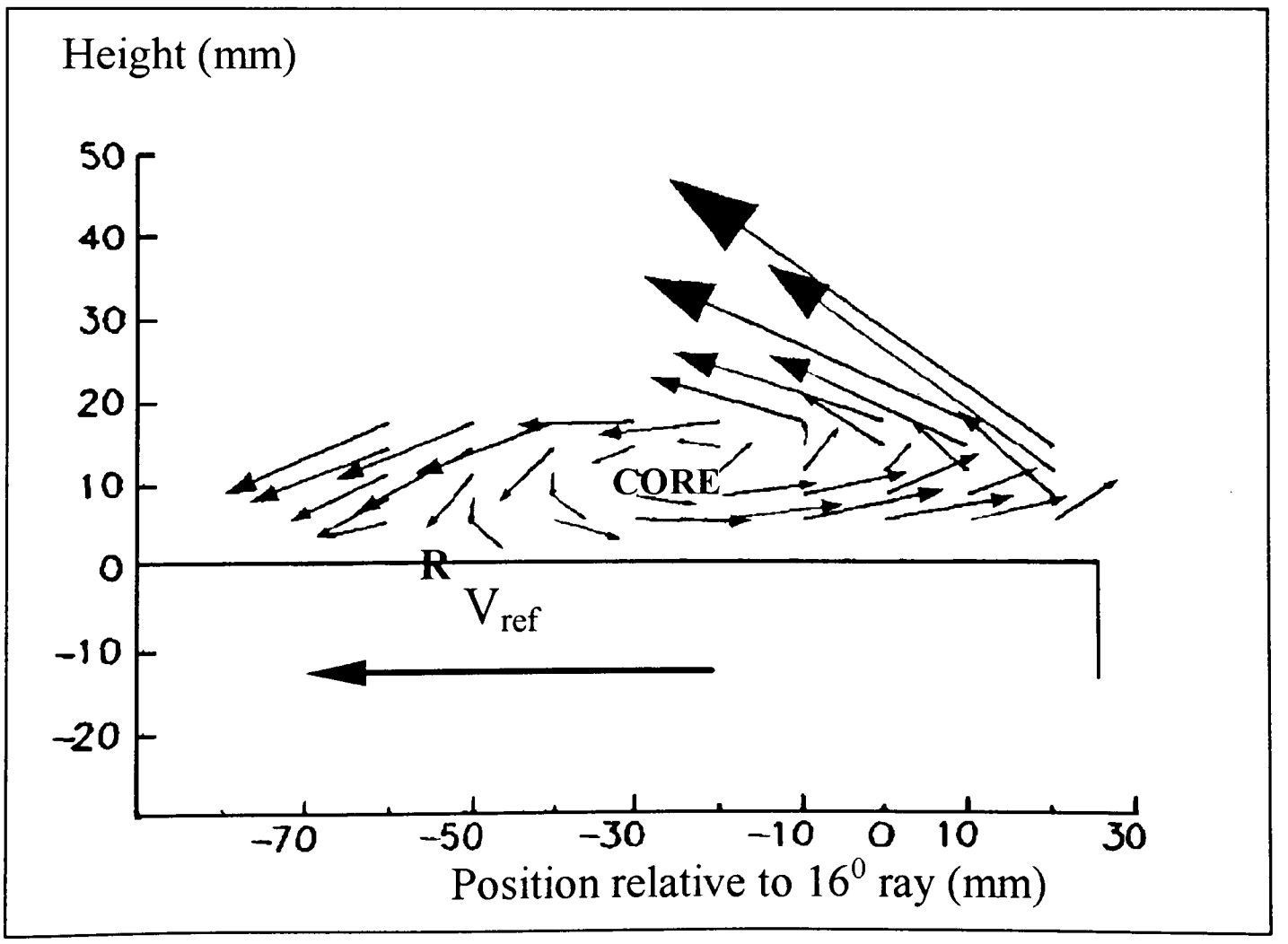

Figure 4-18 Velocity vector plot with $\beta=75^0$ 100mm back from leading corner

4.4.2 Variation in vortex position with azimuth angle

The vector plots in Figs 4-15 to 4-18 show an interesting trend. The vortex becomes larger, and so influences a larger section of the roof, as β increases. This trend is consistent in all the plots. The height of the vortex axis (δ), the angular position of the core relative to the building edge (γ) and the distance from the edge of the model to reattachment all increase with β. This information is summarised in Figs 4-19 and 4-20.

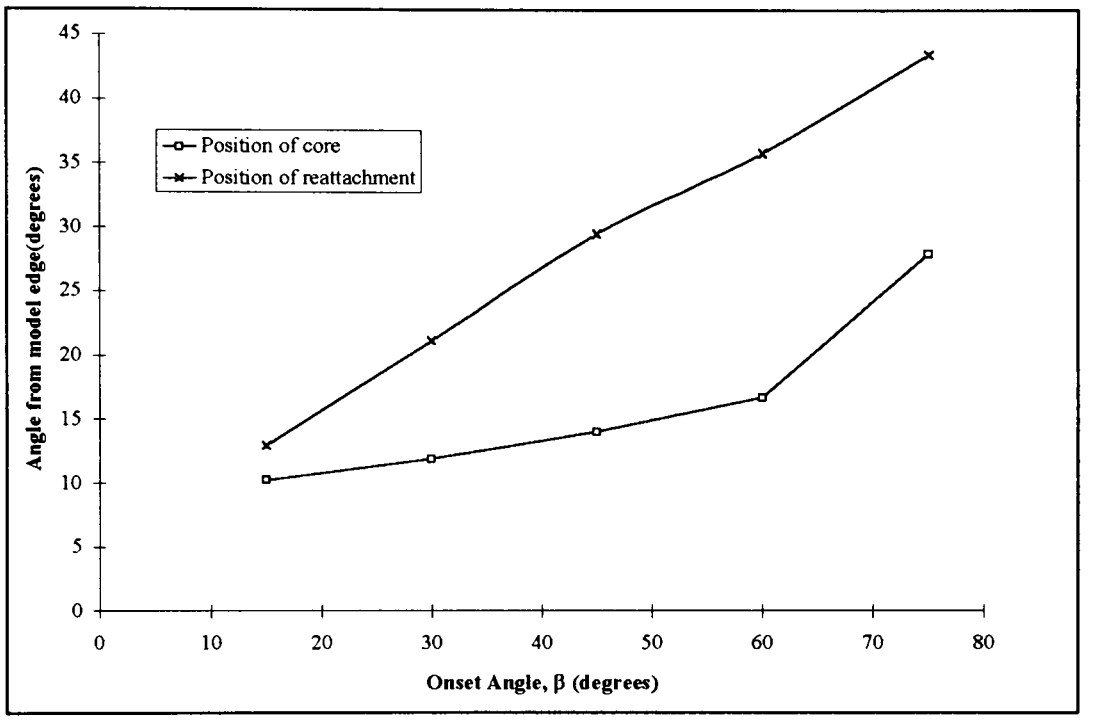

Figure 4-19 Effect of onset flow on vortex angular position

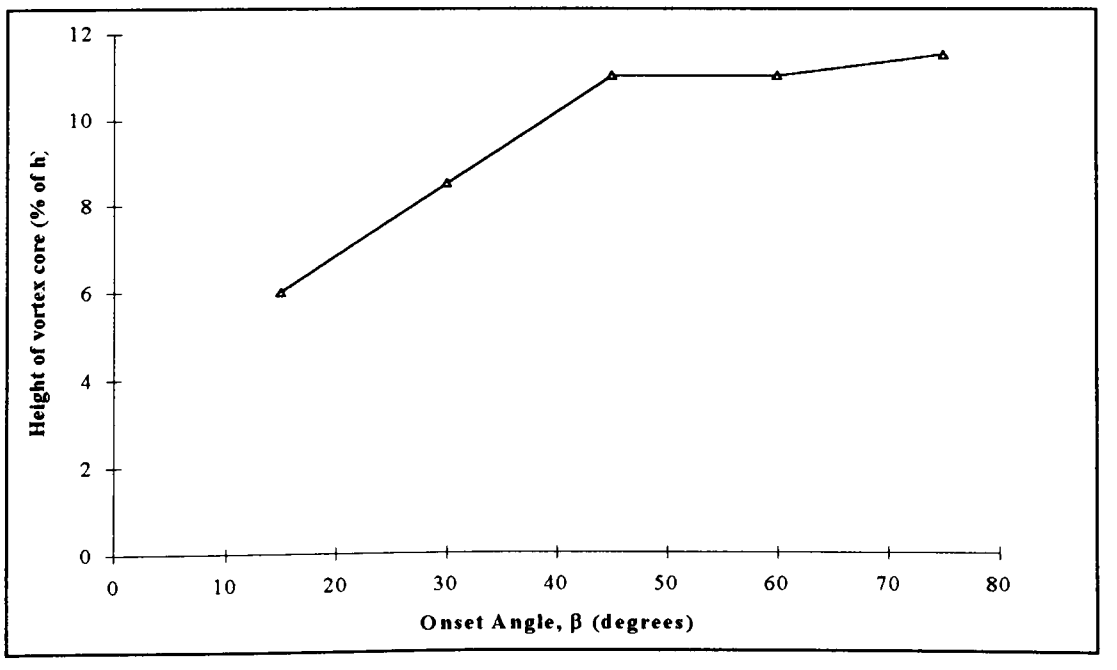

Figure 4-20 Variation of vortex core height with onset angle, β

As the relationship between β, δ and γ is significant, the rate of change of vortex position with changes in onset wind angle is considered below.

$$\frac{d\bar{\gamma}}{d\beta} = 0.17 \qquad (4.8)$$

$$\frac{d\bar{\delta}}{d\beta} = 0.045\ \%h / {}^{\circ} \text{ (at 0.5h from leading corner)} \qquad (4.9)$$

Two other studies have analysed the β–γ relationship. Tieleman et al[1992]) calculated $\frac{d\bar{\gamma}}{d\beta}$ = 0.17 and Williams[1995] $\frac{d\bar{\gamma}}{d\beta} = 0.33$.

This section has only considered the effect of changing mean onset angle (averaged over 60s of sampling which is equivalent to approximately 26 minutes full scale.) However, in turbulent flow, the instantaneous wind angle varies second by second. It is likely that the variations in the instantaneous value of β will produce a similar short time scale variation in the instantaneous vortex position. This idea is assessed at length in chapter 8.

4.4.3 Variation in vorticity field with azimuth angle

A subjective estimation of circulation from the velocity vector plots shown in Figs 4-15 to 4-18 suggests that the vortex becomes stronger as the onset flow approaches being perpendicular to the edge of the building. The circulation appears to be largest when $\beta=60^{0}$.

In order to assess this subjective assessment, the vorticity (ζ) field in the vortex has also been calculated. This was done by applying equation (4.10) to the velocity data used to produce Figs 4-15 to 4-18.

The vorticity of a flow is defined as the circulation in a flow per unit area. For a vw plane it

The vorticity of a flow is defined as the circulation in a flow per unit area. For a vw plane it is defined as:

$$\zeta = \frac{\partial w}{\partial y} - \frac{\partial v}{\partial z} \tag{4.10}$$

Vorticity contour plots for varying values of β are shown in Figs 4-21 to 4-25. The approximate core positions are shown for reference. The plots were based on measured velocity data for between 36 and 80 locations. Due to the relatively small number of data points, the plots do not show any fine detail of the vorticity field (although Fig 4-24 appears to show a concentration of vorticity in the shear layer). However, these plots do show that vorticity over the whole flow field increases as β increases, which supports the subjective assessments described earlier.

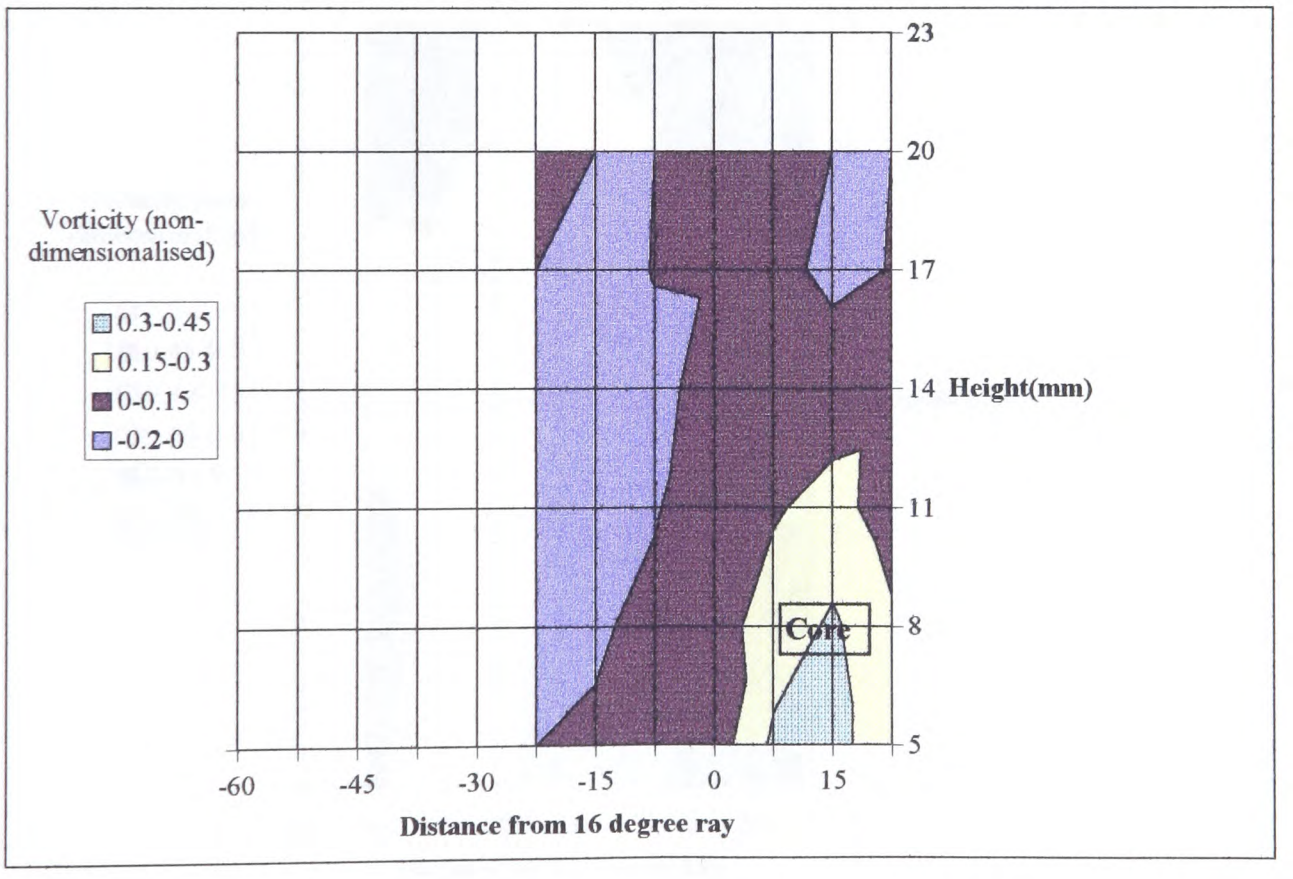

Figure 4-21 Vorticity field at $\beta = 15^0$

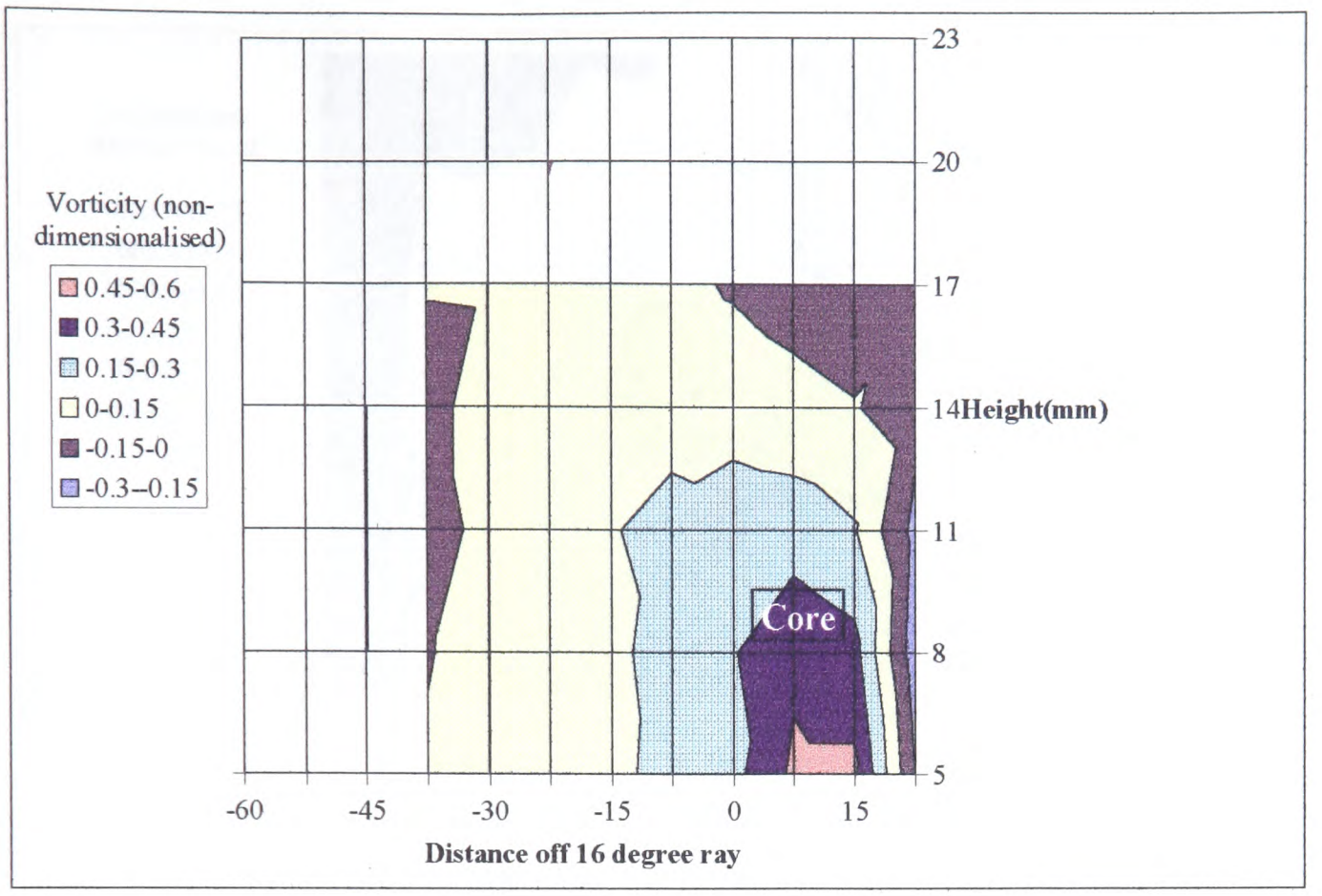

Figure 4-22 Vorticity field at $\beta = 30^0$

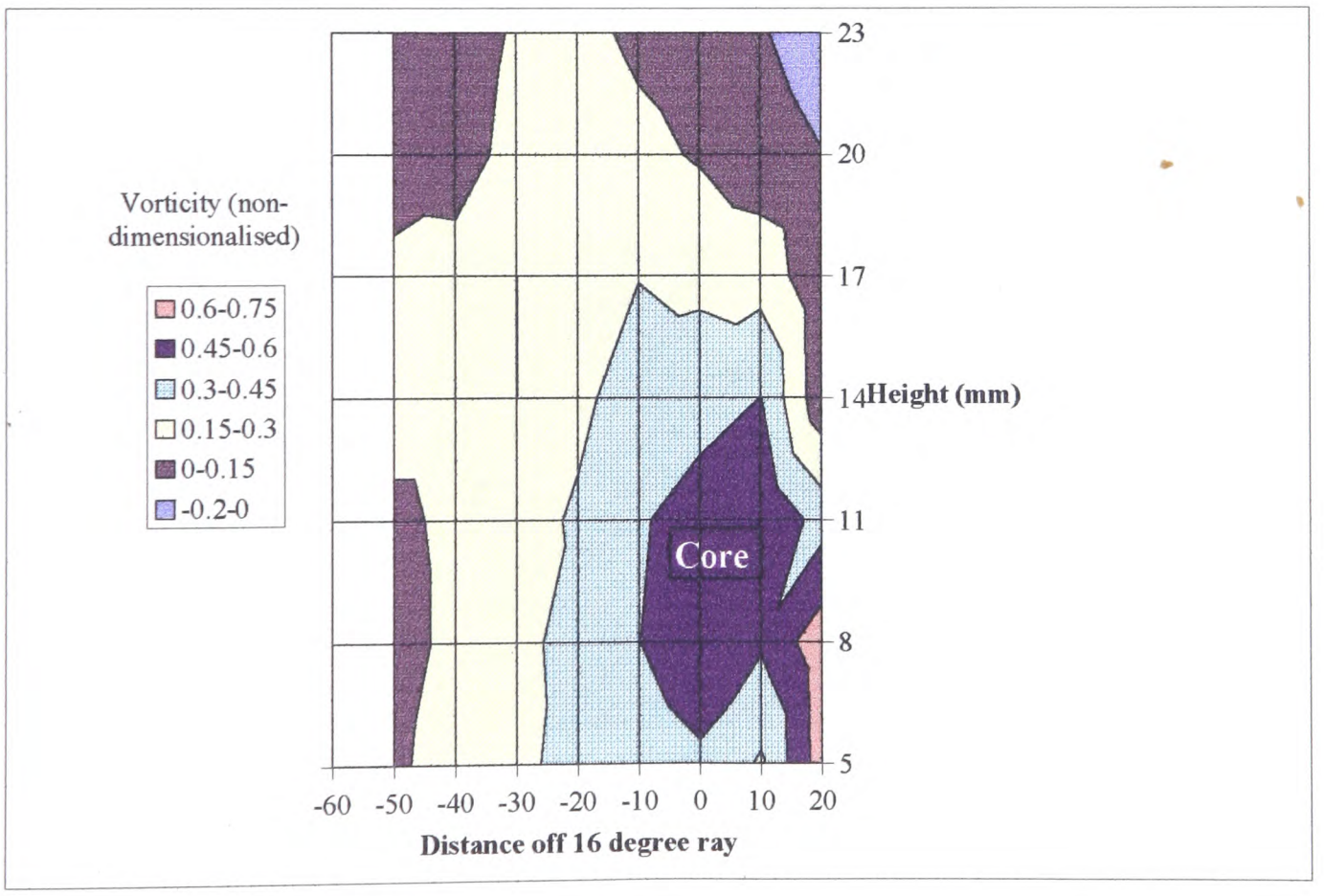

Figure 4-23 Vorticity field at $\beta = 45^0$

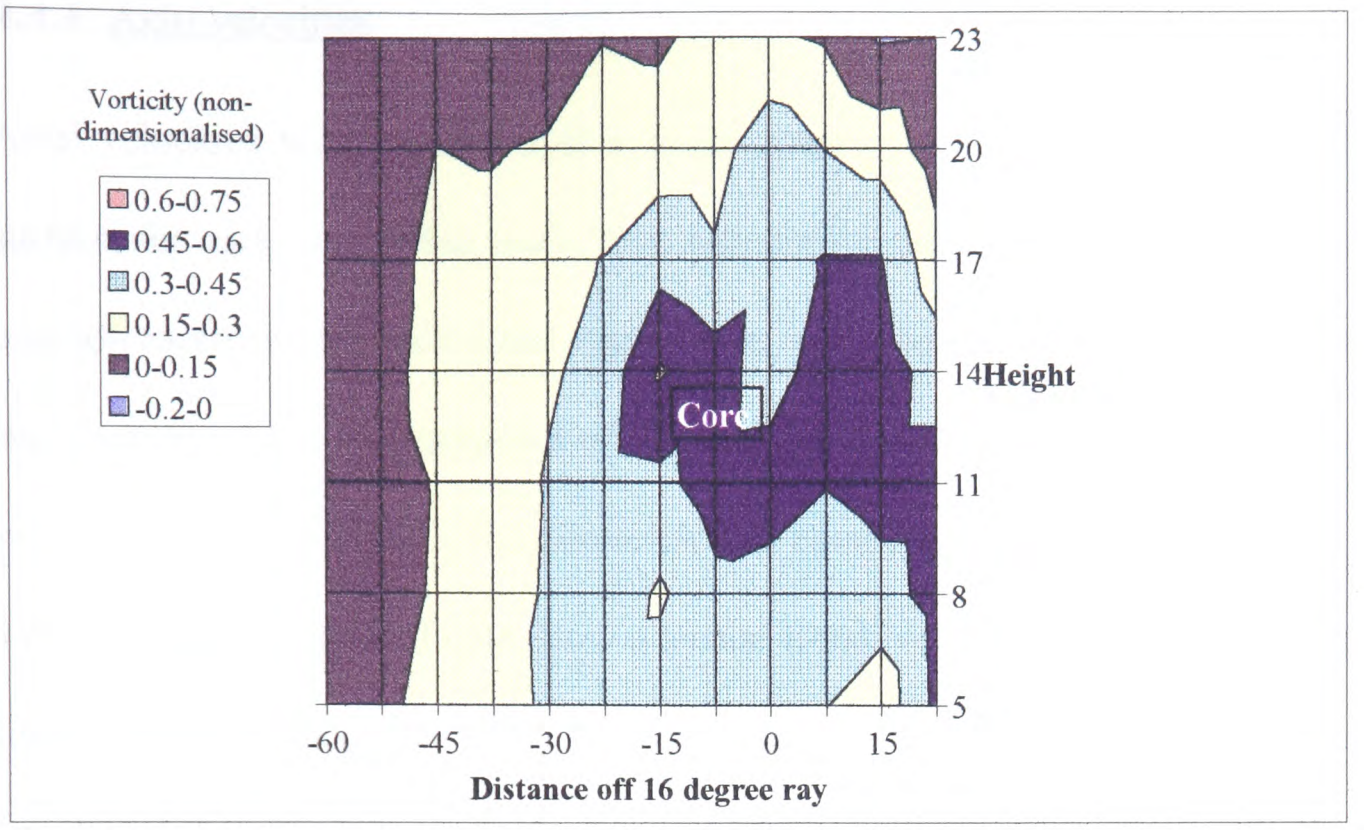

Figure 4-24 Vorticity field at $\beta = 60^0$

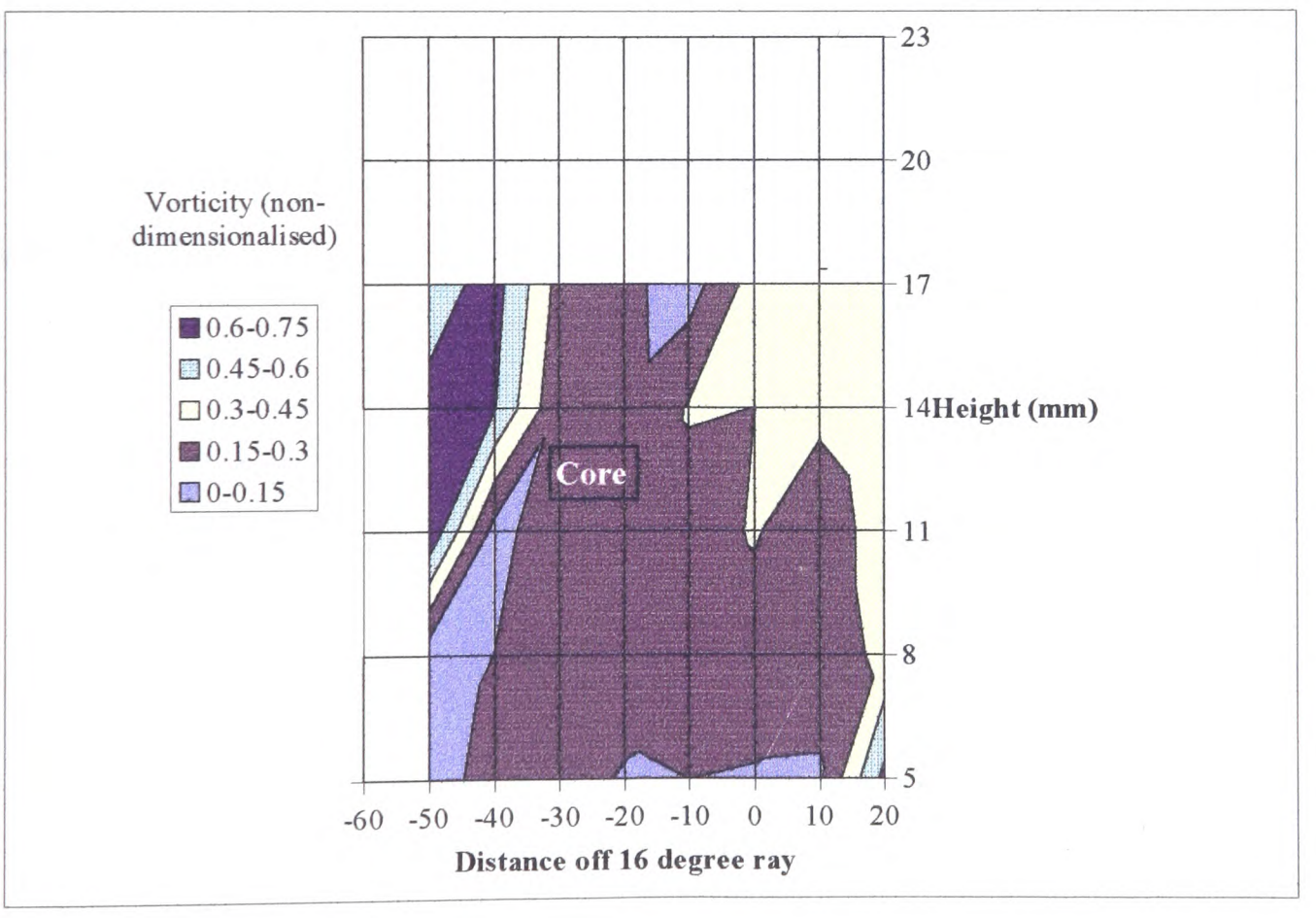

Figure 4-25 Vorticity field at $\beta = 75^0$

4.4.4 Axial velocities

Axial velocities were measured at a single point in the vortex, 11mm above the model surface, for each onset wind angle. This was done both on the 16^0 ray and also at the axis position measured for each onset angle earlier in the section (see Fig 4-19.) The results are shown in Fig 4-26. For purposes of comparison, the figure also includes the velocity that would be expected at that point due solely to a component of the onset velocity.

The two sets of measured data show a similar trend, with measured velocities being greater than the component of free stream velocity acting through the measurement point at oblique onset angles, and smaller than the free stream component as the onset angle becomes more normal to the roof edge nearest the vortex. The transition from the vortex relatively increasing axial velocities, to reducing them, occurs at an onset angle of 55^0 for the 16^0 ray measurements and 52^0 for the vortex axis measurements. This transition could be significant as it shown in the present measurements and elsewhere that largest suctions occur on a roof when $\beta=60^0$ (see 2.1 and 4.5).

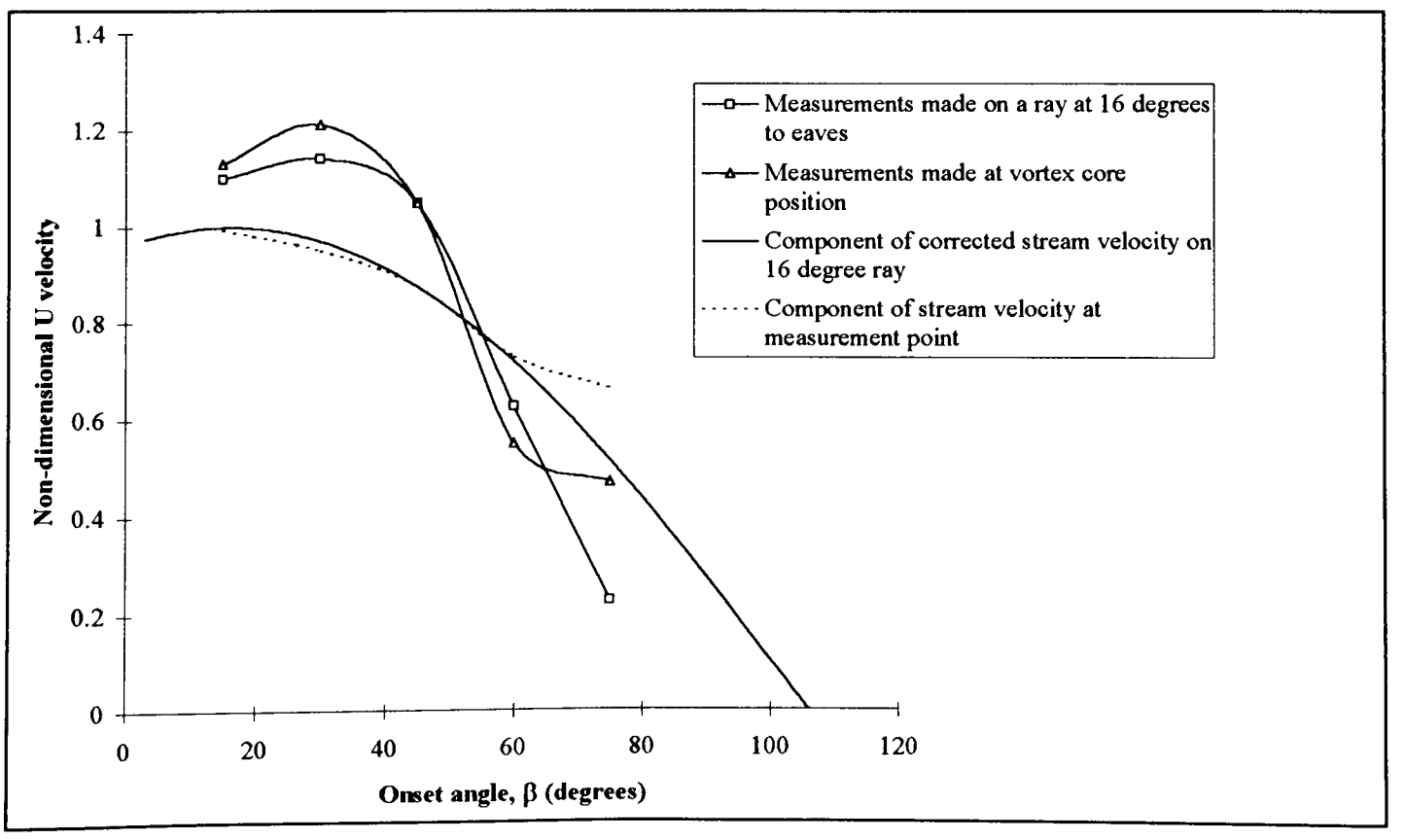

Figure 4-26 Variation in axial velocity with onset wind azimuth

4.5 Mean Pressure Measurement

Many studies have been made of the roof pressure field produced by conical vortices, and their results have been widely published (see 2.1). For this reason, extensive pressure measurements have not been included in this study. The measurements made in this study have simply been made to analyse the effect of onset wind direction on surface pressure.

Pressures were measured at two tappings, both of which were on the ray at 16^0 to the building edge, one 15mm downstream from the leading corner, the other 100mm downstream.

The magnitudes of the suctions with respect to onset angle are shown in Fig 4-27.

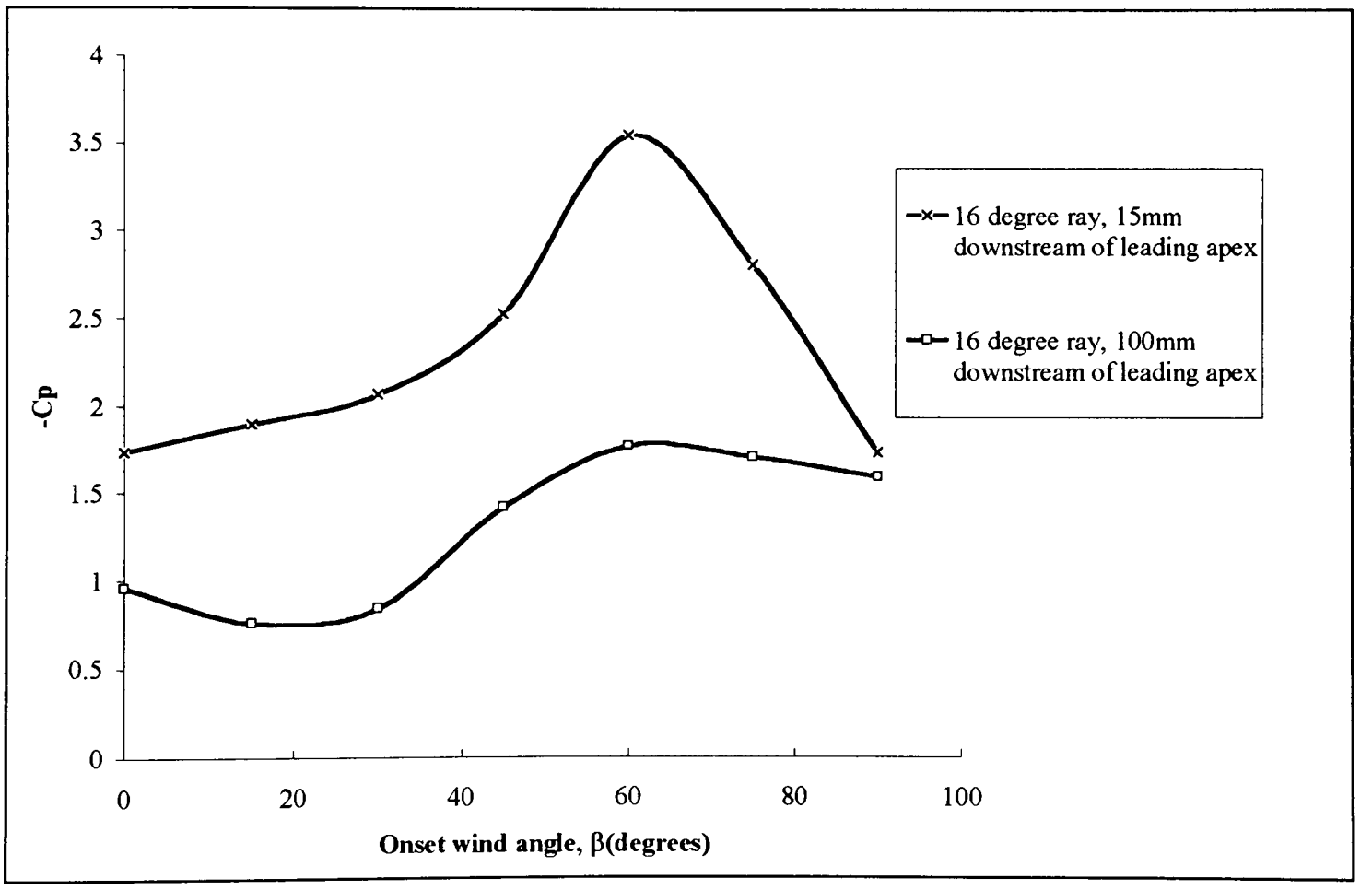

Figure 4-27 Variation in surface suction with β

At both tappings the largest mean suctions occur at $\beta = 60^0$. This is in agreement with published data (see section 2.1).

The pressures at the two tappings are governed by the structure of the conical vortex. Thus, the change in the size, circulation and position of the vortex with β (described in section 4-4), are likely to account for the variation in pressure with differing onset azimuth angles.

It is likely that instantaneous variations in β will cause a variation in the instantaneous position of the conical vortex. If this is the case, then instantaneous pressure may be similarly affected by instantaneous gust angle. This idea is explained in chapter 8.

5. Simultaneous pressure and velocity measurements

5.1 Introduction

It is well established that roof edge vortices are responsible for the high suctions that occur near the edges of roofs, but the mechanism linking vortex structure and surface pressure is little understood.

The primary achievement of this research is the development of a technique to measure simultaneously the velocity field in a conical vortex and the surface pressure at a point beneath the vortex.

There are four major difficulties in producing such simultaneous results.

1. The LDA and pressure measurement systems are physically separate and require a formal procedure to establish a common time datum.

2. The phase lag in the pressure measurement system must be accounted for.

3. The LDA does not sample at a uniform rate.

4. The LDA can measure velocity at only one location at a time.

Sections 5.2.1, 5.2.2 and 5.2.3 discuss the first three problems and section 5.3 the fourth. Having described the measurement system and data analysis, sections 5.4 and 5.5 then present data measured using this technique.

5.2 Combining LDA and pressure time series

5.2.1 Common Time Marker

The simultaneous measurement system is basically a combination of two separate measurement systems, an LDA for measuring velocities, and a Setra pressure transducer to measure surface pressure. Each of these systems has its own data logging PC and software. A diagram of the simultaneous measurement system in shown in Fig 5-1.

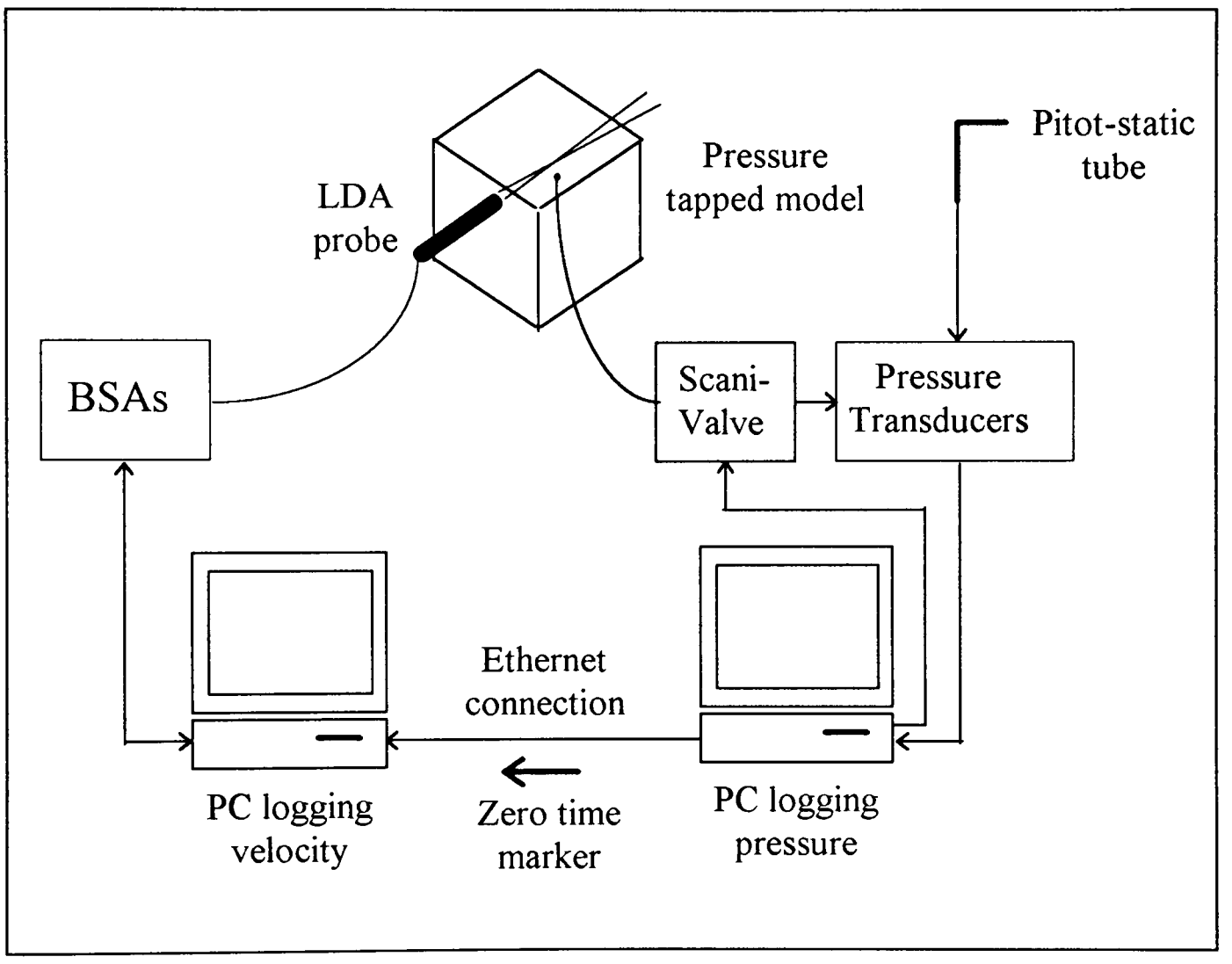

Figure 5-1 Pressure and velocity measurement systems

The two PCs are linked via an ethernet connection. This link allows a common time marker to be transmitted onto both pressure and velocity time histories, as described below.

The LDA and the pressure measurement systems are started independently. The pressure system first measures its zero datum (see section 3.4.4.). Having measured the zero datum,

the Scanivalve is then switched to sample the desired tapping. At this point, a trigger pulse is transmitted via the ethernet connection to the LDA PC. This pulse is the zero time marker. Although two data series are still measured separately, both now have a common time datum.

5.2.2 Accounting for the phase lag in the pressure signal

As was discussed in section 3.4.2, there is a time lag between a pressure occurring at a tapping and it being registered at the transducer. The time lag in the system used in this study was calculated to be 11.6 milliseconds (see equation 3.6). The pressure and velocity time series are offset to account for this time lag.

5.2.3 Converting randomly timed LDA samples into a regular time series

The pressure transducer system samples at a uniform rate of 100Hz, giving pressure values at 10 millisecond intervals. However, the LDA does not produce a uniform time series. It records a velocity sample only when a seeding particle passes through the measuring volume. Fig 5-2 shows the unpredictable occurrence of data points in 0.5 seconds of a typical velocity time series.

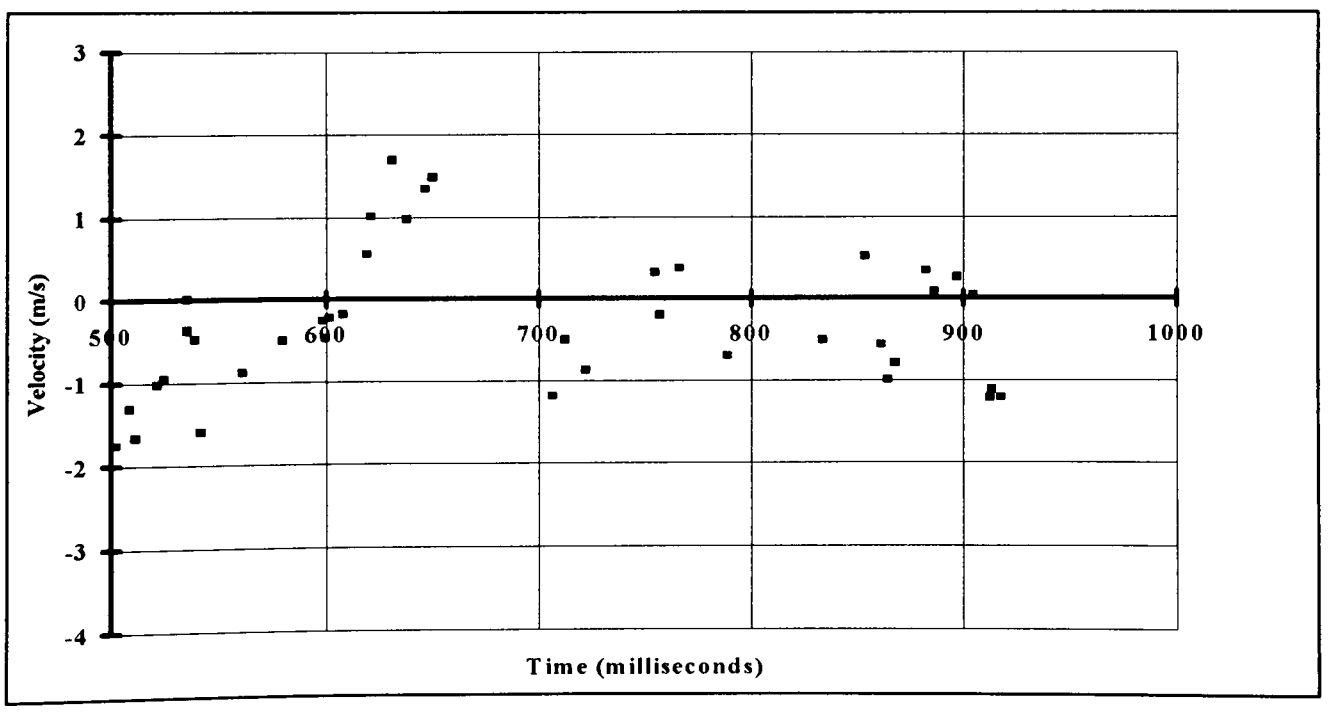

Figure 5-2 Typical velocity time series from LDA

Before such data can be used, it is necessary to construct a uniform velocity time series. To achieve this some form of interpolation must be employed.

Minson[1993] investigated interpolation methods applicable to LDA measurement. He concluded that simple linear interpolation between points was the most reliable method. This method has been used to construct uniform velocity time series in this study.

The interpolation allows data points to be created artificially at uniform 10ms intervals. When applied to the LDA data, this produces a velocity value for every data point in the pressure time series.

5.3 Creation of a Pseudo-simultaneous flow field from single point measurements

5.3.1 The necessity for conditional analysis

The simultaneous pressure-velocity measurement technique described in section 5.2 allows a pressure time history to be considered in conjunction with a velocity time history measured at a single location.

Ideally, in order to study vortex structure, instantaneous velocities at numerous points in the vortex would be measured simultaneously. This could be achieved with Particle Image Velocimetry (PIV, see Appendix B). However, the LDA can only measure at one location on each measurement run and the velocity time series from different measurement locations cannot be combined spatially. In the absence of multi-point simultaneous velocity measurement, conditional analysis is used to construct a pseudo-simultaneous picture of the flow field.

In formal terminology, the procedure described in this section is pressure-conditional analysis of velocity. This technique is justified by the assumption that identifiable pressure events are uniquely caused by identifiable velocity patterns in the flow field. If this

assumption is true, then the repetition of a pressure event implies a repetition of the corresponding flow field. Thus, velocities at different locations, each measured to coincide with identified pressure events, albeit at different times, can be combined to produce a pseudo-simultaneous measurement of the pressure-conditional flow field.

5.3.2 Definition of a reference pressure event

Having decided that velocity values are to be referenced to pressure events, a suitable pressure event must be defined.

The most simple definition of a pressure event would be a single value of measured pressure, for example Cp = -3.0. Therefore, a single velocity would be noted at a time when a pressure value of -3.0 was found in the pressure time series.

It is possible that the assumption 'the repetition of a pressure event implies a repetition of the corresponding flow field' is not entirely true, and a specific pressure event is not always produced by a unique flow pattern. If this is the case then it is better to select all the velocity values associated with the pressure condition, over the entire measurement run, and average them.

Average values are statistically more reliable when a large sample size is considered. If there are few velocity values to average over, then the average value is likely to be subject to significant statistical error. There are two ways to increase the number of velocity samples, associated with a given pressure condition:

The first option is to sample for longer periods, so that a defined pressure event occurs more times during the measurement period. This has the drawback of being time consuming and, more importantly, producing excessively large data files that pose problems in data storage and manipulation. Even with the 120 second samples used in this study, the

manipulation of data files was extremely demanding on computing power and time consuming.

Alternatively, the definition of the pressure event can be relaxed. For example, rather than considering only samples when Cp = -3.0, a reference pressure range of $-3.1 < Cp < -2.9$ could be defined. However, this means that the reference pressure used to select the velocity samples is less distinct and the associated flow structure may not be defined so precisely.

It is desirable to consider values averaged over the same number of points, but defining a fixed pressure bandwidth would mean that the number of velocity values selected would be likely to vary from one measurement run to another. This can be avoided by defining a quantile pressure-condition and always sampling for the same length of time. For example, the pressure condition could be defined as the pressure value that is exceeded for 1% of the total sample duration.

In this study it is the flow structures associated with pressure maxima and minima that are of particular interest and so quantile reference pressure conditions were used. The value of the quantile percentage, and hence the number of points that are averaged over, is discussed in section 5.3.4.

5.3.3 A definition of terminology

The probability of an event B occurring, given that another event A has already happened is termed the probability of B conditional on A, and is denoted P(B|A).

In this study the object is to determine the flow structures associated with specific pressure conditions, so event A is a pressure event and event B is a velocity event.

A velocity determined conditional on a reference pressure is a **pressure-conditional velocity**.

A was discussed in section 5.3.2 a pressure quantile is chosen as a reference condition. Therefore, the velocities associated with the highest or lowest X % of pressures are selected. These selected values make up a **conditional data set**.

Although the conditional data analysis technique was originally devised to produce pressure-conditional velocities, a similar approach can be used to obtain other conditional statistics. For example, in later chapters of this thesis, wind onset angle-conditional pressures are considered. These are pressures referenced to onset wind angle conditions.

5.3.4 Size and bandwidth of a conditional data set

Having selected pressure quantiles as the best method of defining a pressure reference condition, it is necessary to consider the quantile range of the conditional data set.

To demonstrate the effect of the size of a conditional data set, a trial was carried out with random data having a normal distribution. Two sets (set A and set B) of 12000 independent random numbers were generated and grouped in pairs (A,B). These pairs of numbers were sorted into ascending A order. The A-conditional mean B values were then calculated for a variety of A value ranges (and hence conditional data set sizes).

The A-conditional mean B values were compared to the mean of B for the entire sample. Fig 5-3 shows the variation in conditional means with conditional data set size for four such trials.

As expected, the A-conditional mean B values calculated from the smaller conditional data sets show a large discrepancy relative to the mean value of B for the full sample. Since the data was randomly generated the discrepancy does not follow a consistent trend.

In a second experiment the same analysis was carried out on a set of actual pressure-velocity data. In this data there is a definite correlation between the pressure and velocity variables. The pressures become lower as the velocity increases.

The data was grouped so that the smallest conditional sets were associated with the lowest pressures. Fig 5-4 shows that the pressure-conditional mean velocities diverge away from the overall mean as the size of the conditional data set is reduced.

When conditional data sets containing less than 2.5% of the sample (300 records) were used, the conditional mean became erratic and broke away from the consistent trend shown in the rest of the plot.

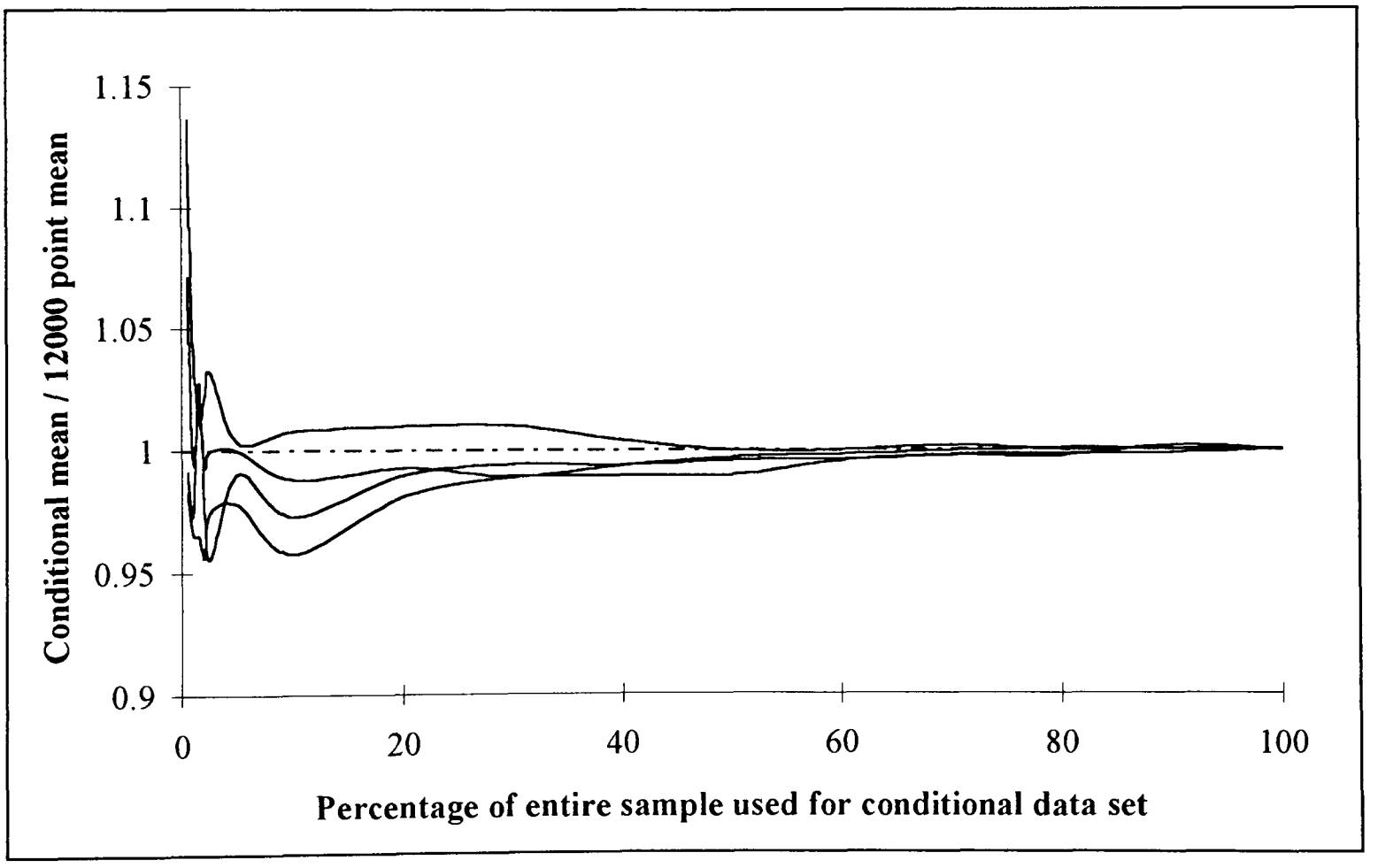

Figure 5-3 Variation in conditional mean with sample size in random, uncorrelated data

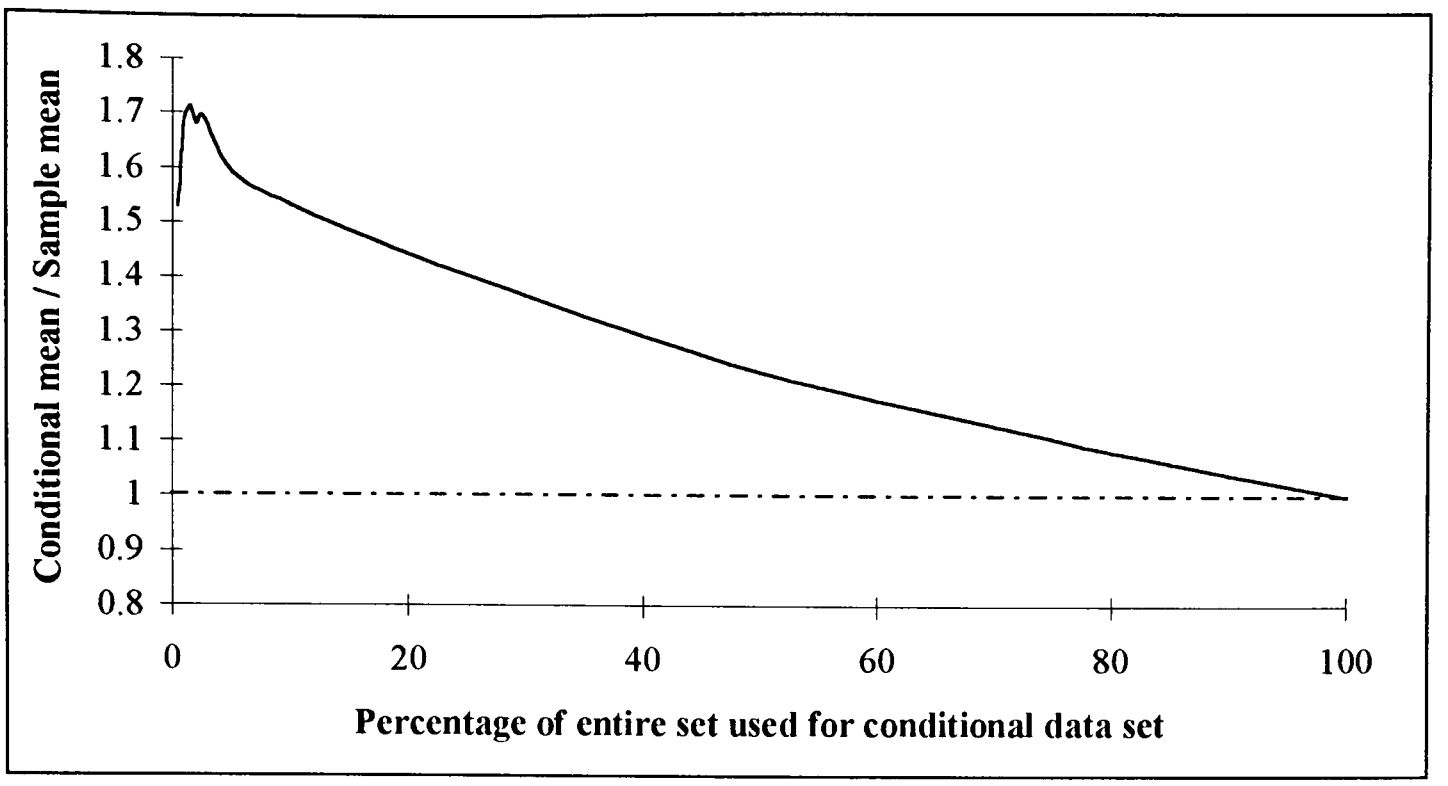

Figure 5-4 Variation of conditional mean with size of conditional data set

The pressure bandwidth associated with a sample of 300 records was determined in order to assess how specific a flow event constituted 2.5% of the total sample. Fig 5-5 shows a histogram of the measured pressures. This figure demonstrates that the lowest 2.5% of the records constitute a data set with a pressure range of -2.7 to -4.

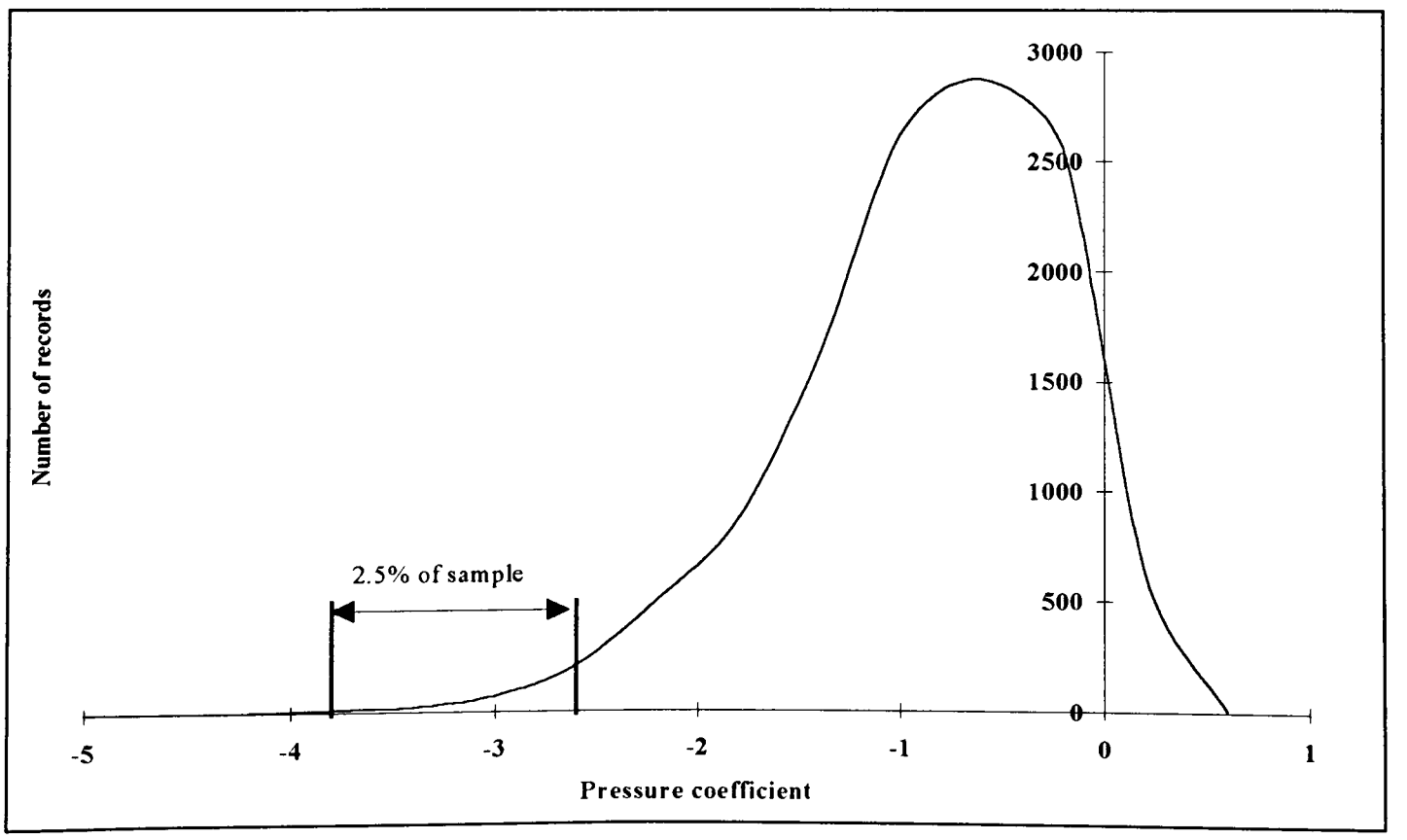

Figure 5-5 Histogram of measured pressures

It is desirable to look at the smallest bandwidth possible, in order to provide the closest association between the velocities and a particular pressure value, but this must be offset against the need to use large enough sets to produce reliable statistics.

From the evidence shown in Figs 5-4 and 5-5, the size of conditional data sets for this study was chosen to be a minimum of 2.5% of the total sample (300 records). This size of conditional data set is large enough to provide reliable statistics, while being associated with a small range of pressures (and hence vortex structures).

5.3.5 Determining pressure-conditional velocities

The previous sections have discussed the theory of conditional analysis. This section briefly describes the technique used to apply conditional analysis to the measured pressure-velocity data.

The assembled simultaneous pressure-velocity time series (as described in section 5.2) takes the form of N records, each of four numbers: time (t), pressure coefficient (Cp(t)), lateral velocity (V(t)) and vertical velocity (W(t)). The series is produced in ascending time order ($t_{n+1} > t_n$). This format is shown in Table 5-1.

In the simultaneous measurements carried out in this study, data was taken over a period of two minutes. With a sampling frequency of 100Hz, this results in 12000 data records, i.e. N=12000.

To consider a pressure-conditional velocity, the simultaneous measurement series is rearranged from time order into ascending pressure coefficient order. There are still N records of data, but now the first record is associated with the lowest pressures and the last is associated with the highest pressures.

t	$C_p(t)$	V(t)	W(t)
t_1	$C_p(t_1)$	$V(t_1)$	$W(t_1)$
t_2	$C_p(t_2)$	$V(t_2)$	$W(t_2)$
t_3	$C_p(t_3)$	$V(t_3)$	$W(t_3)$
		⇓	
t_n	$C_p(t_n)$	$V(t_n)$	$W(t_n)$
		⇓	
t_N	$C_p(t_N)$	$V(t_N)$	$W(t_N)$

Table 5-1 Format of simultaneous data

To consider the pressure conditional velocities associated with the lowest X % of pressures (those which are exceeded for (100 - X)% of the time) the first $\frac{NX}{100}$ data records are chosen from the sorted data series.

The average value of the V(t) samples in the conditional data set (the pressure-conditional mean lateral velocity) can then be calculated. This pressure-conditional velocity is a spatial element of a flow structure that produces a large suction on the roof.

5.4 Pressure-conditional velocity measurements in a conical vortex

Simultaneous pressure-velocity measurements were made at an array of points above a single pressure tapping, with the model angled at 45^0 to the onset flow. Tapping 1 (see Fig 3-8) was chosen for these measurements as, being the tapping closest to the leading apex, it is the measurement location at which the largest suctions occur (Tieleman et al[1992]).

The velocity measurement locations are shown in Fig 5-6. The diagram shows the points when viewed along a ray, at 16^0 to the edge of the building, from downstream of the leading corner.

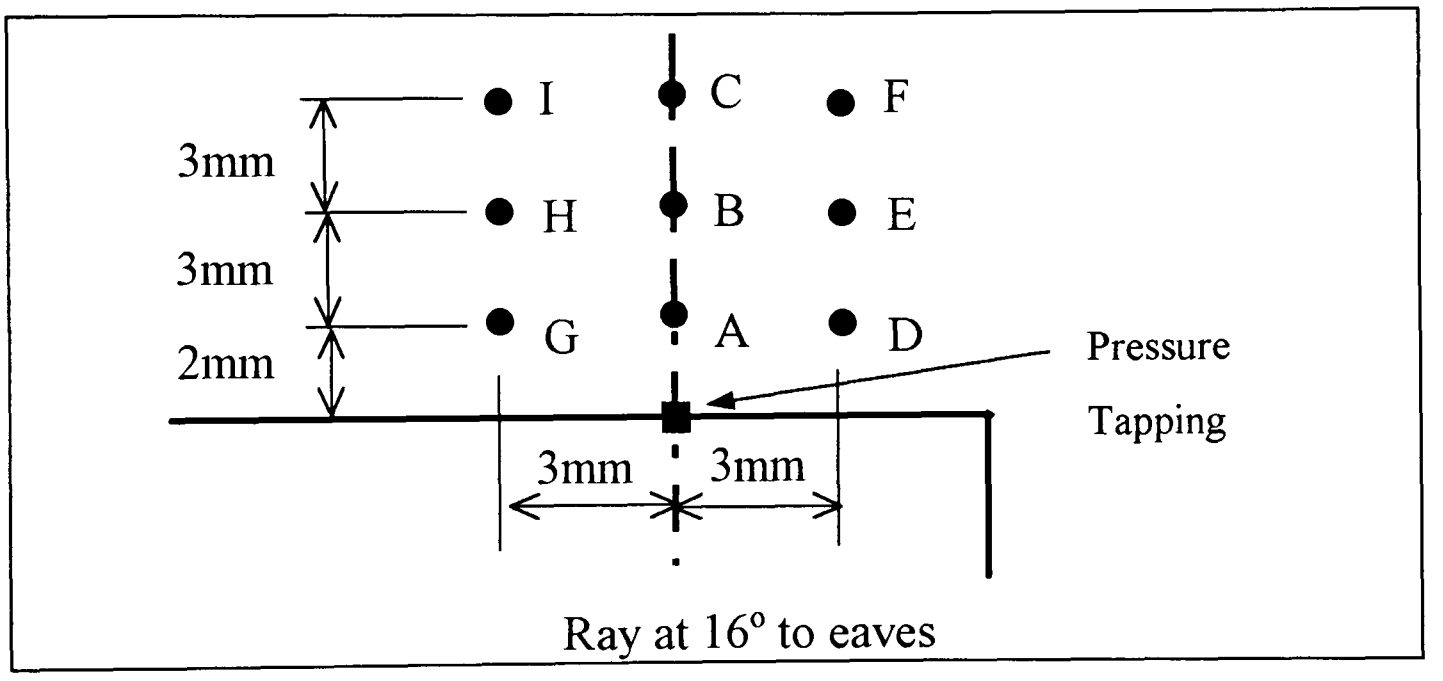

Figure 5-6 Measurement locations 15mm from leading corner

5.4.1 Pressure-velocity correlations

As a first step to investigate the relationship between velocity and pressure fluctuations, the correlation coefficient (r) between the pressure and velocity series was calculated, providing a statistical measure of the degree to which the two arrays of variables, Cp and v, are linked. The correlation coefficient is defined in equation (5.1).

$$r(Cp, v) = \frac{\sum (Cp - \overline{Cp})(v - \overline{v})}{\sqrt{\sum \left(Cp - \overline{Cp}\right)^2 \sum \left(v - \overline{v}\right)^2}} \qquad (5.1)$$

$\overline{Cp}$ and $\overline{v}$ are the mean values of the x and y arrays.

The value of r varies between -1 and 1. Values of r = 1 or -1 shows that the arrays are perfectly linked, i.e. y = f (x). As the magnitude of r reduces, so does the link between the arrays. When r = 0 the arrays are completely independent of each other.

In addition to calculating r(Cp, v), the correlation between pressure and the square of the velocity (r(Cp, v^2)) was also calculated. This was done in order to investigate a Bernoulli form of relationship. Ignoring gravity terms, Bernoulli's equation states that, for an ideal, inviscid fluid of constant density:

$$p + \frac{\rho V^2}{2} = \text{constant} \qquad (5.2)$$

Thus, by Bernoulli, pressure varies with the square of the velocity.

The correlation results are tabulated in Tables 5-2 and 5-3.

Location	Lateral	Vertical	Axial
A	-0.11	-0.13	-0.046
B	0.35	-0.46	0.107
C	0.614	-0.416	0.112
D	-0.332	0.014	-0.130
E	0.52	-0.47	0.133
F	0.64	-0.46	0.122
G	0.23	0.272	-0.017
H	0.07	0.29	0.128
I	0.57	0.285	0.036

Table 5-2 Correlation between pressure and velocity components

Location	v^2	w^2	u^2
A	-0.08	-0.07	-0.08
B	0.17	-0.05	-0.04
C	0.67	-0.31	0.08
D	-0.13	-0.15	-0.23
E	0.63	-0.53	0.08
F	0.74	-0.44	-0.05
G	-0.08	-0.02	-0.11
H	0.05	-0.05	-0.0002
I	0.27	-0.02	0.04

Table 5-3 Correlation between pressure and the square of velocity components

Observing the correlation results suggests the following:

- the axial velocity has little effect on the pressures under the vortex
- there is a high (magnitude of $r > 0.4$) correlation between pressure and lateral velocity
- there is some correlation between vertical velocity and surface pressure, although this correlation is less marked than the lateral velocity-pressure correlation
- the correlations between the pressures and the square of the lateral velocity component are consistently larger than for the correlations between pressure and the unsquared velocity. This supports a Bernoulli form of relationship.
- the measurements made at the lowest positions (points A, D and G) show positive correlations for the lateral component, whereas those above them (B, C, E, F, H and I) have a negative correlation. This shows that, at locations above the vortex core an increase in the lateral velocities *away from* the roof edge leads to a reduction in surface pressure. In contrast, at locations below the vortex core, larger lateral velocities *towards* the roof edge surface produce a similar increase in suction. Therefore, the pressure under the vortex decreases with increased circulation around the vortex axis.

It has been shown that the surface pressure does not to vary with the axial velocity. Section 4.4 explains this. Fig 4-24 shows that the largest axial velocities are associated with oblique (low β) onset flow angles. However, these oblique angles produce smaller velocities in the vw plane (see Figs 4-13 to 4-16). Thus, there is less vorticity in the vortex (see Figs 4-19 to 4-23). Therefore it is likely that the reduction in vorticity negates any effect on suctions produced by higher axial velocity.

5.5 Pressure-conditional velocities in a conical vortex

The pressure-velocity correlation results discussed in section 5.4 support the idea of a link between velocities in the vortex and surface pressure. In order to investigate further the pressure-velocity link, the simultaneous velocity-pressure time series were analysed using pressure-conditional statistics. Only vertical and lateral velocity components were considered as the correlation results suggest that there is no link between axial velocity and surface pressure

The data was sorted into three pressure-conditional data sets, those records associated with pressures having a 10% chance of exceedance, records associated with pressures having a 90% chance of exceedance and a set containing the rest of the records in the sample. Larger conditional data sets (10% of the data rather than the minimum value of 2.5% discussed in section 5.3.4) were chosen, as probability distributions within the conditional sets were to be calculated, rather than single mean values.

Pressure-conditional velocity histograms were plotted by calculating the probabilities of certain velocities occurring within each of the three conditional data sets. These histograms therefore represent the velocity ranges that cause the highest, lowest and most common pressures, respectively. These histograms are shown in Figs 5-7 to 5-24.

These pressure-conditional histograms confirm the conclusions drawn from the correlation experiments carried out in section 5.4. The histograms for points B, C, E, F and I show a very clear relationship between pressure and velocity, demonstrating that larger velocities lead to lower surface pressures.

The histograms for points A, D and G all show an interesting trend. If we consider Fig 5-7, the horizontal velocity for point A, we see that the mode velocity from the largest suction

histogram is in the positive direction i.e. towards the model edge. In contrast, the mode velocity from the smallest suction histogram is in the negative velocity direction i.e. away from the model edge.

Fig 5-25 demonstrates this point very clearly. It shows two vector plots of pressure-conditional mode velocities, one for the highest suctions and one for the lowest. These show the presence of the vortex and the apparent absence of the vortex. This demonstrates that the flow is either not recirculating when the smallest suctions occur or the recirculating velocities have occurred below the measurement positions, i.e. the vortex axis is closer to the model surface.

These results demonstrate that a larger and more strongly rotating vortex structure is responsible for increases in surface suctions. This is contrary to the findings of Letchford[1995], who suggested, from observing full scale flow visualisations,

'...it is possible to say that peak pressures are associated with a tightening of the vortex probably driven by incident turbulence.'

The effect of incident turbulence is investigated extensively in the later chapters of this thesis.

Another interesting result can be seen in Fig 5-8 which shows the vertical velocity histograms for point A. The peaks of the smallest and largest suction histograms lie on opposite sides of the w = 0 axis. This shows that the vortex varies in position relative to the edge of the model. This variation in position, and its effect on surface suctions, is investigated at length in Chapter 7.

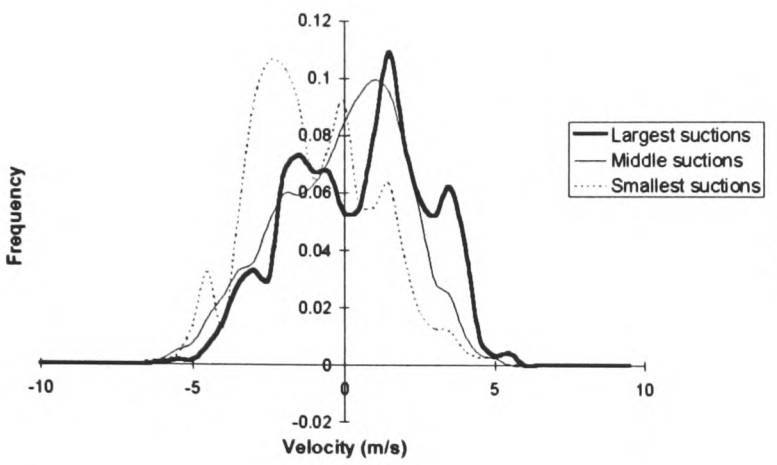

Figure 5-7 v velocities at point A

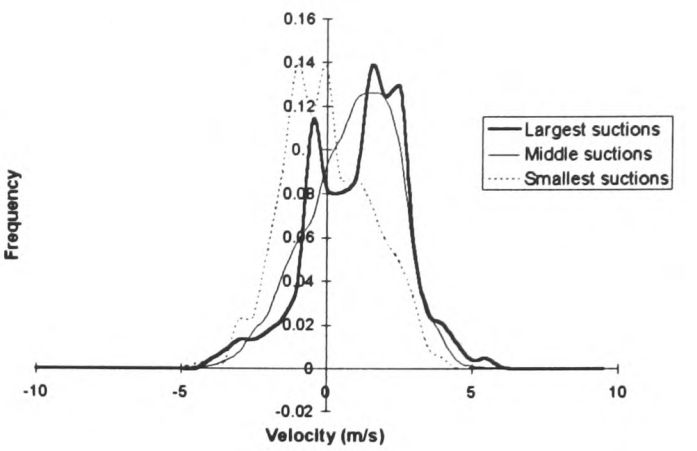

Figure 5-8 w velocities at point A

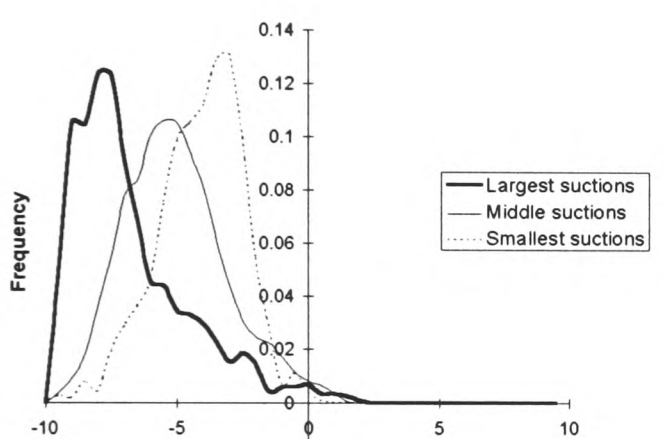

Figure 5-9 v velocities at point B

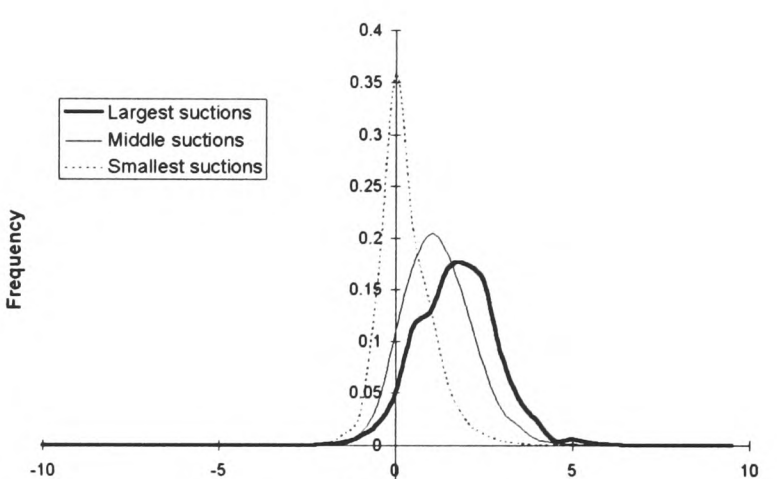

Figure 5-10 w velocities at point B

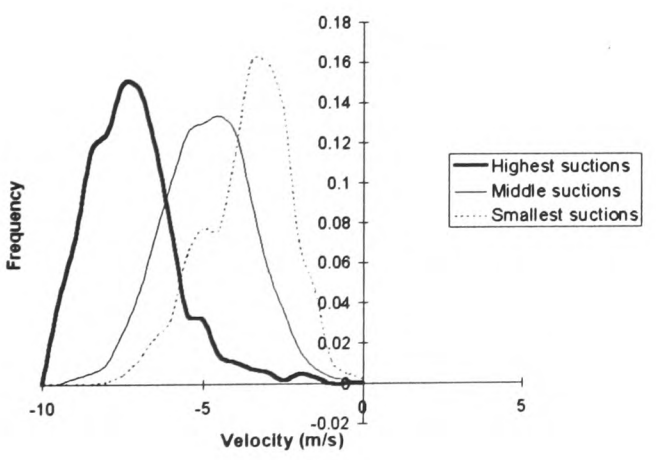

Figure 5-11 v velocities at point C

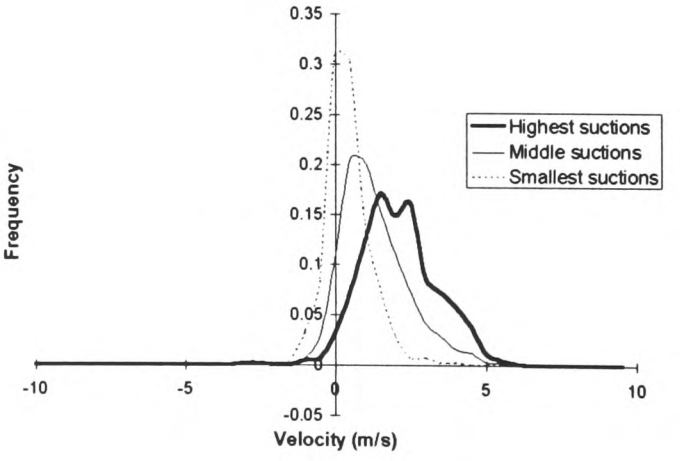

Figure 5-12 w velocities at point C

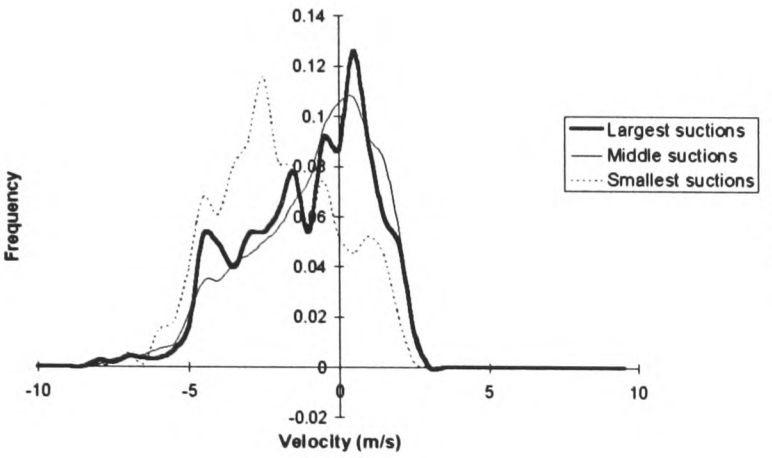

Figure 5-13 v velocities at point D

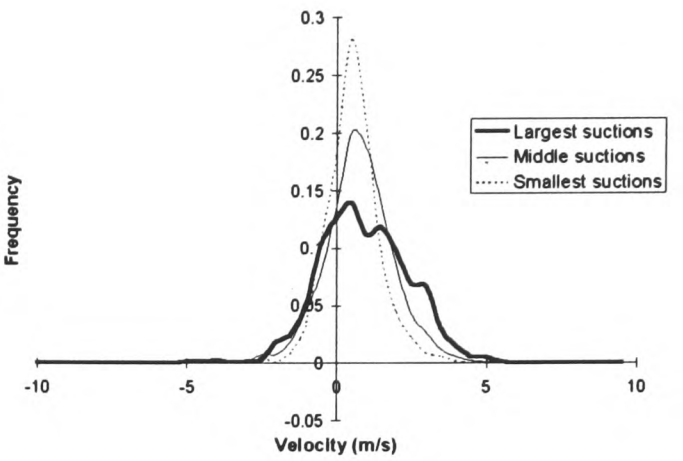

Figure 5-14 w velocities at point D

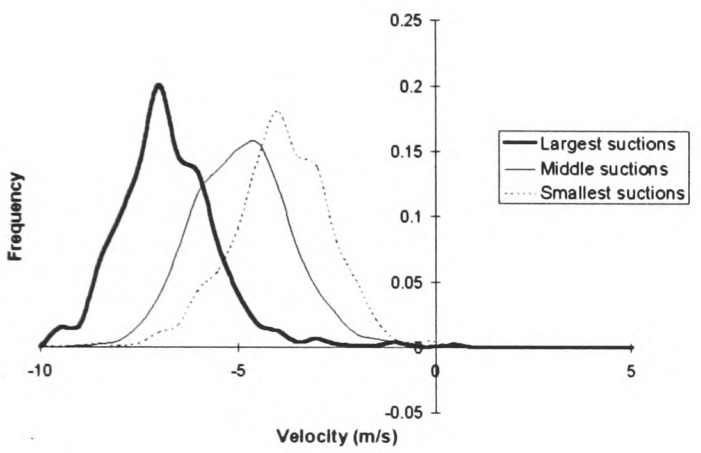

Figure 5-15 v velocities at point E

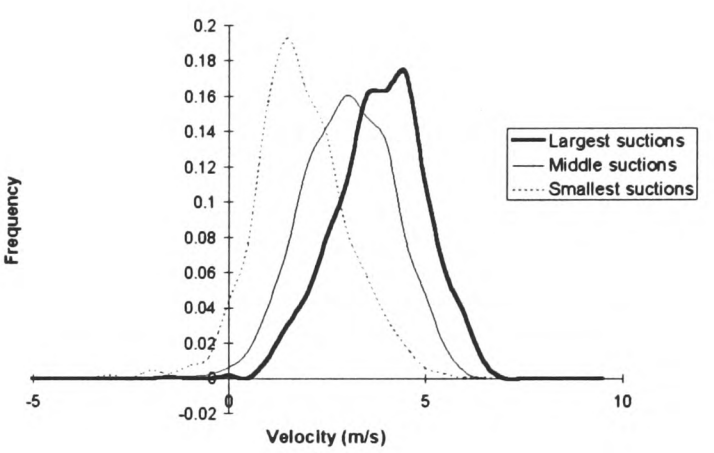

Figure 5-16 w velocities at point E

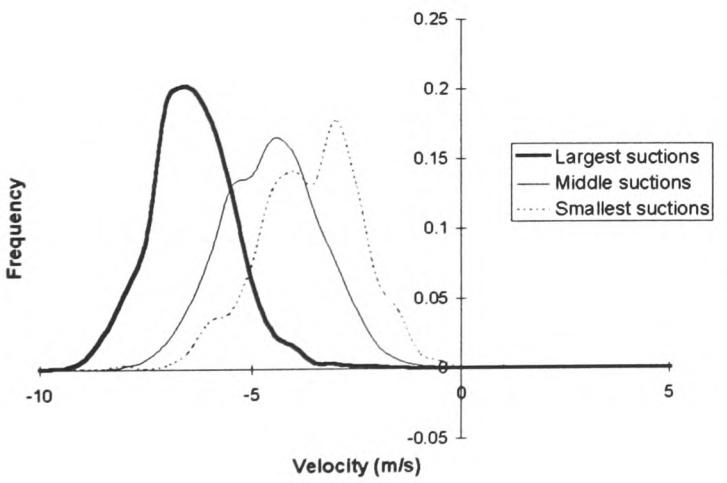

Figure 5-17 v velocities at point F

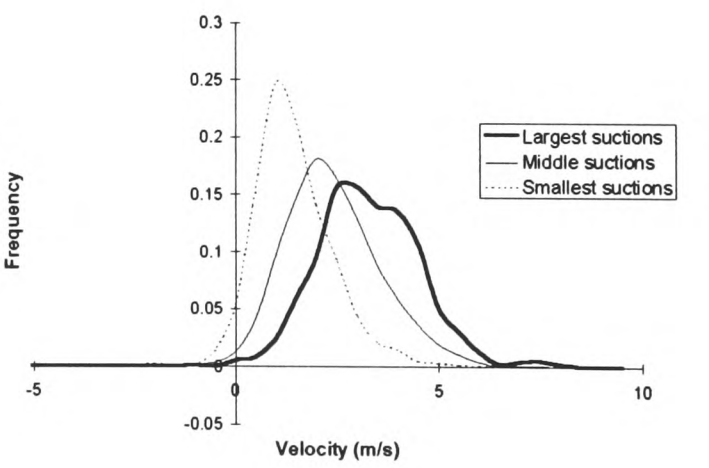

Figure 5-18 w velocities at point F

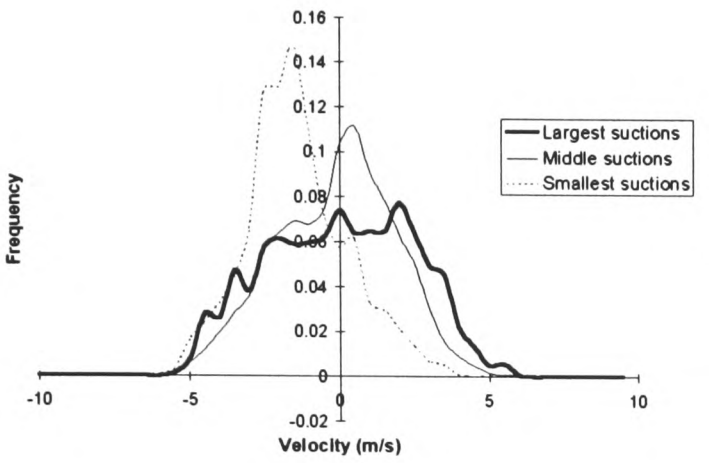

Figure 5-19 v velocities at point G

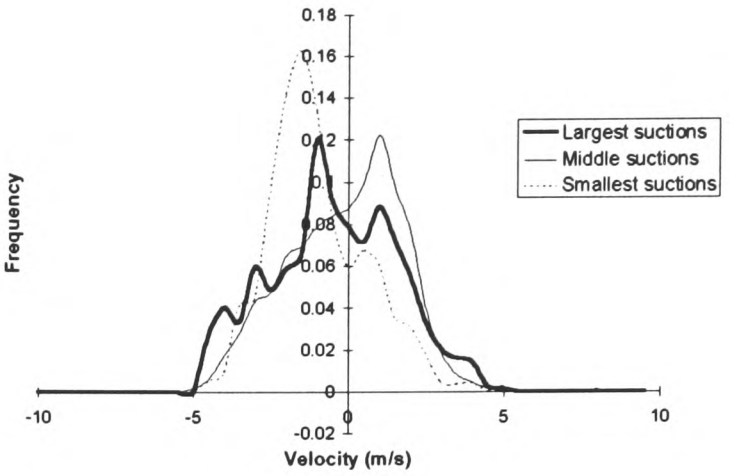

Figure 5-20 w velocities at point G

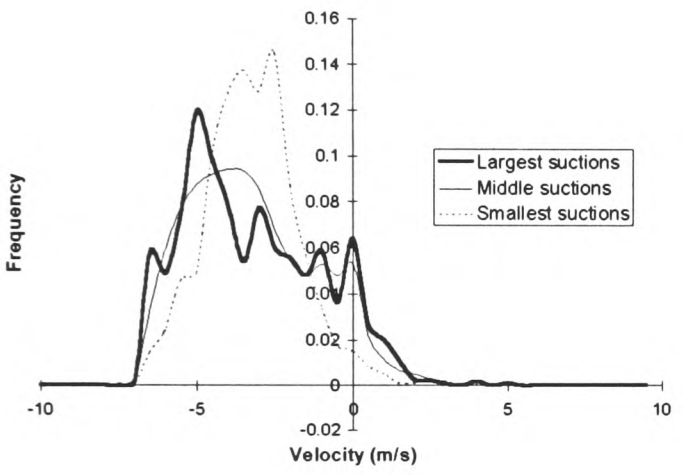

Figure 5-21 v velocities at point H

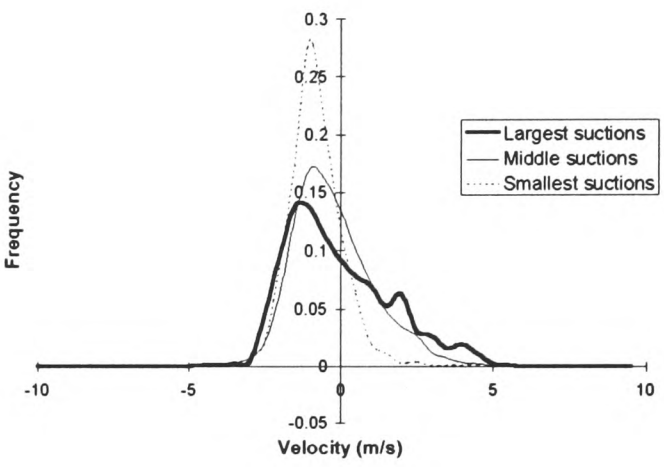

Figure 5-22 w velocities at point H

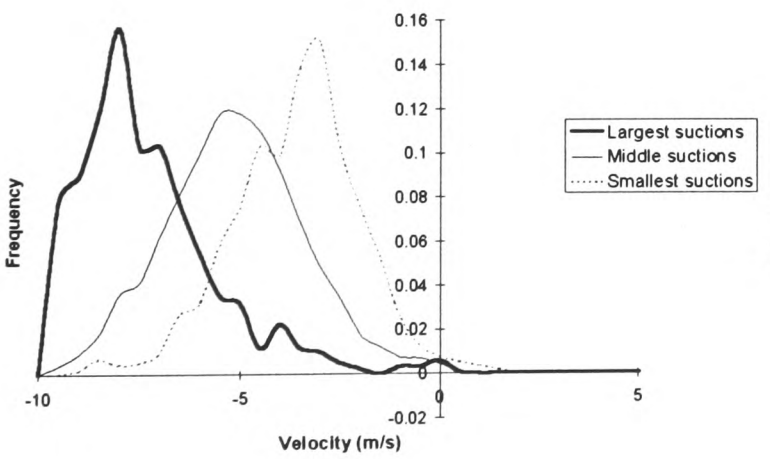

Figure 5-23 v velocities at point I

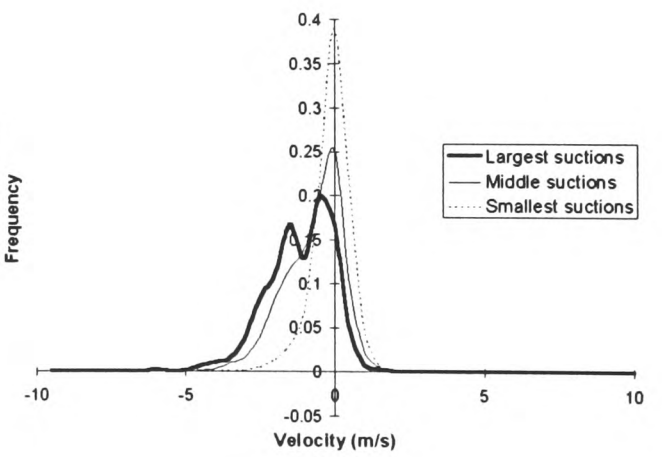

Figure 5-24 w velocities at point I

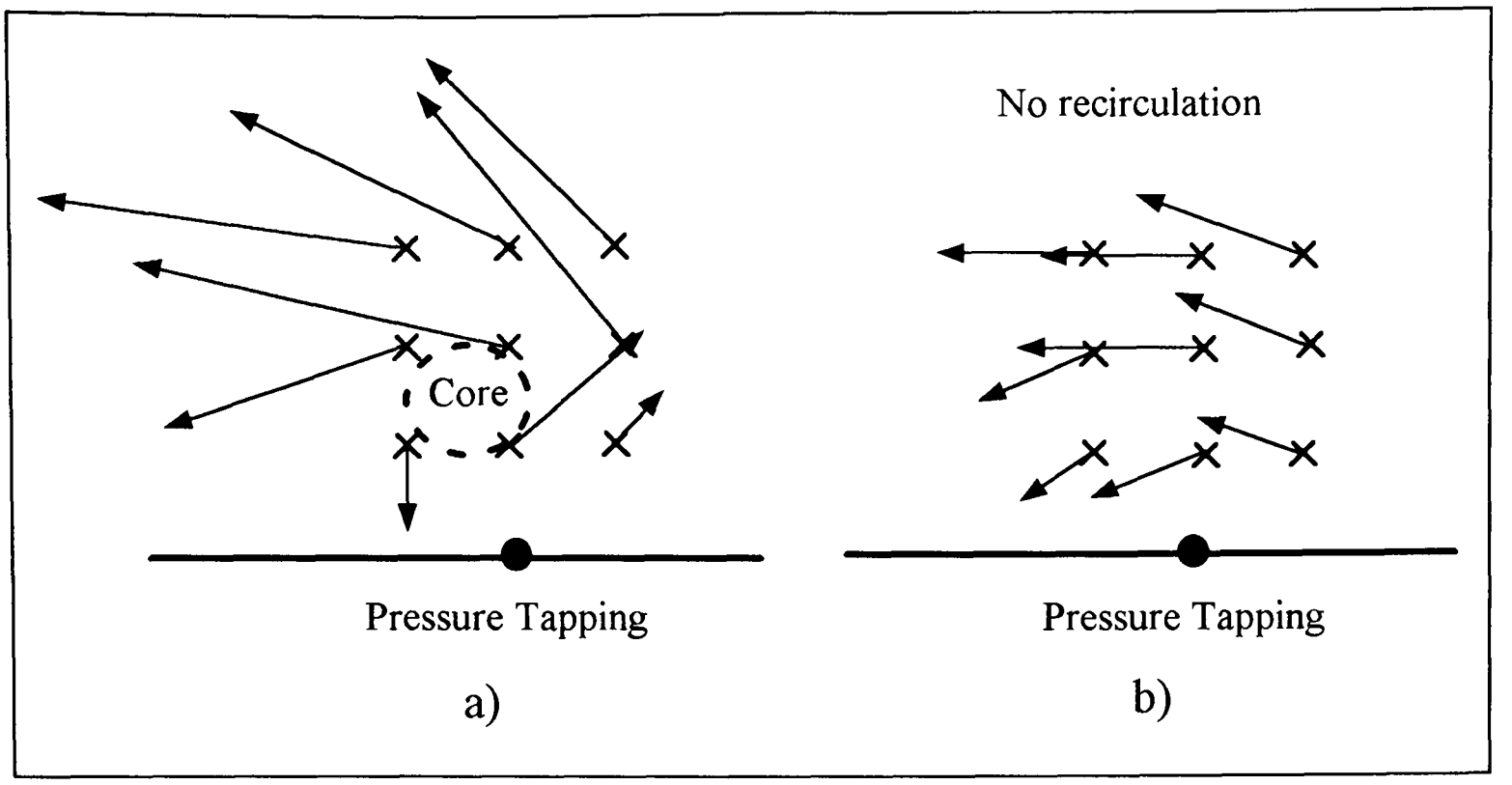

Figure 5-25 Pressure conditional mode vw velocities

a) Lowest pressures b) Highest pressures

6. Vortex Intermittency

6.1 Smoke visualisation

Minson and Wood[1992] suggested from flow visualisation experiments that the presence of the conical vortex is intermittent:

'...the conical vortex was intermittently swept away leaving no identifiable flow structure until another vortex developed.'

It is possible that this observed intermittency was due to the smoke sometimes not getting into the vortex, rather than the vortex not being present.

In the same work, vector plots of velocities in the vortex were presented. These plots showed similar elliptical shapes to those in the plots presented in Chapter 4. At that time, it was thought that the elliptical shape was due to the transience observed in the visualisation. The elliptical shape was hypothesised to be a time-averaged structure formed by averaging two flow events - the presence of a conical vortex, and a condition with no recirculation in the flow.

The intermittent presence of the vortex was also observed in full scale visualisation work carried out at both the Silsoe Research Establishment and the Texas Tech research building. In the latter of these studies, Letchford[1995] suggested that lateral turbulence in the onset flow was responsible for the periodic destruction of the vortex.

Results presented in section 5.5 suggest that the recirculating flow associated with the separated flow is sometimes not present. These results support the observations made from the earlier smoke visualisation experiments. A further investigation is carried out in this chapter.

6.2 Effect of onset stream turbulence

The smoke visualisation experiments performed by Minson and Wood were repeated by this author (see photographs in Fig 1-2 and 1-3). The intermittency of the vortex was again observed in this repeated experiment.

The experiment was carried out on a building model in a turbulent onset flow ($z_0 = 0.25$m, a turbulence intensity of 20% at model height). In order to assess the role of turbulence in the onset flow, the same visualisation experiment was repeated in a low turbulence flow (turbulence intensity less than 1% at model height) with a uniform velocity profile.

A low turbulence flow was produced in the wind tunnel by removing the inlet grid and the upstream roughness elements. Additionally, the model was placed on a platform 1 metre above the floor of the tunnel. This was done to avoid the boundary layer that grows naturally on the floor of the tunnel along its length.

In the low turbulence flow, the vortex was visible in the smoke at all times, i.e. there was no apparent intermittency.

Clearly, it is turbulence in the onset flow which produces the intermittent nature of the vortex.

6.3 Effect of onset flow direction

In the smoke visualisation experiments described in sections 6.1 and 6.2, the model was placed at 45^0 to the mean onset flow. However, the instantaneous wind angle varies greatly due to the onset turbulence. Thus, although the mean onset wind direction is 45^0, the instantaneous onset direction can sometimes be markedly different from this mean.

This variation in instantaneous azimuth direction was determined done by measuring simultaneously the streamwise (u) and lateral (v) velocity components upstream of the model with the LDA. The instantaneous azimuth angle is given by:

$$\beta = \tan^{-1}\left(\frac{v}{u}\right) + 45^0 \qquad (6.1)$$

The measurement location was 50mm (0.25h) upstream of the model, at roof height (200mm), in both the $z_0 = 0.25$m simulated turbulent boundary layer and the low turbulence flow.

Fig 6-1 shows histograms of the instantaneous azimuth directions in both the high and low turbulence flows.

Fig 6-2 shows a 20 second time history of azimuth wind angle. During the 20 second sample there are 4 times when the instantaneous onset angle varies from the mean onset angle by approximately 40^0 or more. The duration of these gusts constitutes only 0.5% of the total sample period.

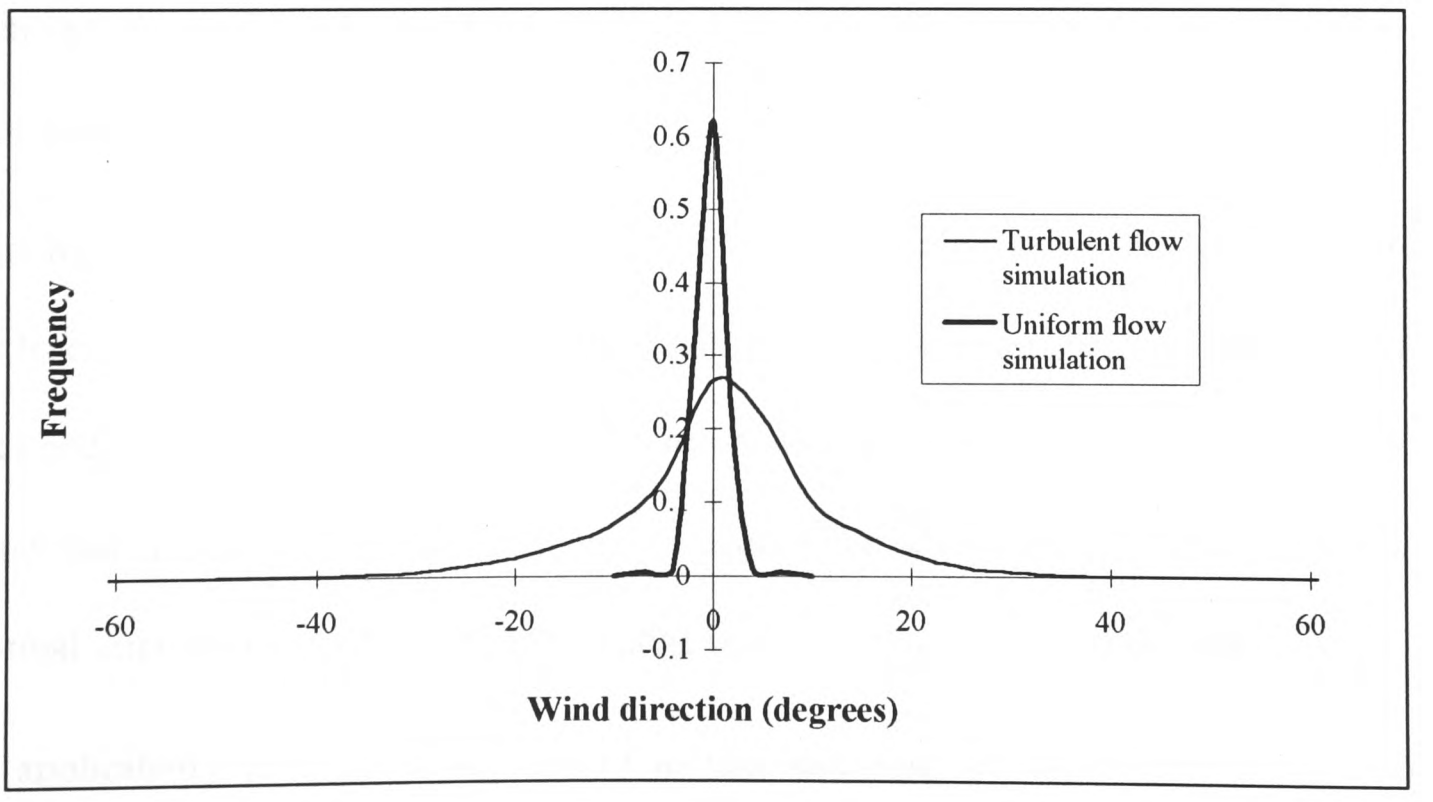

Figure 6-1 Histograms of instantaneous azimuth angles

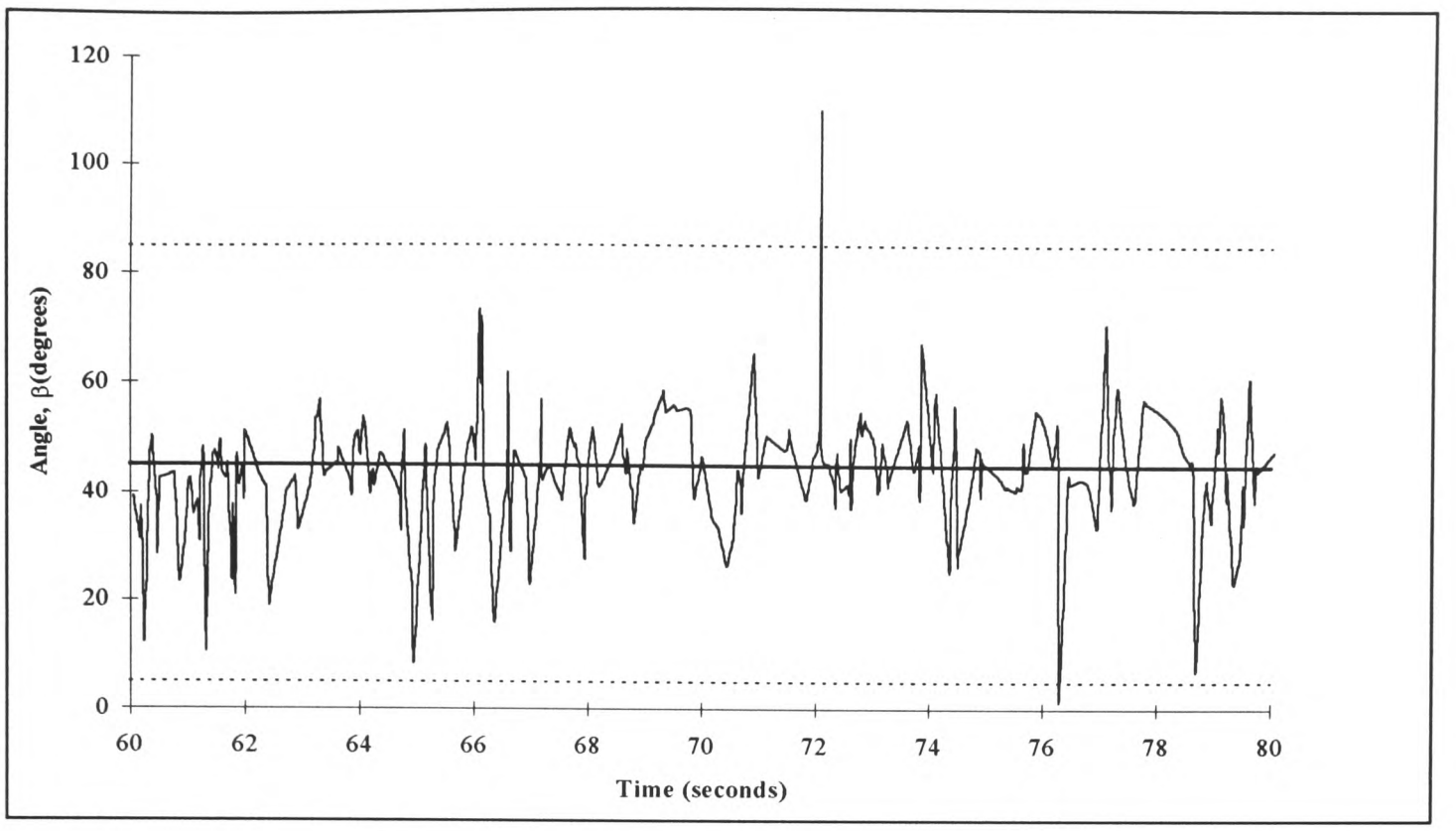

Figure 6-2 Instantaneous wind angle time history

Quasi-steady theory assumes that flow patterns respond to atmospheric turbulence as if the gusts it produces were changes in mean wind speed and direction. If the vortex behaviour is quasi-steady then an instantaneous onset flow angle which is parallel to one of the model's leading edges will not produce any flow separation on that edge, and no vortex will be formed. However, it is possible that the vortex can still persist in a transient state even when the instantaneous flow angle produces no separation at that edge, and the vortex behaviour is not quasi-steady.

Apart from the particular case when one face of the modèl is perpendicular to the stream, two leading edges are presented to the onset flow. Therefore, there are two separation edges and two conical vortices. When the instantaneous onset angle becomes perpendicular to one leading edge, it is parallel to the other edge. Thus, under the quasi-steady hypothesis, a normal separation bubble forms at one edge but no vortex forms at the other.

The applicability of quasi-steady theory to the behaviour of the vortex is discussed in Chapter 8.

7. Variations in instantaneous vortex position

7.1 Previous studies

As far as the author is aware, Kind[1986] was the first author to suggest that the instantaneous position of a conical roof edge vortex varies:

'Approach-flow direction fluctuations due to turbulence cause a "wandering" of the flow pattern and thus a "smearing" of mean suction peaks.'

However, it was not until the work of Kawai and Nishimura[1994] that vortex movement was studied in detail. Kawai and Nishimura measured pressures at a number of locations simultaneously on the roof of a model building placed at 45^0 to a turbulent onset flow. The correlation between instantaneous pressures measured at various pairs of locations was calculated. These correlation results showed that as the suction near one leading edge of roof increased the suction on the other edge decreased. Kawai and Nishimura concluded that the vortex position did vary and that the flow mechanism was driven by lateral turbulence (similar to the behaviour discussed in section 6.3.) The extent of the vortex movement was not quantified.

The results presented in section 5.4 provided further evidence that the instantaneous position of the conical vortices varies, both in height above the model roof and in angular position to the model edge.

In this chapter, the effect of turbulence in the onset flow on the vortex position is assessed. Vortex position was measured in both a simulated turbulent boundary layer and a low turbulence flow. Conditional analysis is used to determine the relationship between vortex position and roof surface pressures.

7.2 Measuring vortex position

The simultaneous measurement technique and conditional analysis developed in this thesis was used to determine vortex position. Both the height of the vortex above the surface of the model, and its angular position relative to the roof edge were measured.

The vortex positions producing specific surface suctions were determined by simultaneously measuring surface pressures and velocities in the vortex and noting the change in direction of lateral and vertical pressure-conditional velocity components.

Fig 7-1 illustrates the significance of velocity component direction in determining vortex axis position. The axis of a vortex lies at the intersection of the planes x = 0 and y = 0. Where x = 0, v = 0 and similarly, where y = 0, w = 0.

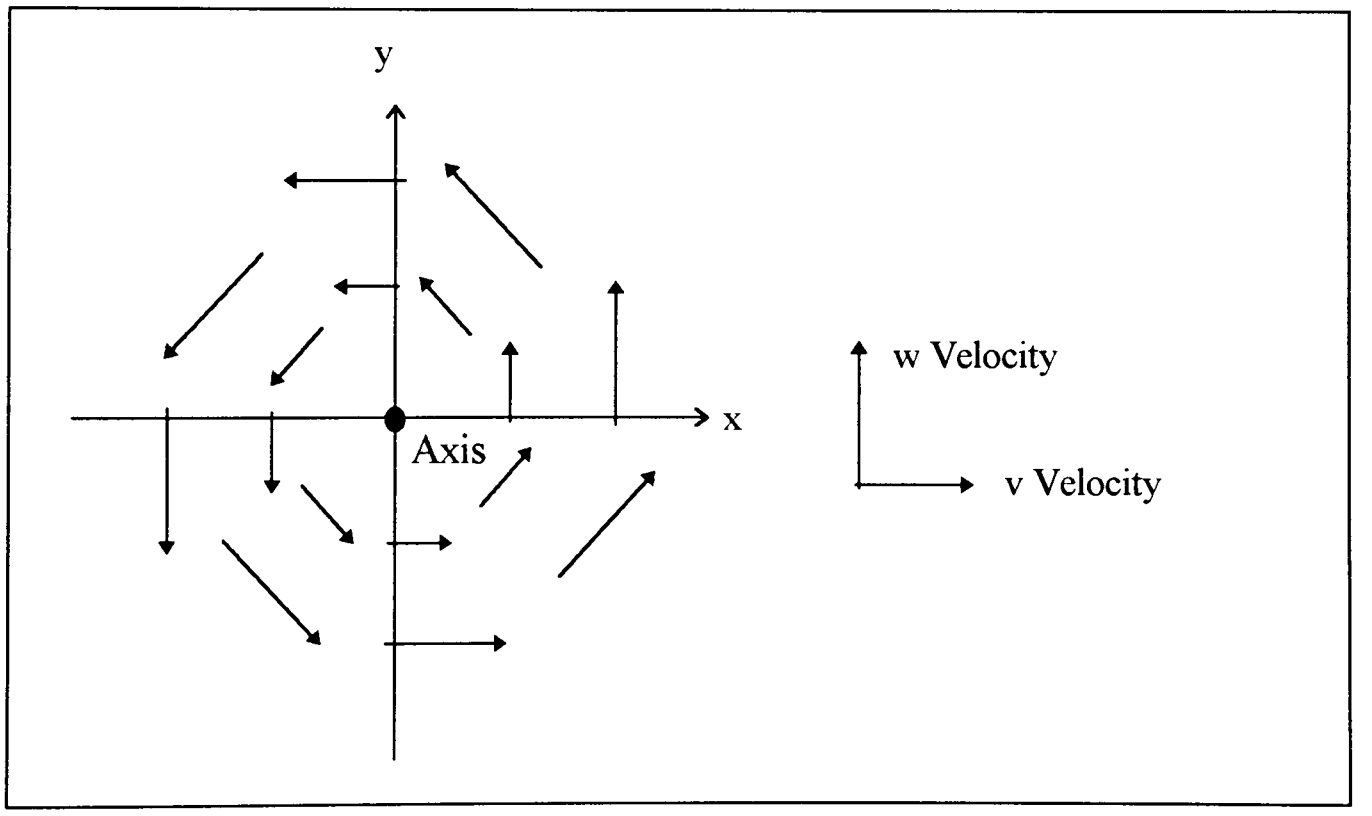

Figure 7-1 Velocities around vortex axis

The position of the vortex axis was determined by measuring one velocity component at a series of locations on a plane perpendicular the vortex axis plane of interest. Horizontal

velocities were measured on a vertical line to find the vertical position of the vortex and vertical velocities on a horizontal line to find the horizontal position. Determining the locations at which v = 0 or w = 0 determines the positions of the y = 0 and x = 0 planes respectively.

The vortex positions associated with three flow structures were considered:

1. that which produces the mean surface suctions

2. that producing surface suctions with a 2.5% of exceedance

3. that producing surface suctions exceeded 97.5% of the time

7.2.1 Vortex position results

This section presents the results from pressure-conditional vortex position measurements. These measurements were made with the model building placed at 45^0 to the mean onset flow direction.

Two different onset flows were used, a high turbulence flow (a turbulence intensity of 20% at model height) and a low turbulence (a turbulence intensity of less than 1% at model height.)

Vortex position was measured at three locations in the turbulent flow, 0.25h, 0.5h and 0.75h downstream of the leading apex of the model.

Two positions were measured in the low turbulence flow, 0.25 and 0.5h downstream of the leading corner.

7.2.1.1 High turbulence onset flow results

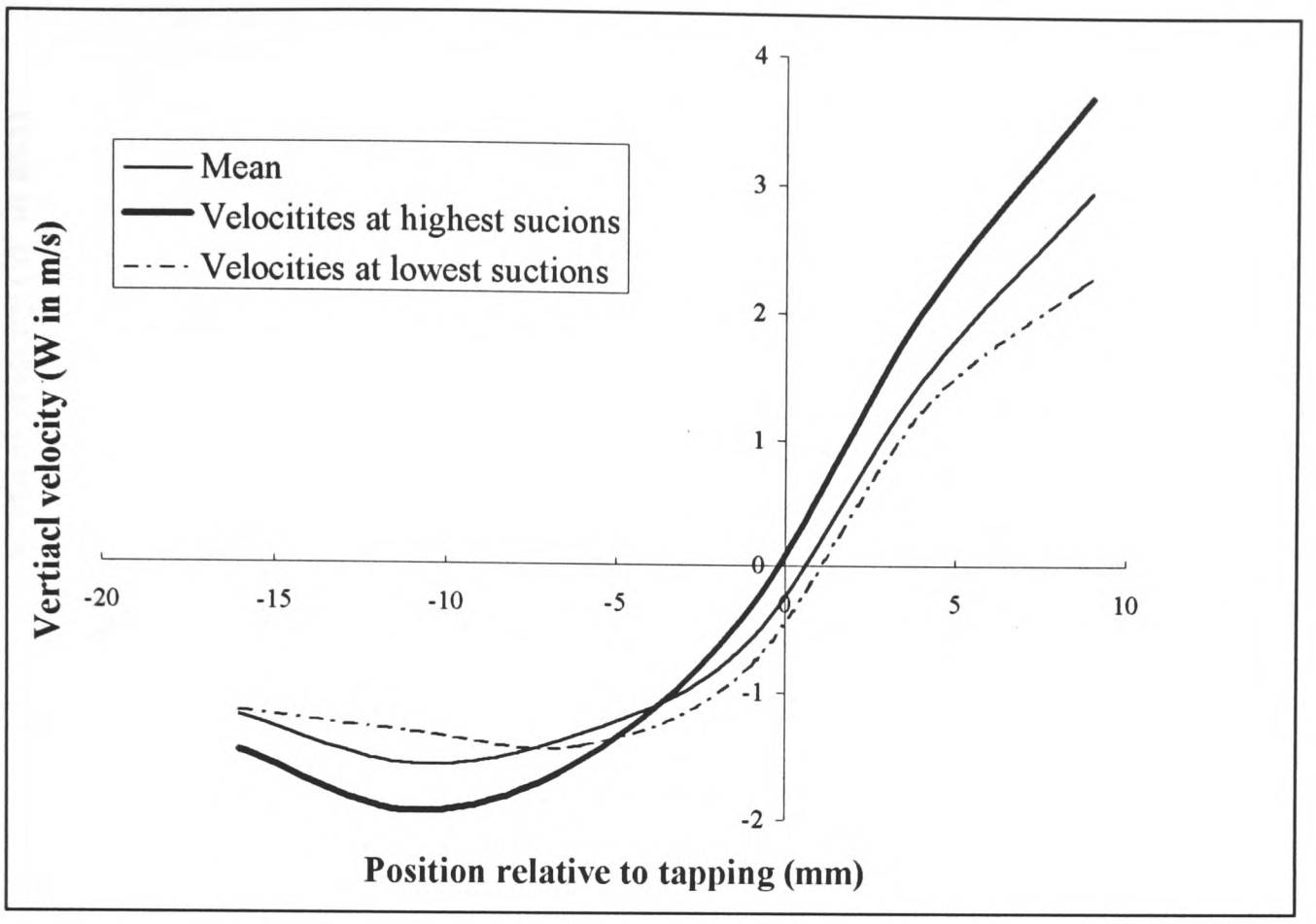

Figure 7-2 Vertical velocities 0.25h downstream (w = 0 shows vortex axis)

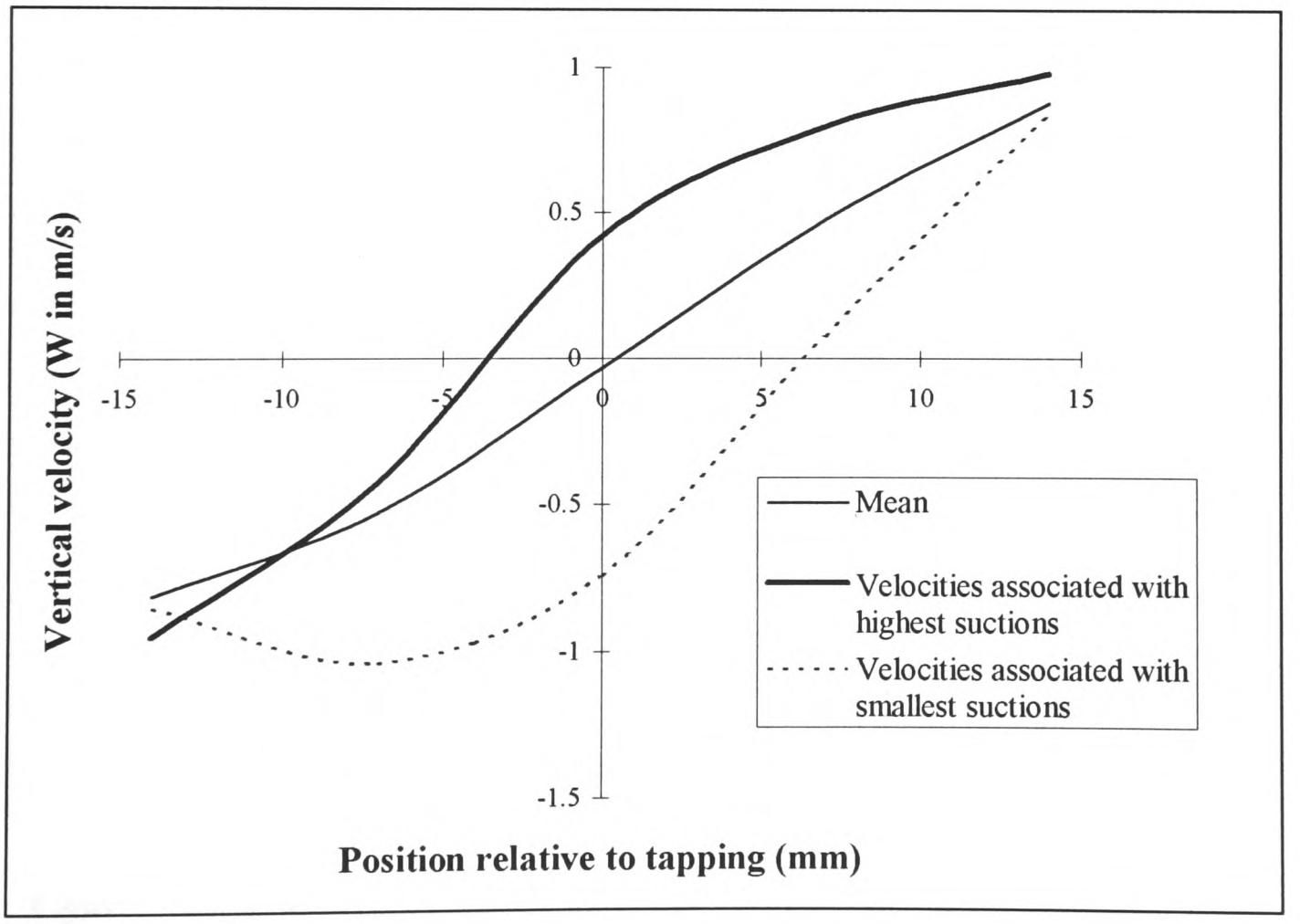

Figure 7-3 Vertical velocities 0.5h downstream (w = 0 shows vortex axis)

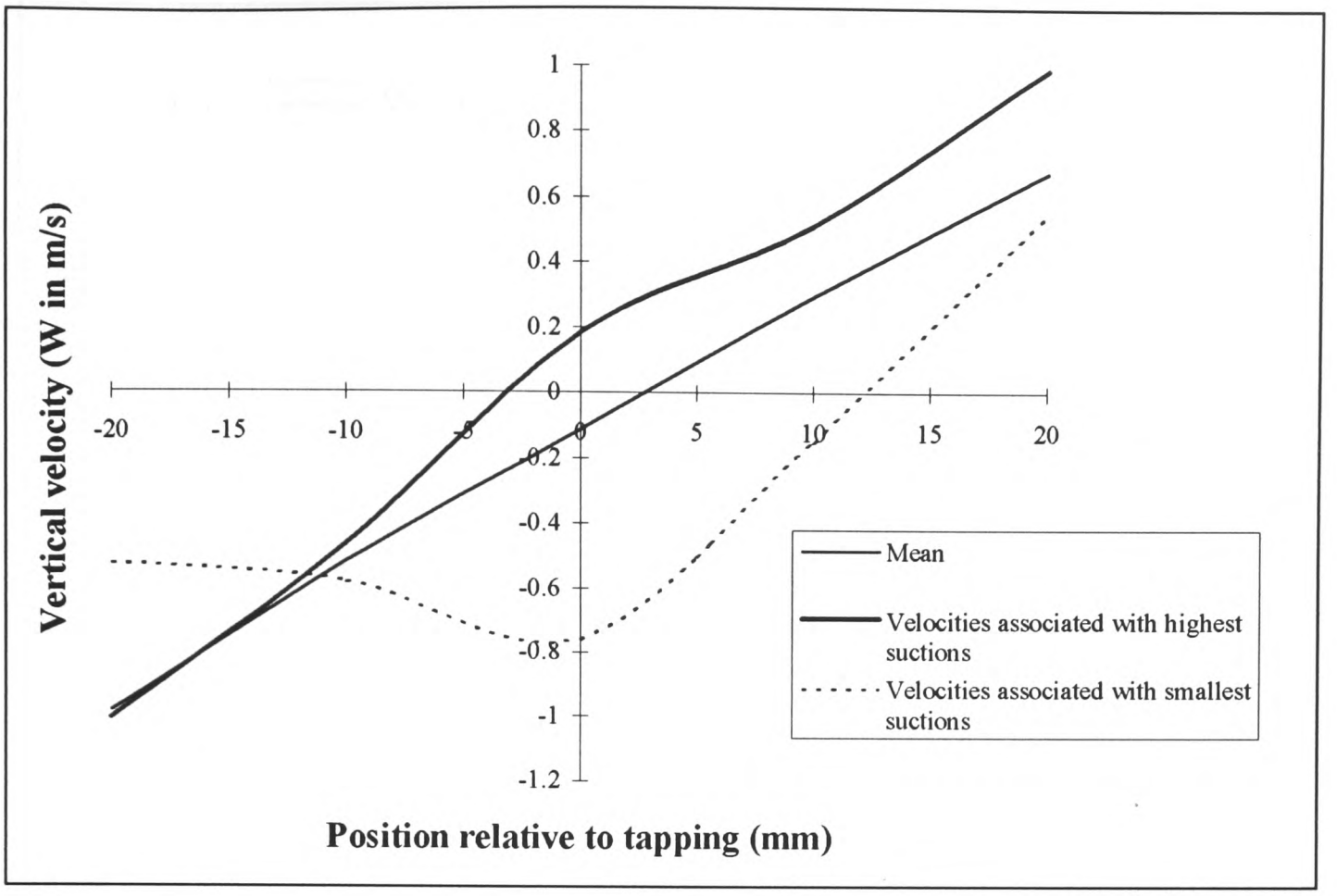

Figure 7-4 Vertical velocities 0.75h downstream (w = 0 shows vortex axis)

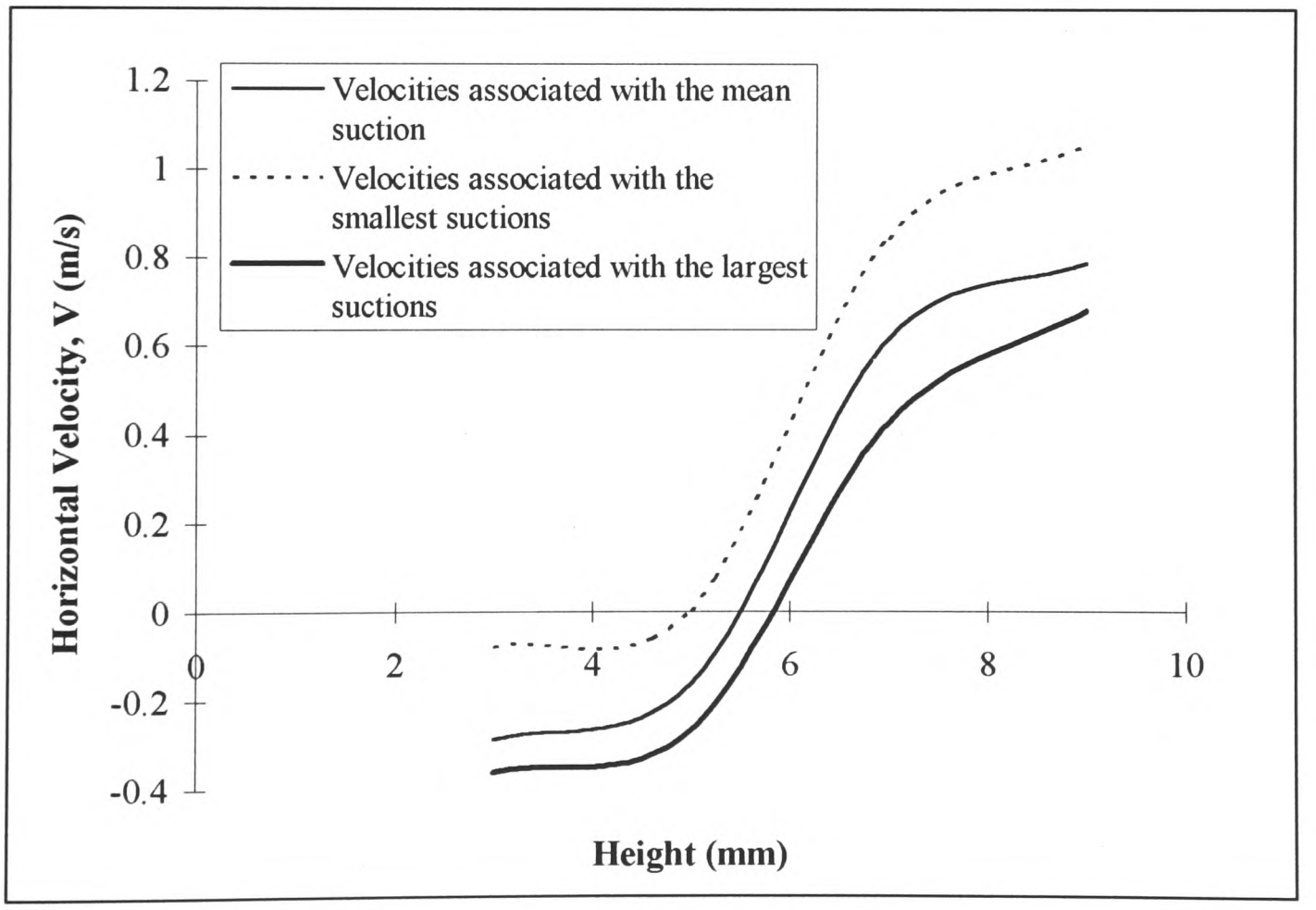

Figure 7-5 Horizontal velocities 0.25h downstream (v = 0 shows axis height)

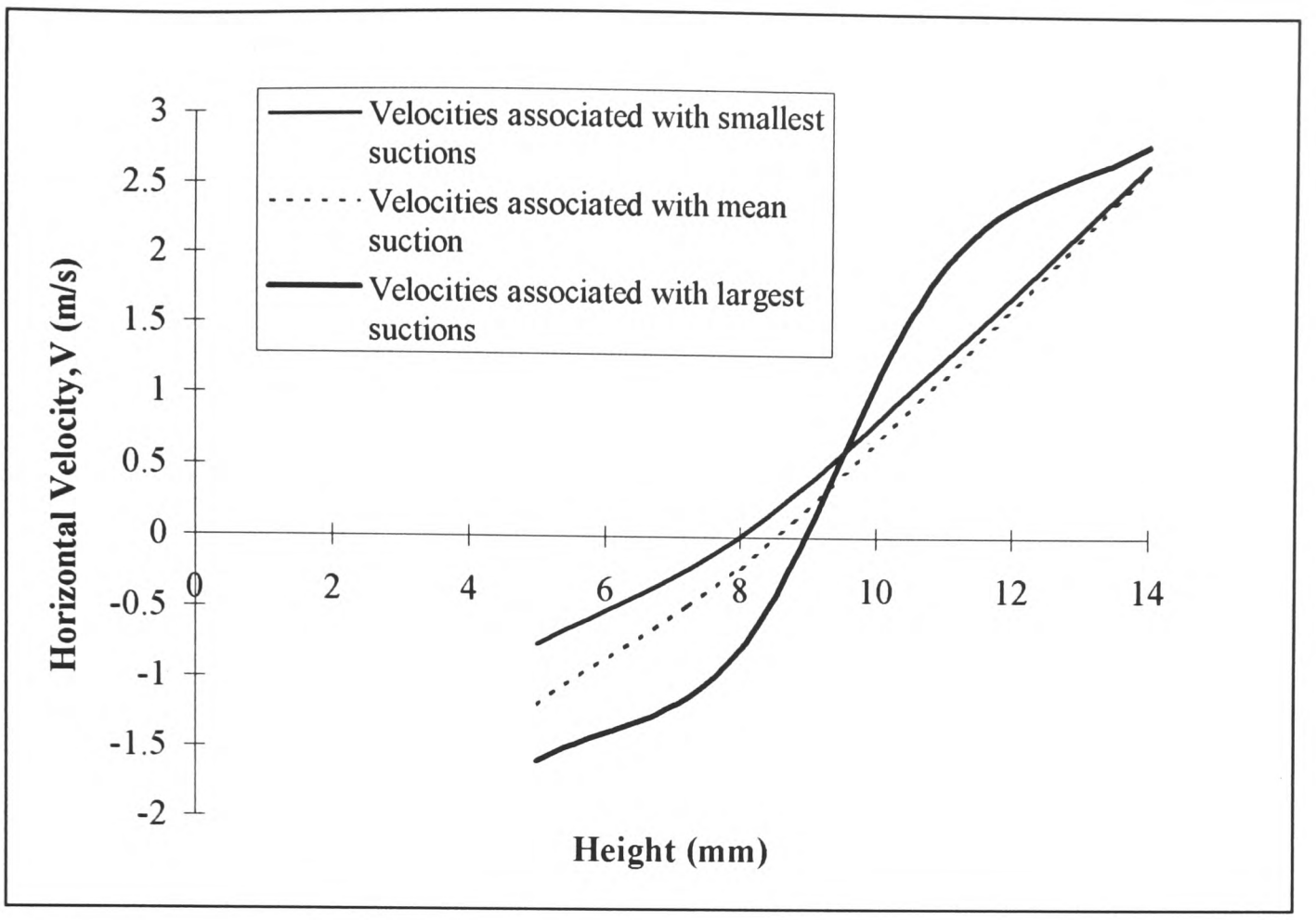

Figure 7-6 Horizontal velocities 0.5h downstream (v = 0 shows axis height)

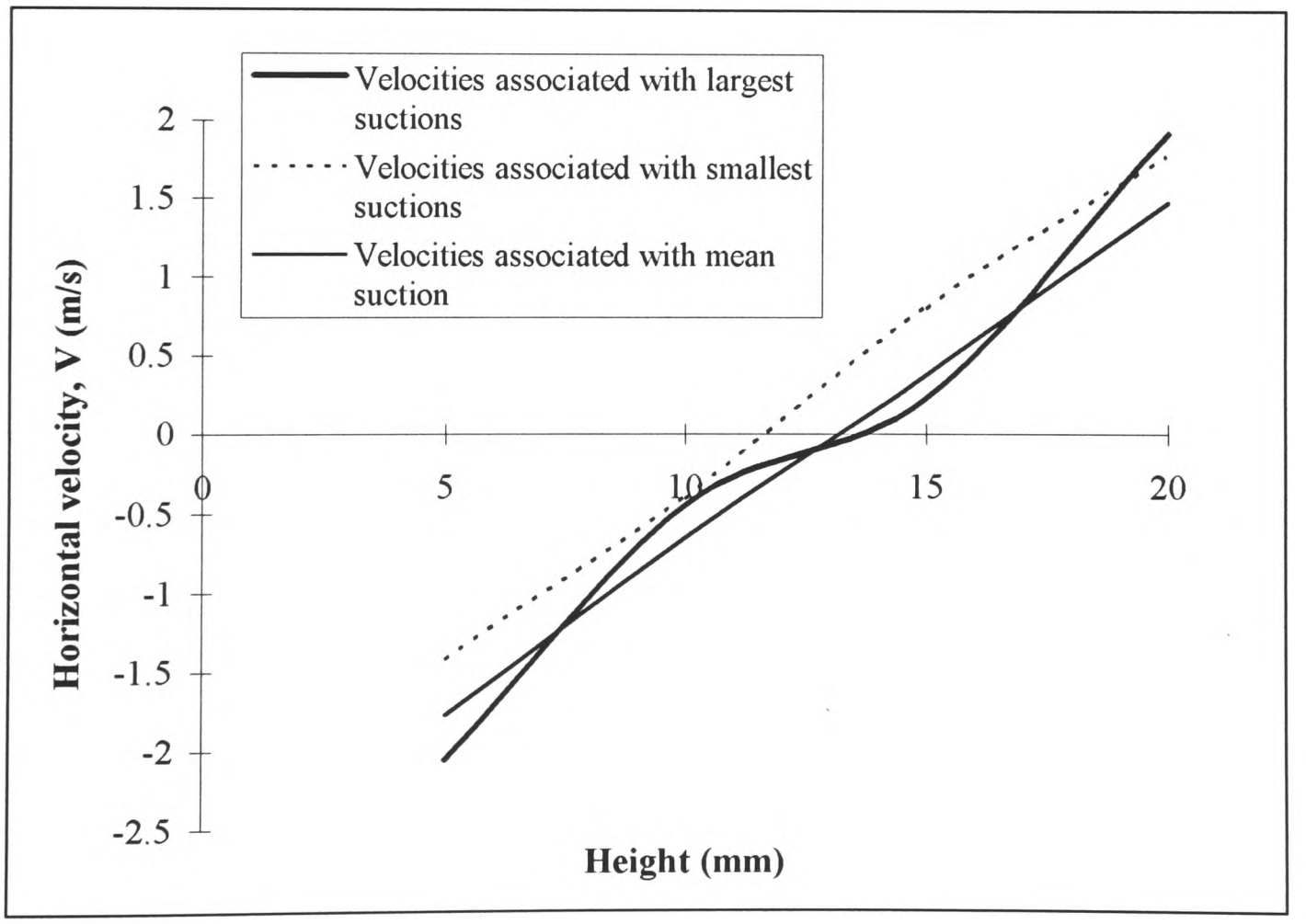

Figure 7-7 Horizontal velocities 0.75h downstream(v = 0 shows axis height)

7.2.1.2 Low turbulence onset flow results

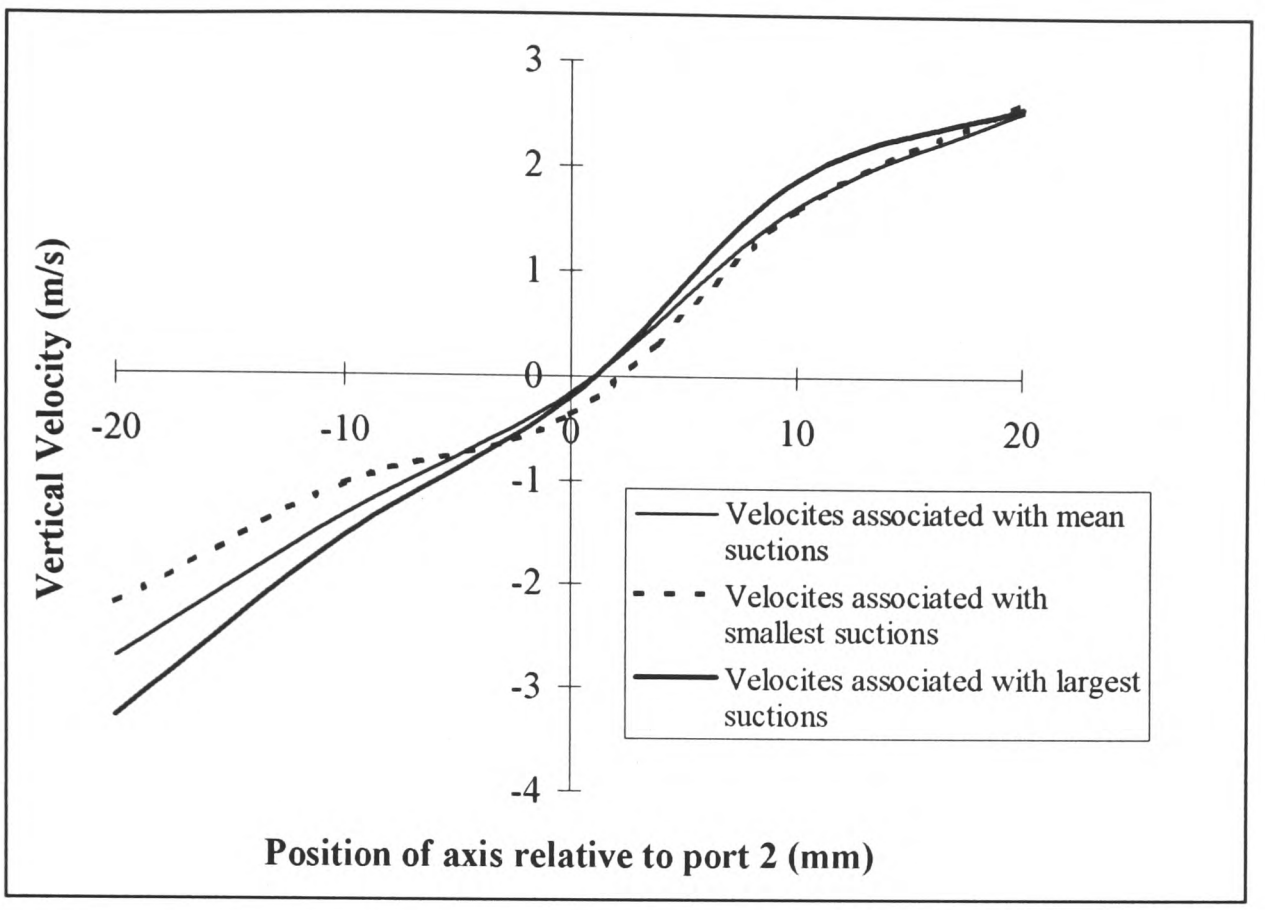

Figure 7-8 Vertical velocities 0.25h downstream (w = 0 shows vortex axis)

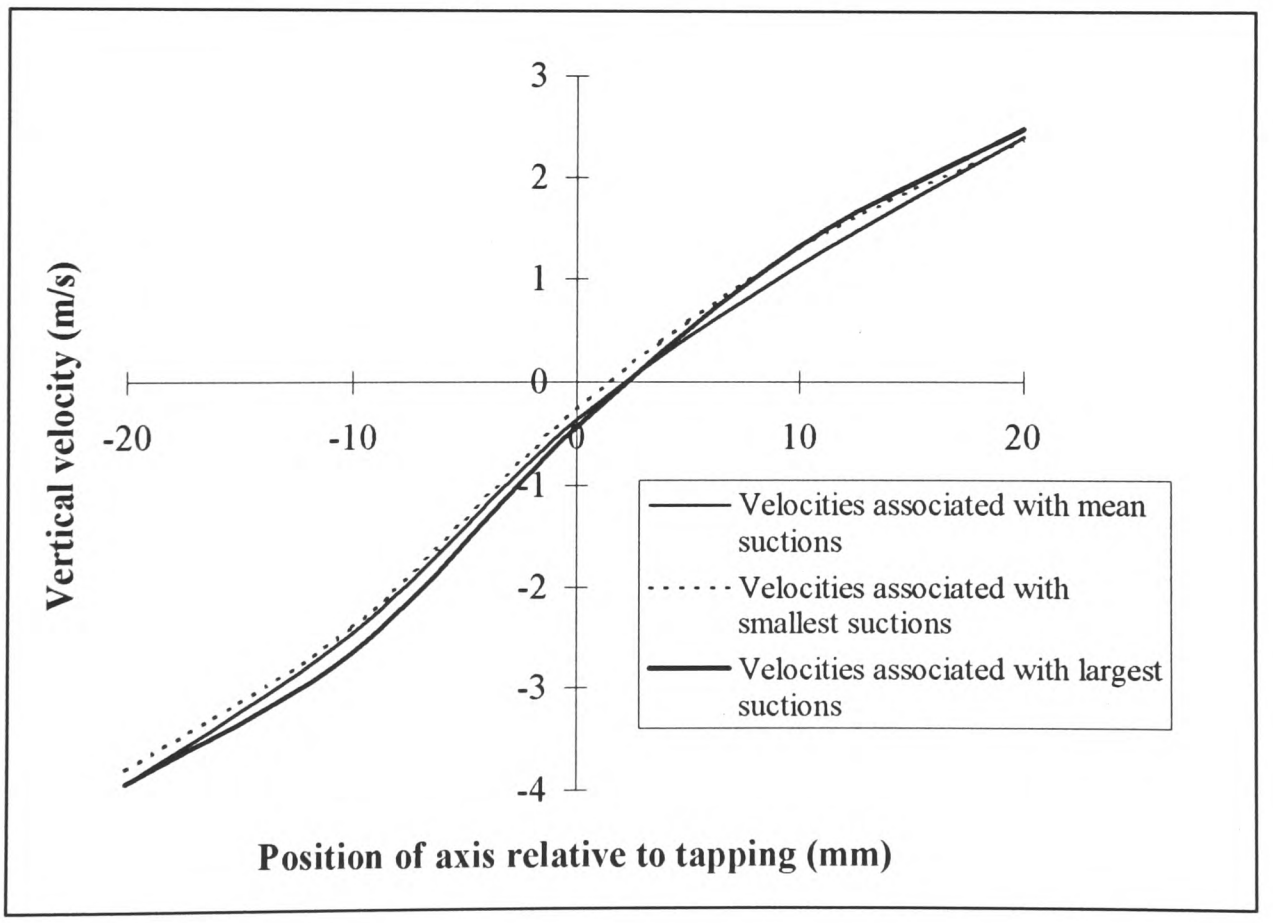

Figure 7-9 Vertical velocities 0.5h downstream (w = 0 shows vortex axis)

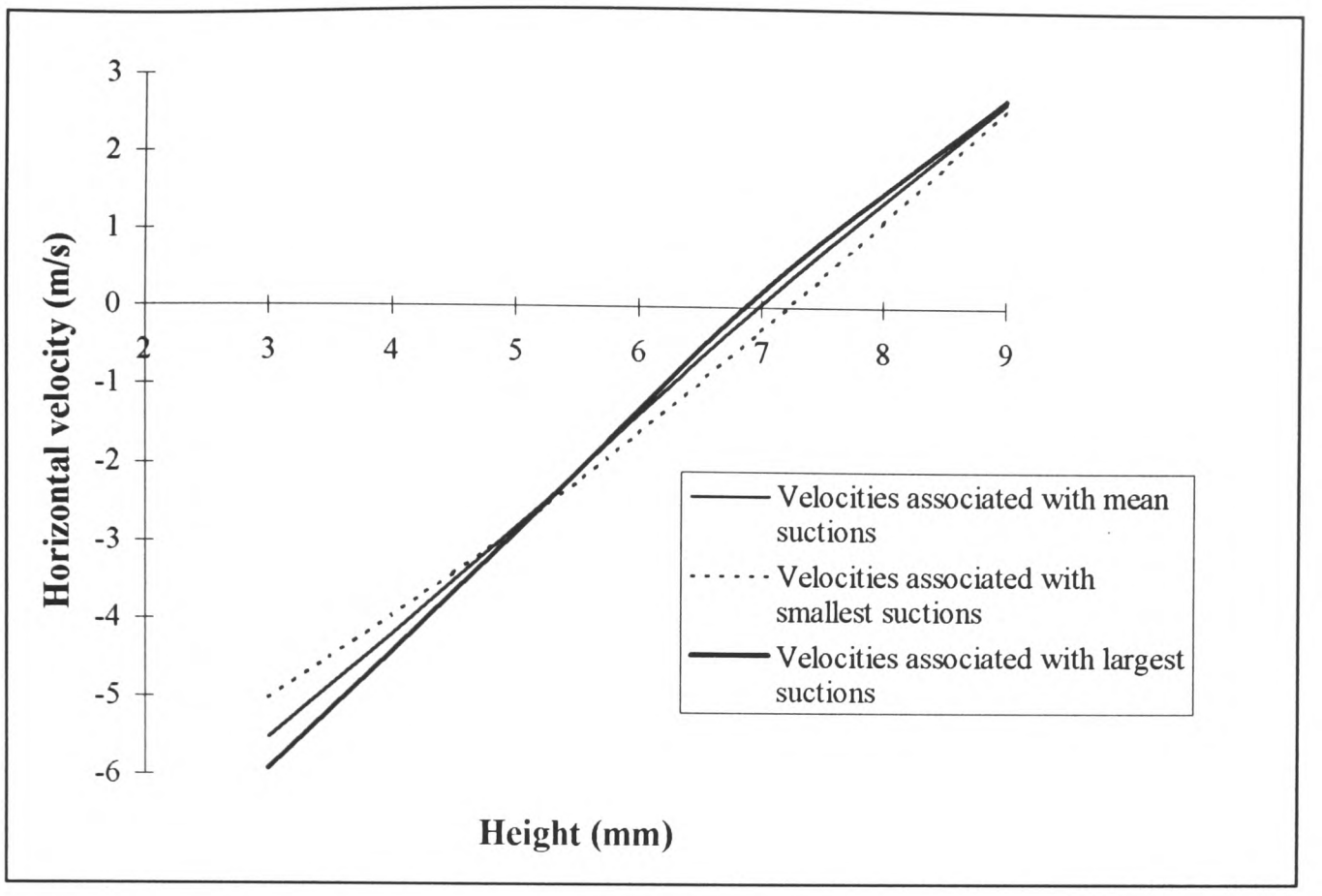

Figure 7-10 Horizontal velocities 0.25h downstream (v = 0 shows vortex height)

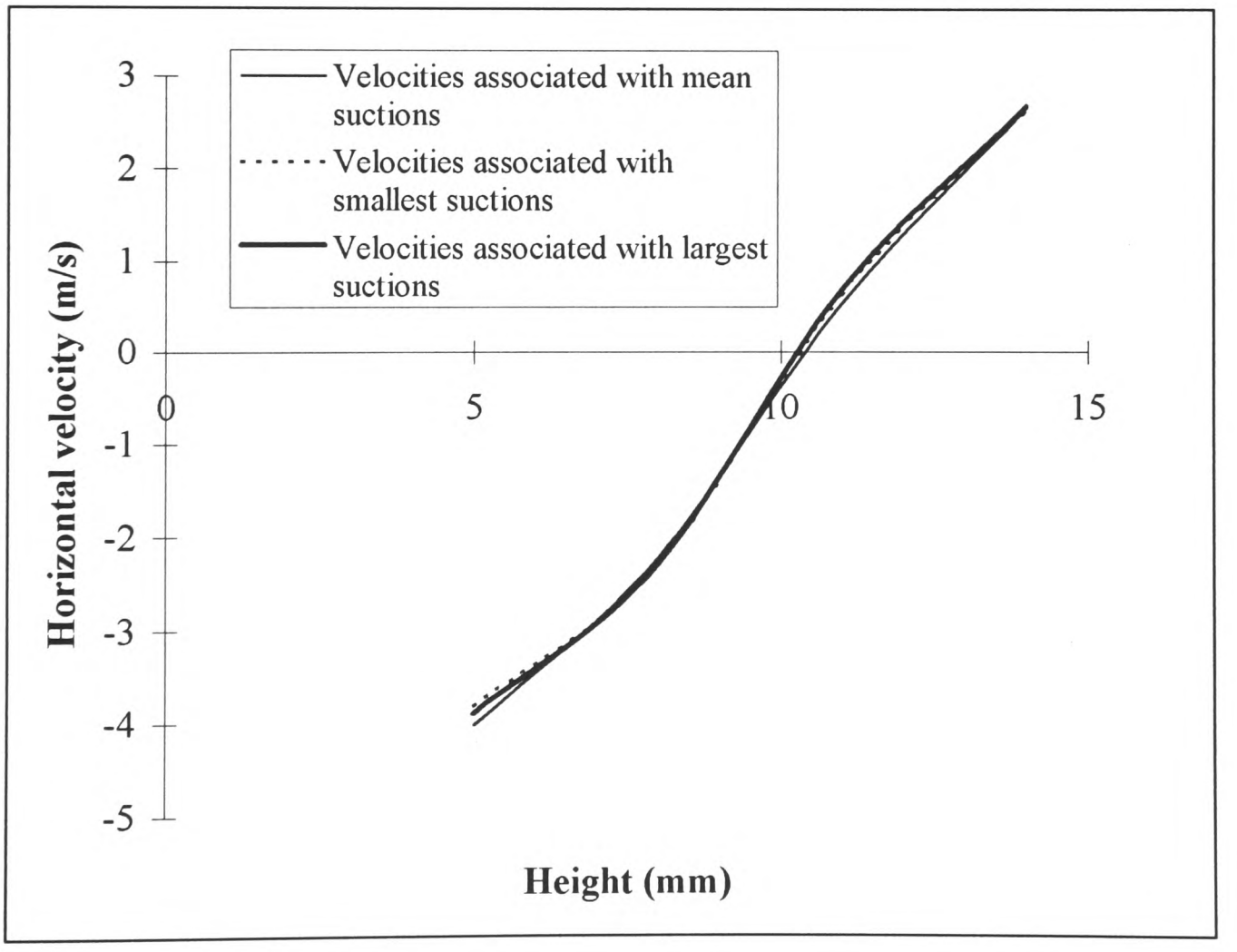

Figure 7-11 Horizontal velocities 0.5h downstream (v = 0 shows vortex height)

7.3 Discussion of results

The results presented in sections 7.2.1 and 7.2.2 highlight a number of interesting aspects of vortex behaviour which are discussed in the following sections.

7.3.1 Effect of onset turbulence

Variations in vortex position are greater in the high turbulence flow than in the low turbulence flow. Therefore, the vortex movement is driven by onset turbulence.

7.3.2 Ratio of lateral position variation to vertical position variation

The measured variations in horizontal position are larger than the variations in vertical position. This is the flow mechanism which produces the elliptical appearance of the vortex in the mean velocity vector plots (see chapter 4).

7.3.3 Vortex intermittency

Both the vertical and lateral pressure-conditional mean velocities show changes of direction, even when the highest surface pressures are considered. This means that the typical flow event constructed by pressure-conditional velocities within the conditional data set is a recirculating vortical structure.

This is somewhat contrary to the results discussed in section 5.5 (see Fig 5-25), which suggested that the presence of the vortex is intermittent. This contrast may be due to a vortex being present, albeit at varying strengths, for all but very short periods. The pressure-conditional velocities used to determine vortex position were calculated from data sets comprising 2.5% of the entire measurement sample, whereas the pressure-conditional mode velocity plot in Fig 5-25 (b) is based on conditional data sets containing 10% of the

measurement sample. The apparent absence of recirculation in Fig 5-25 (b) is most likely to be due to the reversed flow in the vortex occurring below the lowest measurement location.

7.3.4 Pressure-conditional vortex position relative to the roof edge

Lower surface pressures are produced when the vortex core is further from the edge of the roof. This observation supports the findings of Tieleman et al[1992]. Tieleman's work showed that although the maximum mean suctions under a corner vortex occurred on a ray at 15^0 to the roof edge, peak instantaneous suctions occurred on a ray at 18^0 to the roof edge.

7.3.5 Pressure-conditional vortex height relative to the roof surface

Lower surface pressures are produced when the vortex axis is further from the model surface. This was the most surprising outcome of the vortex position measurements. Conventional vortex theory predicts that, for a vortex of constant strength, the lowest pressures occur on a surface when the vortex is closest to that surface. Therefore, the conical vortex must increase in strength when the lowest surface pressures occur. This increase in strength was measured in the experiments discussed in section 5.5. The pressure-conditional velocity component histograms (Figs 5-7 to Fig 5-24) show that velocities in the vortex increase when lower surface pressures occur.

8. Quasi-steady vortex behaviour

Sections 4.4 and 4.5 showed that both the time averaged vortex position and mean surface pressures varied with mean onset wind angle. The mean position of the vortex axis was found to be furthest from the roof edge and roof surface when the mean onset angle was more perpendicular to the leading edge of the model.

The pressure-conditional vortex position results discussed in sections 7.3.4 and 7.3.5 showed that lower instantaneous surface pressures occur when the axis of the conical vortex is further from the roof edge and higher from the roof surface.

This chapter aims to test quasi-steady theory to relate the time averaged variables measured in Chapter 4 to the instantaneous variables measured in Chapter 7.

8.1 Quasi-steady theory

Quasi-steady theory is based on the assumption that the surface pressures generated on a building respond to atmospheric turbulence as if the gusts were merely differences in mean wind speed and direction. Thus, it is implied that instantaneous pressures correspond to instantaneous wind velocity vectors.

If Quasi-steady theory is valid then the instantaneous pressure, p(t), is given by:

$$p(t) - p_{datum} = \tfrac{1}{2}\rho V(t)^2 \overline{Cp}(\alpha(t),\beta(t)) \qquad (8.1)$$

p_{datum} is the pressure that measured values are being compared to. e.g. transducer back pressure.

V(t) is the magnitude of instantaneous wind velocity.

$\overline{Cp}(\alpha(t),\beta(t))$ is the quasi-steady pressure coefficient for the instantaneous wind directions, pitch, $\alpha(t)$ and azimuth, $\beta(t)$. This is determined by measuring time averaged pressure coefficients for specific mean azimuth and pitch angles.

The magnitude, V(t), of the wind velocity vector is given by:

$$V(t)^2 = (U+u)^2 + v^2 + w^2 \tag{8.2}$$

U is the mean onset wind speed.

u, v and w are the streamwise, lateral and vertical fluctuating velocity components which result from turbulence.

Expanding equation (8.2),

$$V^2(t) = U^2 + 2Uu + u^2 + v^2 + w^2 \tag{8.3}$$

u, v and w are very much smaller than U and so second order terms containing them contribute little to the value of $V^2(t)$. Therefore,

$$V^2(t) \approx U^2 + 2Uu \tag{8.4}$$

The instantaneous pitch and azimuth onset flow angles deviate from the mean wind directions $\bar{\alpha}$ and $\bar{\beta}$ due to the turbulence components u, v and w.

$$\alpha(t) = \bar{\alpha} + \tan^{-1}\left(\frac{w}{U+u}\right) \tag{8.5}$$

$$\beta(t) = \bar{\beta} + \tan^{-1}\left(\frac{v}{U+u}\right) \tag{8.6}$$

Substituting equations (8.4), (8.5) and (8.6) in (8.1) produces the equation:

$$p(t) - p_{datum} \approx \tfrac{1}{2}\rho(U^2 + 2Uu)\left(\overline{Cp}(\bar{\alpha},\bar{\beta}) + \tan^{-1}\left(\frac{w}{U+u}\right)\frac{\partial\overline{Cp}}{\partial\alpha} + \tan^{-1}\left(\frac{v}{U+u}\right)\frac{\partial\overline{Cp}}{\partial\beta}\right) \qquad (8.7)$$

Dividing each side of equation (8.7) by $\frac{1}{2}\rho U^2$ to obtain a pressure coefficient, and expanding, gives:

$$\begin{aligned} Cp\,(\alpha(t), \beta(t)) - Cp_{datum} \approx\ & \overline{Cp}(\bar{\alpha}, \bar{\beta}) + \tan^{-1}\left(\frac{w}{U+u}\right)\frac{\partial\overline{Cp}}{\partial\alpha} + \tan^{-1}\left(\frac{v}{U+u}\right)\frac{\partial\overline{Cp}}{\partial\beta} \\ & + \left(\frac{2u}{U}\right)\overline{Cp}(\bar{\alpha}, \bar{\beta}) + \left(\frac{2u}{U}\right)\tan^{-1}\left(\frac{w}{U+u}\right)\frac{\partial\overline{Cp}}{\partial\alpha} \\ & + \left(\frac{2u}{U}\right)\tan^{-1}\left(\frac{v}{U+u}\right)\frac{\partial\overline{Cp}}{\partial\beta} \end{aligned} \qquad (8.8)$$

For small angles $\tan x \approx x$ (in radians). Deviations from the mean flow angles are generally small (although at times large deviations, such as those discussed in chapter 6 invalidate this assumption) and so substituting this approximation and discarding small second order terms gives:

$$Cp(\alpha(t),\beta(t)) - Cp_{datum} \approx \left(1 + \frac{2u}{U}\right)\overline{Cp}(\bar{\alpha},\bar{\beta}) + \left(\frac{w}{U+u}\right)\frac{\partial\overline{Cp}}{\partial\alpha} + \left(\frac{v}{U+u}\right)\frac{\partial\overline{Cp}}{\partial\beta} \qquad (8.9)$$

Time averaging equation (8.9) produces the expected result:

$$\overline{Cp(\alpha(t),\beta(t))} = \overline{Cp}(\bar{\alpha},\bar{\beta}) \qquad (8.10)$$

u, v and w are assumed to be independent and so can be expressed as component turbulence intensities, I_u, I_v and I_w. Using these turbulence intensities the following equation for the fluctuating pressure coefficient, σ_{Cp}, can be produced:

$$\sigma_{Cp} \approx \sqrt{(2I_u Cp(\bar{\alpha}, \bar{\beta}))^2 + \left(I_w \frac{\partial Cp}{\partial \alpha}\right)^2 + \left(I_v \frac{\partial Cp}{\partial \beta}\right)^2} \qquad (8.11)$$

$\frac{\partial \overline{Cp}}{\partial \beta}$ and $\overline{Cp}(\beta)$ data is readily available from a large number of full scale and model scale investigations (see section 2.1). However, $\frac{\partial \overline{Cp}}{\partial \alpha}$ and $\overline{Cp}(\alpha)$ data has not been widely reported to date.

Due to the paucity of pitch angle data, the α terms in equation (8.11) are typically neglected. This is deemed to be acceptable because near to the ground the vertical turbulence has approximately half the magnitude of the horizontal turbulence. Hence, terms containing α are assumed to be relatively small.

The work of Letchford and Marwood[1995] presents measured $\frac{\partial \overline{Cp}}{\partial \alpha}$ data. This data was obtained by varying mean pitch angle by tilting the roof of a specially designed model. $\frac{\partial \overline{Cp}}{\partial \alpha}$ terms were found to be small compared to the mean and $\frac{\partial \overline{Cp}}{\partial \beta}$ terms. Therefore, the previous assumption that α terms can be neglected from quasi-steady equations is valid and equations (8.9) and (8.11) can be simplified to:

$$Cp(\alpha(t),\beta(t)) - Cp_{datum} \approx \left(1 + \frac{2u}{U}\right)\overline{Cp}(\bar{\beta}) + \left(\frac{v}{U+u}\right)\frac{\partial \overline{Cp}}{\partial \beta} \qquad (8.12)$$

$$\sigma_{Cp} \approx \sqrt{(2I_u \overline{Cp}(\bar{\beta}))^2 + \left(I_v \frac{\partial \overline{Cp}}{\partial \beta}\right)^2} \qquad (8.13)$$

Figs 8-1 and 8-2 are figures from Letchford and Marwood[1995]. These plots compare measured σ_{Cp} values with those predicted by equations (8.11) and (8.13). The graphs show that the quasi-steady predictions without the I_w term included (equation (8.13)) are more accurate.

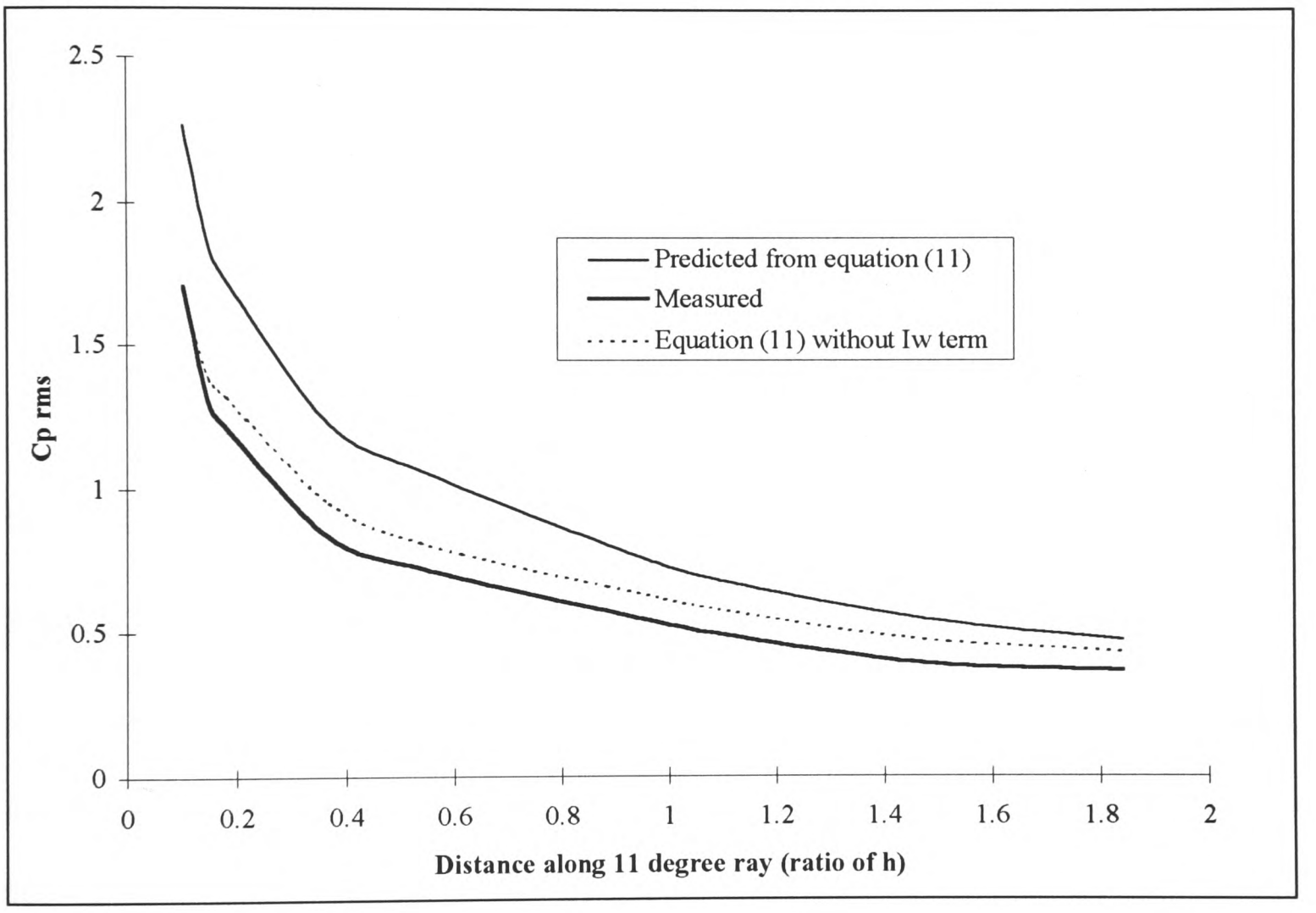

Figure 8-1 Comparison of measured and quasi-steady predicted pressures

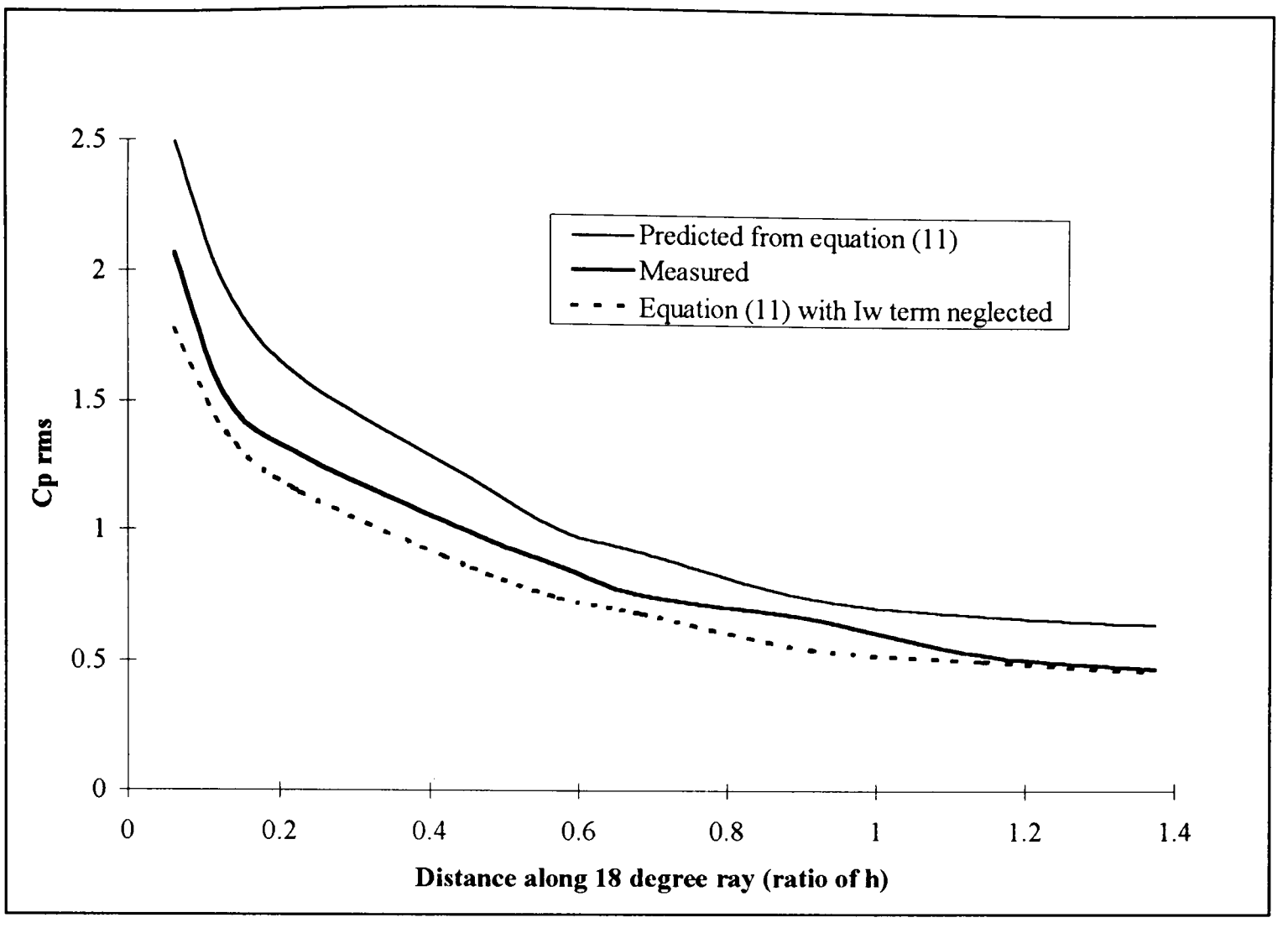

Figure 8-2 Comparison of measured and quasi-steady predicted pressures

8.2 Distortion of turbulence

8.2.1 Building generated turbulence

For the quasi-steady assumption to hold, all velocity fluctuations, and therefore pressure fluctuations must occur only as a result of turbulence in the onset flow. However, the onset flow is distorted as it flows over and around the building, by the presence of the building itself. This distortion is commonly termed 'building generated turbulence'.

The effect of such building generated turbulence is illustrated by considering peak pressures. Quasi-steady theory predicts that peak suctions on a building are the result of the largest velocity gusts in the onset flow. If we define the gust factor, G as:

$$G = \frac{u_{peak}}{U} \tag{8.14}$$

Quasi-steady theory predicts:

$$Cp_{peak} = \overline{Cp} \times G^2 \tag{8.15}$$

The accuracy of this prediction is tested by considering the pseudo-steady coefficient, Cp_{pseudo}, which is defined as:

$$Cp_{pseudo} = \frac{Cp_{peak}}{G^2} \tag{8.16}$$

Clearly if all pressure fluctuations are due to onset turbulence, equation (8.15) predicts that:

$$Cp_{pseudo} = \overline{Cp} \tag{8.17}$$

However, as reported in Letchford et al[1993], $\left|Cp_{pseudo}\right| > \left|\overline{Cp}\right|$. This indicates that onset turbulence is being enhanced by building generated turbulence.

8.2.2 Effect of building generated turbulence on quasi-steady assumption

Quasi-steady theory assumes that all pressure fluctuations on a building are caused only by velocity fluctuations in the onset wind. However, this assumption is invalidated by the generation of building generated turbulence.

An experiment was conducted in order to assess the degree to which the onset flow is distorted as it approaches the building. Onset velocity components (streamwise component, U, lateral component, V, and vertical component, W) and roof pressure were

simultaneously measured. The correlation between the velocity components and the magnitude of the roof suction was then calculated.

The measurements were carried out using two different building models, the 200mm cubic model used previously in this thesis, and also a 300mm x 300mm x 140mm high model. The second of these models was the tilting roof model used in the experiments of Letchford and Marwood[1995].

Pressure was measured at tapping 1 on the cubic model (0.075h along a ray at 16^0 to the model edge) and 0.065h downstream of the leading apex at 18^0 to the roof edge on the Letchford and Marwood model. Both models were placed at 45^0 to the mean onset flow direction.

Correlations between each upstream velocity component and the corresponding roof pressure, for a range of upstream measurement positions, are shown in Figs 8-3 and 8-4.

Figs 8-3 and 8-4 show that the correlation between the roof suction and the lateral velocity component is high when the onset velocity is measured at small distances upstream of the model. There is also a significant correlation between the roof suction and the vertical velocity component. However, the correlation between roof suction and streamwise velocity is small.

The correlation between the roof suction and lateral and vertical velocity components increases with decreasing distance upstream of the model. In contrast, the correlation between the roof pressure and streamwise velocity component reduces at measurement locations close to the model. This reduction is due to the onset flow being deflected around and over the cube, distorting streamwise velocity into the lateral and vertical directions.

The strong correlation between roof suction and the lateral velocity component shows that instantaneous roof pressures are primarily governed by the azimuth angle, β, of the onset wind.

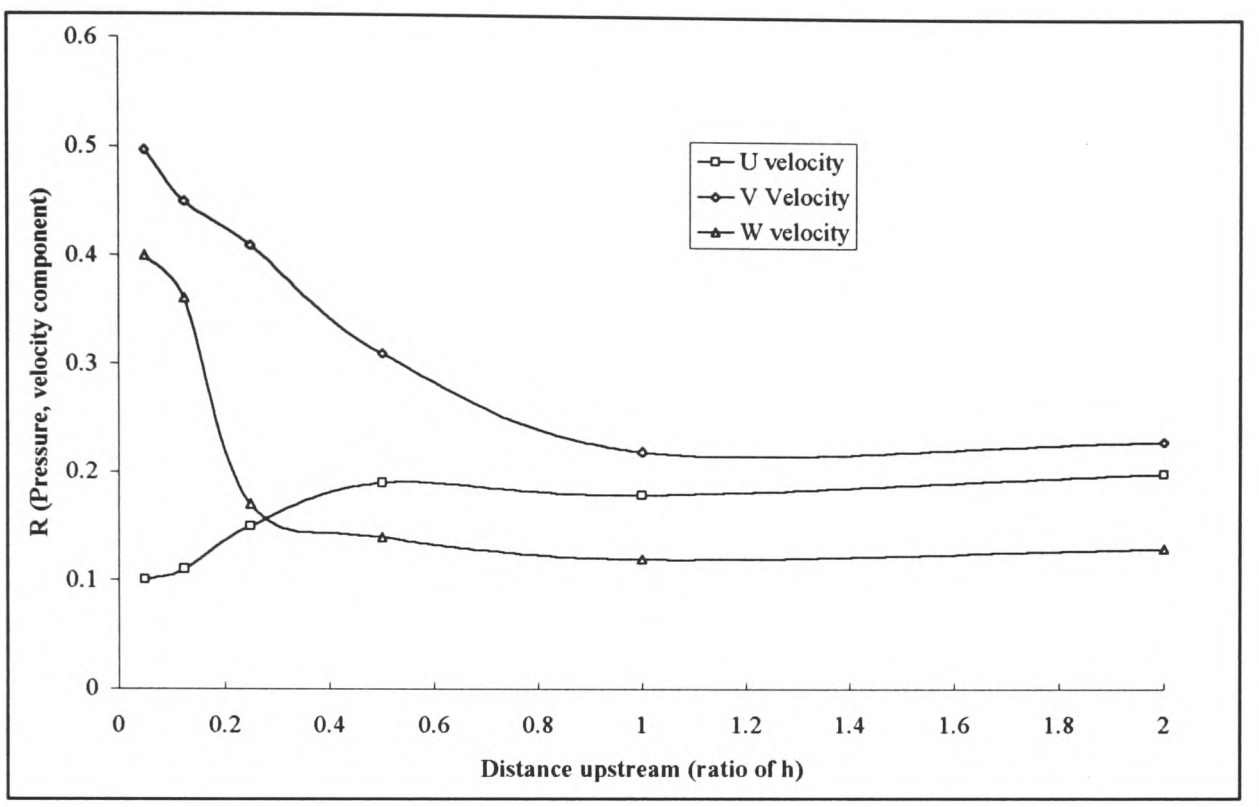

Figure 8-3 Correlation of roof pressure with upstream velocity components (200mm x 200mm cubic model)

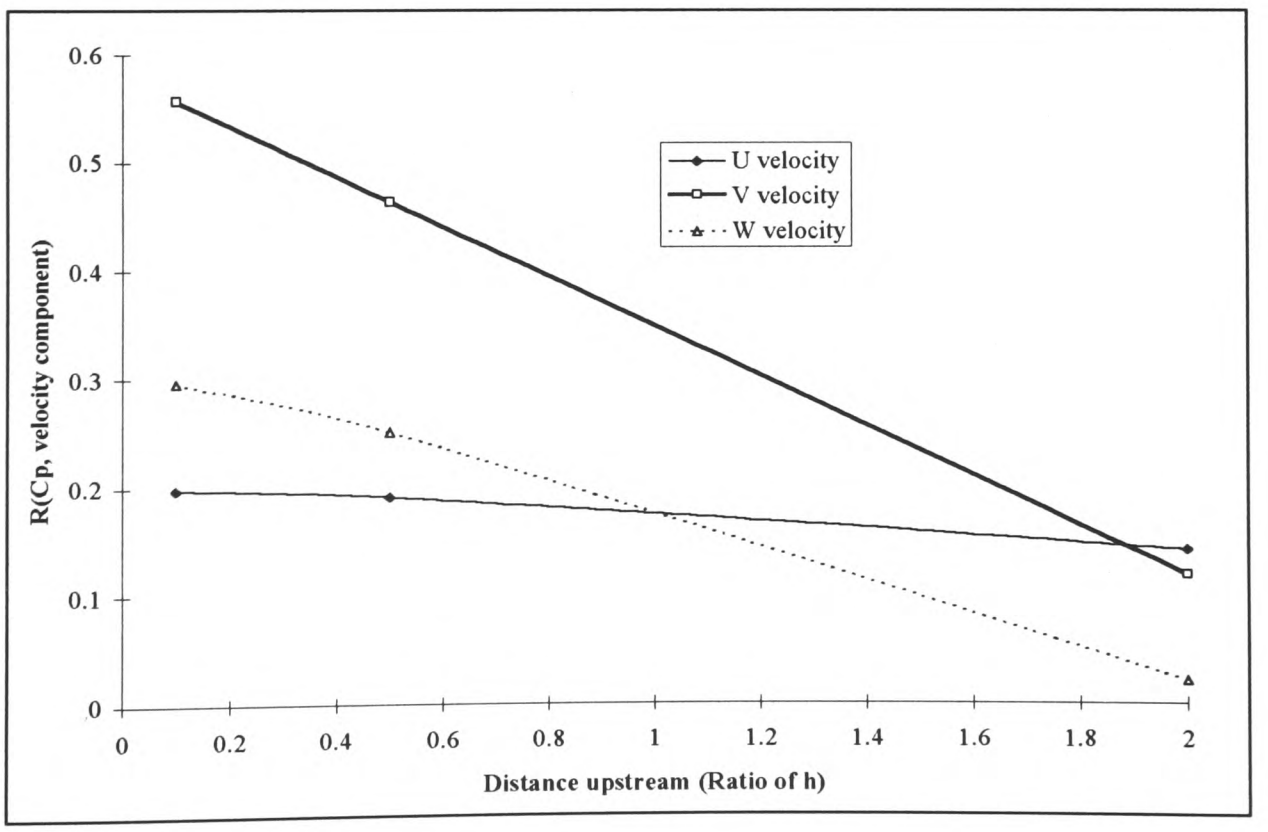

Figure 8-4 Correlation of roof pressure with upstream velocity components (300mm x 300mm model)

8.3 The applicability of the Quasi-steady assumption for conical vortex flow

In chapter 4 it was shown that the mean position of the vortex relative to the edge of the model varies with the mean azimuth angle of the onset flow. Mean pressure at a point on the roof was also shown to vary with mean azimuth angle. This suggests that roof pressure varies with vortex position. Also, from the results presented in section 8.2, it was concluded that instantaneous roof pressures are governed by instantaneous onset wind azimuth.

If instantaneous pressures respond to instantaneous azimuth angles in the same way that mean pressures respond to mean azimuth angle, then the central assumption of quasi-steady theory is valid.

An experiment was carried out to determine whether quasi-steady theory is applicable to pressures induced by conical vortices. Roof pressures were measured at tappings 1 and 3 on the 200mm cubic model and at the same time, measurements of the streamwise and lateral velocity components were made. The velocity components were measured with the LDA at model height, 50mm (0.25h) upstream.

Conditional data sets were formed by sorting the data records into instantaneous azimuth angle ranges. The mean value of the pressures in each conditional set was calculated. In this way, angle-conditional mean pressures were calculated.

Fig 8-5 compares the angle-conditional mean pressures with the mean pressures measured by varying the mean onset azimuth angle (see section 4.5). The angle-conditional pressures and the mean azimuth pressures agree well, which shows that the quasi-steady assumption is valid.

It is noteworthy that at high azimuth angles ($\beta > 60^0$), the angle-conditional pressure coefficients are larger than the mean angle coefficients.

Richards et al[1995] showed that the value of $Cp(\bar{\beta})$ for regions of peak pressures must be obtained carefully. This is because instantaneous wind direction varies greatly and $Cp(\bar{\beta})$ actually includes a range of onset angles, $\beta \pm \delta\beta$. If the mean azimuth angle is the same as that which will produce the largest instantaneous suctions, then the directional variation will lead to a scenario where $|Cp(\bar{\beta})| < |Cp(\beta)|$.

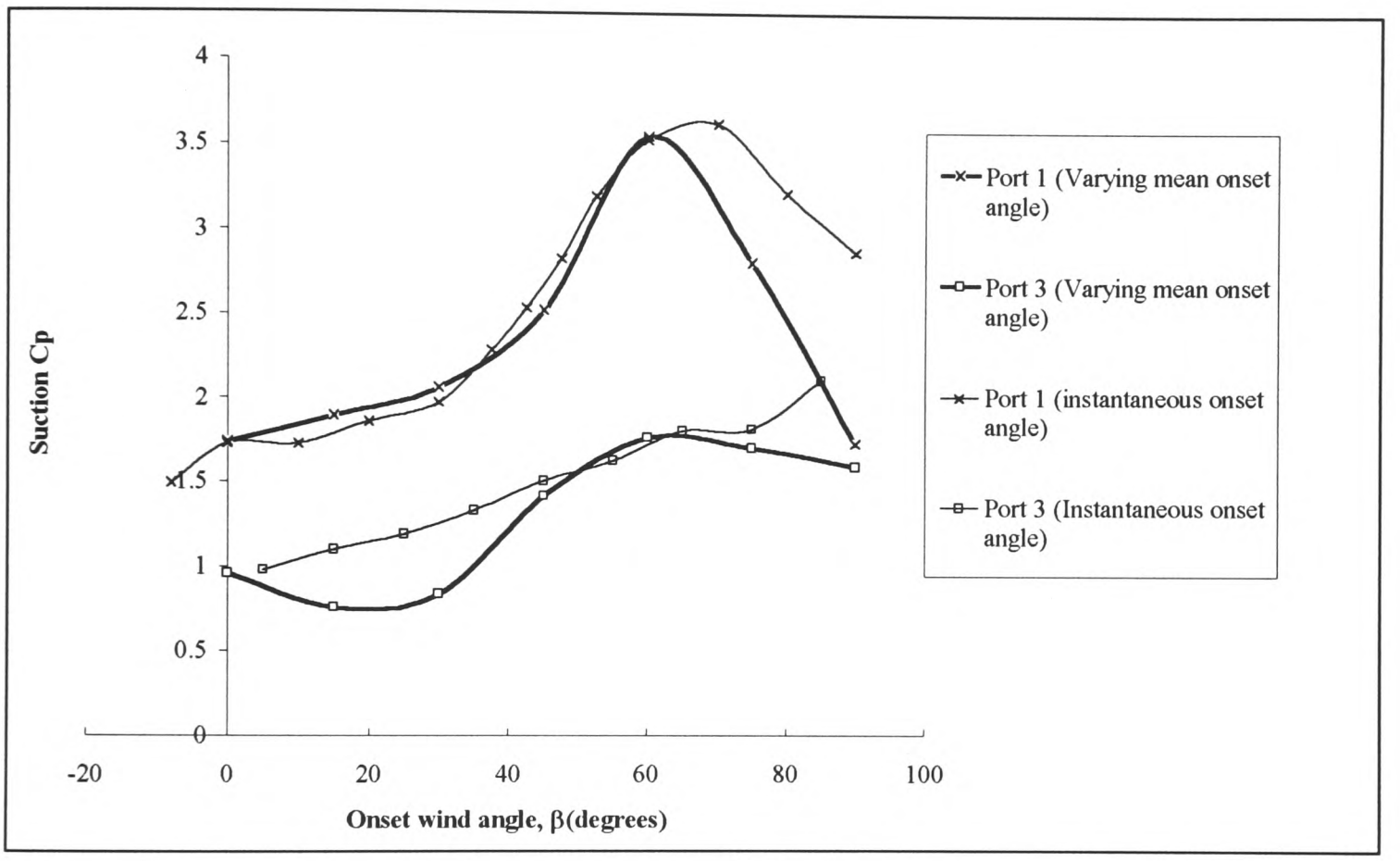

Figure 8-5 Instantaneous wind angle-conditional pressures

The experiment was repeated using the Letchford and Marwood model. This model has a roof which can be tilted to allow the mean pitch angle to be varied. Pitch angle-conditional pressures were compared to mean pitch angle pressures to confirm that pitch angle terms can be removed from the quasi-steady equations. Instantaneous pitch angle was determined by measuring vertical and streamwise velocities.

$$\alpha = \tan^{-1}\left(\frac{w}{u}\right) \tag{8.18}$$

Once again the model was placed at 45^0 to the onset flow. The onset velocities, and hence the onset pitch and azimuth angles, were measured 14mm (0.1h), 70mm (0.5h) and 280mm (2h) upstream of model height.

Figs 8-6 and 8-7 shows the Cp-β and Cp-α relationships for the Letchford and Marwood model.

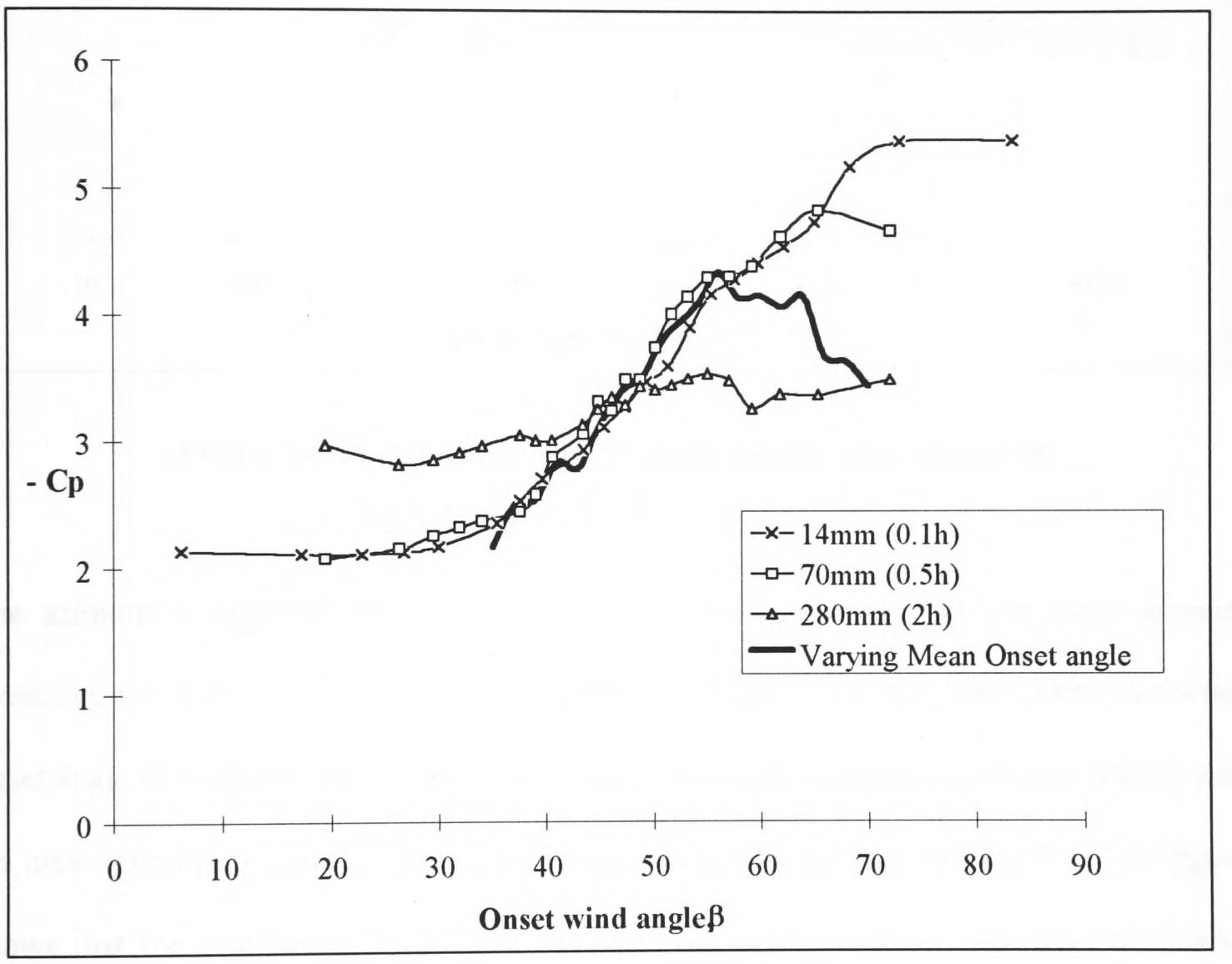

Figure 8-6 Instantaneous azimuth angle conditional pressures for Letchford and Marwood model

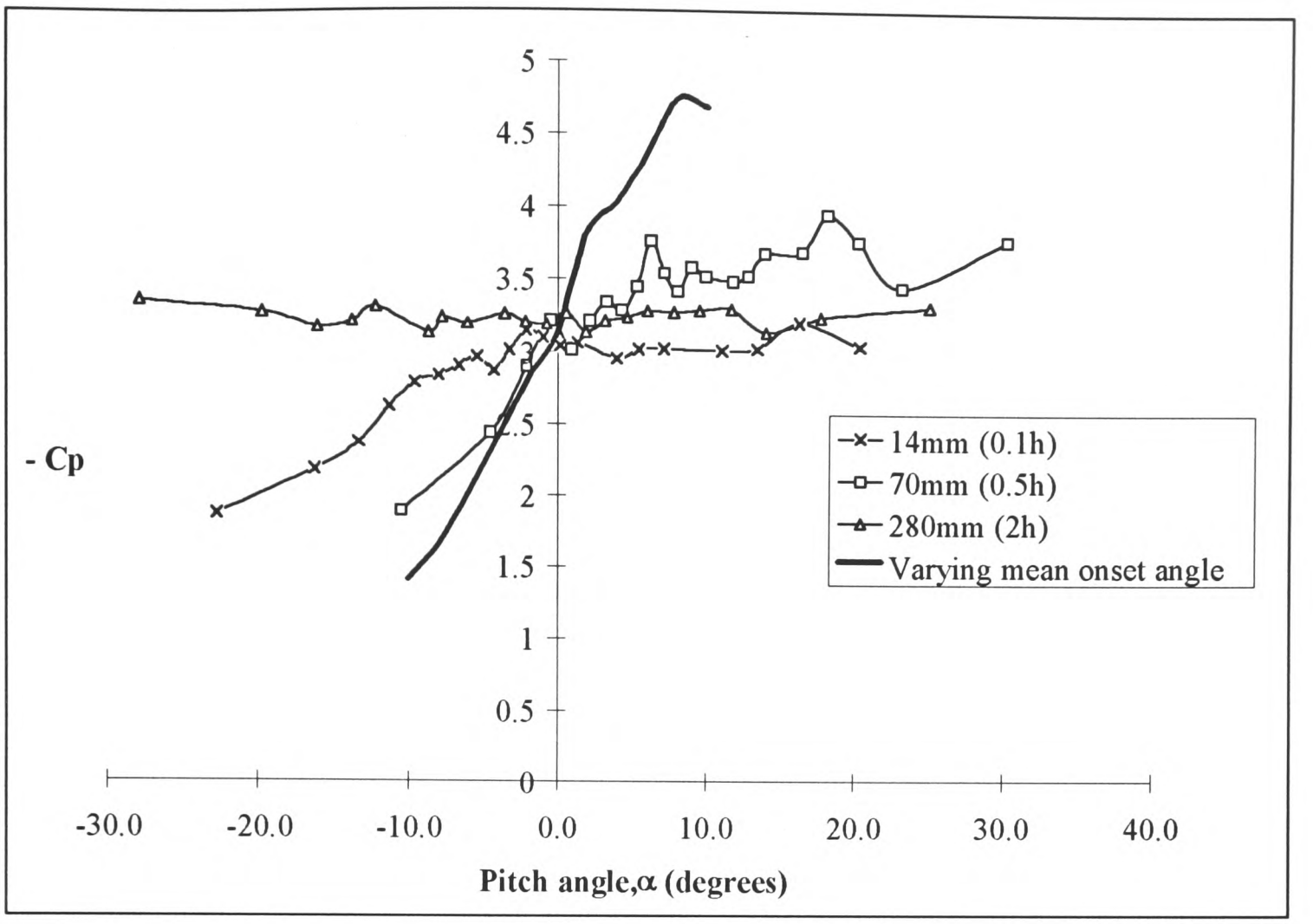

Figure 8-7 Instantaneous pitch angle conditional pressures for Letchford and Marwood model

The azimuth angle-conditional pressure are in good agreement with the mean azimuth pressures when the onset angle is measured at 0.1h and 0.5h upstream. However when onset angle is measured 2h upstream the angle-conditional pressures agree very poorly with the mean azimuth pressures. This result is not surprising if we consider Fig 8-4. This figure shows that the roof suctions correlate well with the upstream lateral velocity only within 0.5h of the model.

As with the measurements made using the 200mm cubic model, the azimuth angle-conditional pressures are lower than the mean azimuth pressure when $\beta > 55^0$.

The pitch angle-conditional data is presented in Fig 8-7. This shows that there is no agreement between pitch angle-conditional pressures and mean pitch angle pressures for any

upstream measurement locations. This can be explained by considering Fig 8-4, which shows that the vertical velocity component is only weakly correlated with roof pressures.

To summarise, the results in this section have shown that the conical vortices respond in a quasi-steady fashion to instantaneous azimuth angle, but not to instantaneous pitch angle.

Generally only azimuth angle is considered in design. The results presented in this section have shown that a quasi-steady model, which is the basis of all national design codes, is valid for instantaneous changes in azimuth angle. Vertical velocity component (and hence pitch angle) terms need not be included in the quasi-steady equations.

This section has highlighted a cause for concern regarding peak loads estimated by quasi-steady theory. At azimuth angles approaching perpendicular to the roof edge, the azimuth angle-conditional suctions have consistently been larger than the mean azimuth pressures.

9. Conclusions

This study has, for the first time, measured velocities in a conical roof edge vortex with a laser Doppler anemometer (LDA). Additionally, these measured velocities have been related to the pressures produced on the roof by the vortex.

A measurement system has been designed to simultaneously measure pressure and velocity. Also, a conditional data analysis technique has been developed to analyse the simultaneous pressure-velocity data.

9.1 Simultaneous velocity-pressure measurement technique

This study has developed a technique to link a pressure measurement system with a laser Doppler anemometer (LDA) velocity measurement system. This has allowed velocities in a conical vortex to be measured simultaneously with the pressures exerted on a surface beneath the vortex.

The LDA can only measure velocity at one location at a time. Mean flow patterns in the vortex can be studied by making LDA measurements at a number of locations. However, determining instantaneous vortex structure is problematic. Velocity measurements can only be made at one location at a time and, since measured instantaneous velocities are statistically random, no measurement run can be repeated. Therefore, velocity time series measured at various locations cannot be combined to construct a time history for the entire flow field. A conditional sampling technique has been developed to overcome this problem.

In conditional sampling, instantaneous velocities measured at a range of locations are referenced to surface pressures measured simultaneously at a single pressure tapping. It is then assumed that specific flow events produce specific surface pressure. Thus, by selecting

all the velocities that were measured at a specific reference pressure, the instantaneous flow pattern producing that specific surface pressure can be synthesised.

In the absence of Particle Image Velocimetry (PIV), which can measure the velocity field in a two dimensional plane rather than just at a single point, conditional analysis offers the best opportunity to study the effect of conical vortex structure on surface pressures.

9.2 Vortex Behaviour

As part of this work, mean velocities were measured in the conical vortex which is formed on the top surface of a sharp edged model in oblique flows. These measurements showed that the size, position and circulation of the vortex are strongly dependent on the azimuth angle of the model to the onset flow.

As the onset flow azimuth angle increases towards $\beta=90^0$, the vortex forms further from the roof edge and higher above the surface. The circulation of the vortex also appears to increase as the onset flow becomes more perpendicular to the separation edge.

An azimuth angle of 60^0 produces the lowest roof pressures. A subjective assessment of vortex circulation, based on observations of the mean velocity vector plots, suggests that an azimuth angle of 60^0 produces the most strongly circulating vortex.

Oblique azimuth angles produce a vortex with high mean axial velocities. As the azimuth angle increases the mean axial velocities in the vortex reduce.

Onset angle-conditional pressure measurements have shown that the vortex reacts to the instantaneous azimuth changes of onset gusts in the same way that it would to changes in mean onset flow. The instantaneous onset azimuth varies constantly and so the position of the vortex also varies constantly, both in relation to the roof edge and in height from the surface of the roof.

Very large changes in instantaneous azimuth angle can bring the onset flow parallel to one edge of the building. If this occurs, the vortex at that edge breaks down. This vortex intermittency has been observed in smoke visualisations at both model and full scale.

This vortex movement and intermittency, along with the accompanying changes in onset gust speeds, produces the large pressure fluctuations measured under conical roof edge vortices.

The lowest instantaneous surface pressures have been measured when the flow approaches being normal to the leading edge of the model. This is the onset flow that produces the biggest vortex, i.e. the vortex core position is furthest from the roof edge and roof surface.

The fact that the lowest pressures are produced when the vortex is further from the roof surface is perhaps the most surprising discovery of this work. Up to this point it has been thought that peak suctions are caused by the vortex being very close to the surface.

9.3 Quasi-steady modelling

Onset angle-conditional pressure measurements have shown that conical vortices react to instantaneous changes in onset azimuth angle in the same way that they would to changes of mean onset wind angle. Hence, the vortex behaviour is quasi-steady.

This quasi-steady behaviour does not apply to instantaneous pitch angle, but pressure fluctuations can be accurately predicted by the quasi-steady model without considering pitch angle terms.

In design codes, only azimuth angle is generally considered. The results presented in this thesis have shown that the quasi-steady model, which is the basis of all national design codes, is valid for instantaneous changes in azimuth angle.

The one question concerning quasi-steady modelling regards peak loads. When the instantaneous azimuth angle approaches being normal to the roof edge, the measured angle-conditional pressures were consistently lower than those that would be expected from mean onset flow measurements.

9.4 Suggestions for further work

This work could be enhanced greatly with PIV technology as PIV can provide simultaneous velocity vectors over an entire flow field. Although this technique has yet to be applied to wind engineering, all investigations suggest that it is likely that a system could be set up to achieve meaningful measurements.

The problem of overcoming the measurement problems that would be encountered in the Oxford boundary layer wind tunnel (such as seeding density in an open circuit wind tunnel, seeding wake or vortex regions and positioning of system components so as not to interfere with the flow being measured) could form a substantial part of a D.Phil. thesis, in the same way that simultaneous pressure-velocity measurement did in this thesis, or the use of LDA did in Minson[1994].

In the absence of PIV several avenues of research can still be pursued:

1. The investigation of normal separation bubbles ($\beta = 90^0$) by using simultaneous velocity-pressure measurements and conditional statistics. An important consideration would be seeding and data rate on the LDA. Separation bubbles are less stable than conical vortices and so high data rates would be necessary to detect vortex transience.

2. Further investigation of the discrepancy between $Cp(\beta)$ and $Cp(\bar{\beta})$ at high azimuth angles. This study would tie in closely with the investigation of normal separation bubbles described above.

3. The making of more extensive simultaneous pressure-velocity measurements in the vortex. This would allow better pressure-conditional velocity vector plots to be constructed. This exercise is similar to the one which could be undertaken using PIV, only much more time consuming.

Appendix A - Design against vortex effects

The main body of this thesis dealt in detail with the nature of roof edge vortices. This appendix looks at the significance of conical vortex induced loading to building design. Design strategies to reduce the high roof loads that the vortices cause are also discussed.

How important are vortex effects?

The loading induced by conical vortices is limited to roof edge regions, and contributes little to overall roof loads. However, the vortices can cause severe localised damage from which larger scale damage can propagate.

The damage caused to buildings by wind storms represents a large financial loss to society and a significant danger to lives. A Building Research Establishment (BRE) survey found that between 1962 and 1976 approximately £200 million of damage was caused (Cook[1985]). Another BRE study found that between 1962 and 1981 74 people were killed and 751 injured (and this statistic regarding the number injured is thought to an underestimate) by incidents directly attributable to wind.

Fig A-1 shows the breakdown by cause for fatal accidents and Fig A-2 a similar breakdown for injuries(data from Cook[1985]).

As Figs A-1 and A-2 show, failure of roofing materials, which are the principal interest of this thesis, is a major cause of fatal accidents and the primary cause of injury. The uses of modern building codes already mean that the majority of structures can withstand the structural loading imposed by even the strongest winds. This was demonstrated during the 'Great Storm' in the South of England, on the 15th and 16th of October 1987. In this storm no structures that had been designed with reference to

wind loading codes were significantly structurally damaged (structural damage being defined as damage that reduces the stability of the building). However, there were many cases of damage to cladding, roof tiles, aerials and chimneys and 10 people were killed and many more injured.

Clearly, although such 'minor' damage does not effect the integrity of the building, it must be reduced because the cost of such failures can be high, both financially and in terms of danger to life. Much of this localised damage is the result of vortex action and so work furthering the understanding of damage mechanisms must be incorporated into design codes.

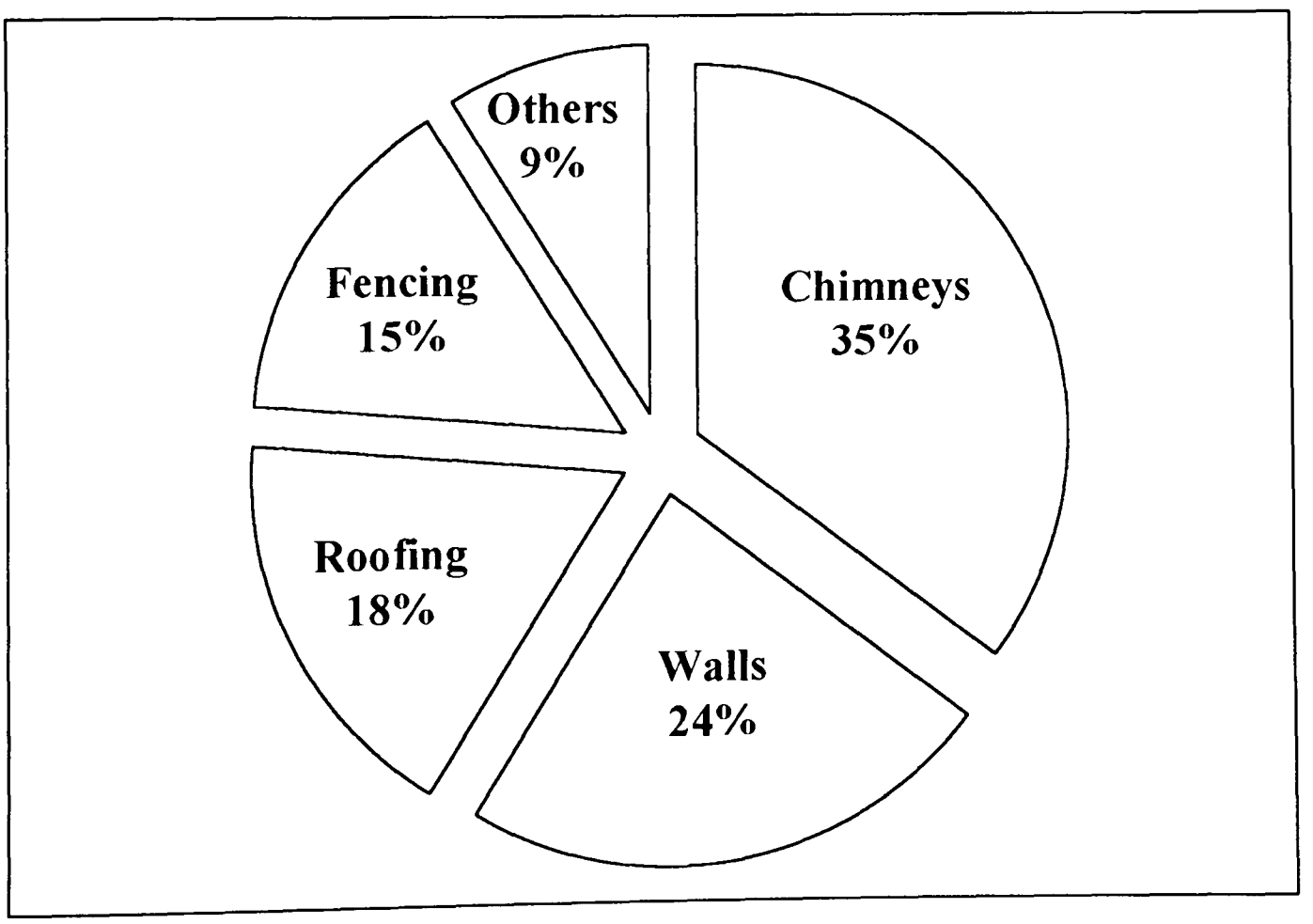

Figure A-1 Breakdown of causes of fatal wind related accidents

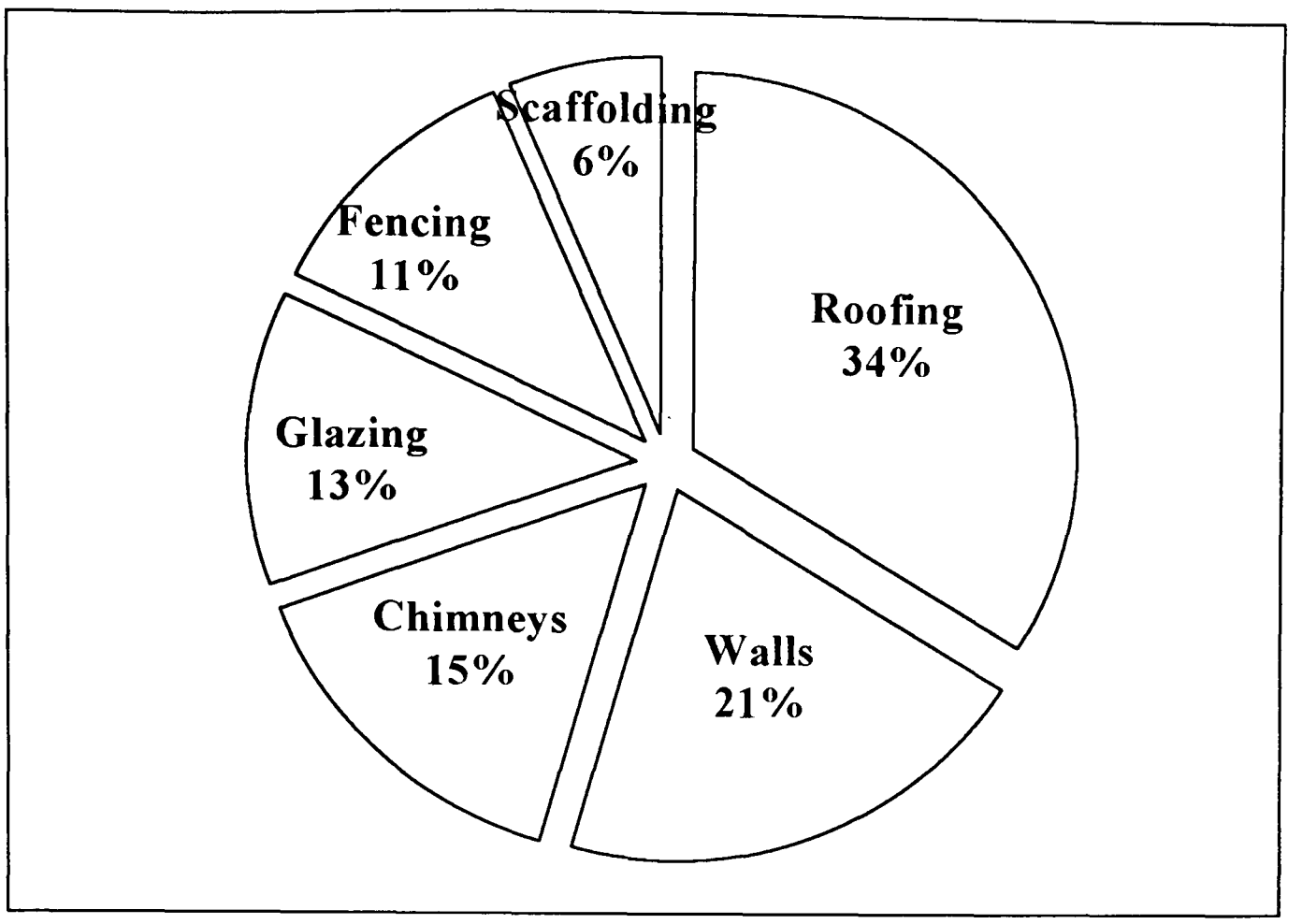

Figure A-2 Breakdown of injuries caused by directly wind attributable accidents.

Design strategy

Having established that the consideration of the effect of conical vortices is important to building design, two strategies are available:

1. To accept that the high roof suctions are inevitable and to design the cladding and attachments accordingly. This is the method typically employed at the moment.
2. To encourage collaboration between architects and wind engineers to modify building design to produce buildings that are subject to smaller wind loads due to the way in which they are constructed.

This section concentrates on the latter of these options and reviews methods that have been proposed to reduce loading.

Four design aspects are reviewed for their effect on roof corner suctions; roof edge profiles, vortex disrupters, parapets and permeable roofs.

Roof edge profiles

The majority of roof pressure studies have been made on models with square roof edges. This section looks at the effect of having rounded or chamfered edges.

Blackmore[1988] looked at the effect of chamfering the edges of a building, as shown in Fig A-3. Various chamfer angles were tried and it was found that shallower chamfers produced the greatest reductions in roof corner suctions. A 30° chamfer was shown to produce a 70% reduction in corner suctions.

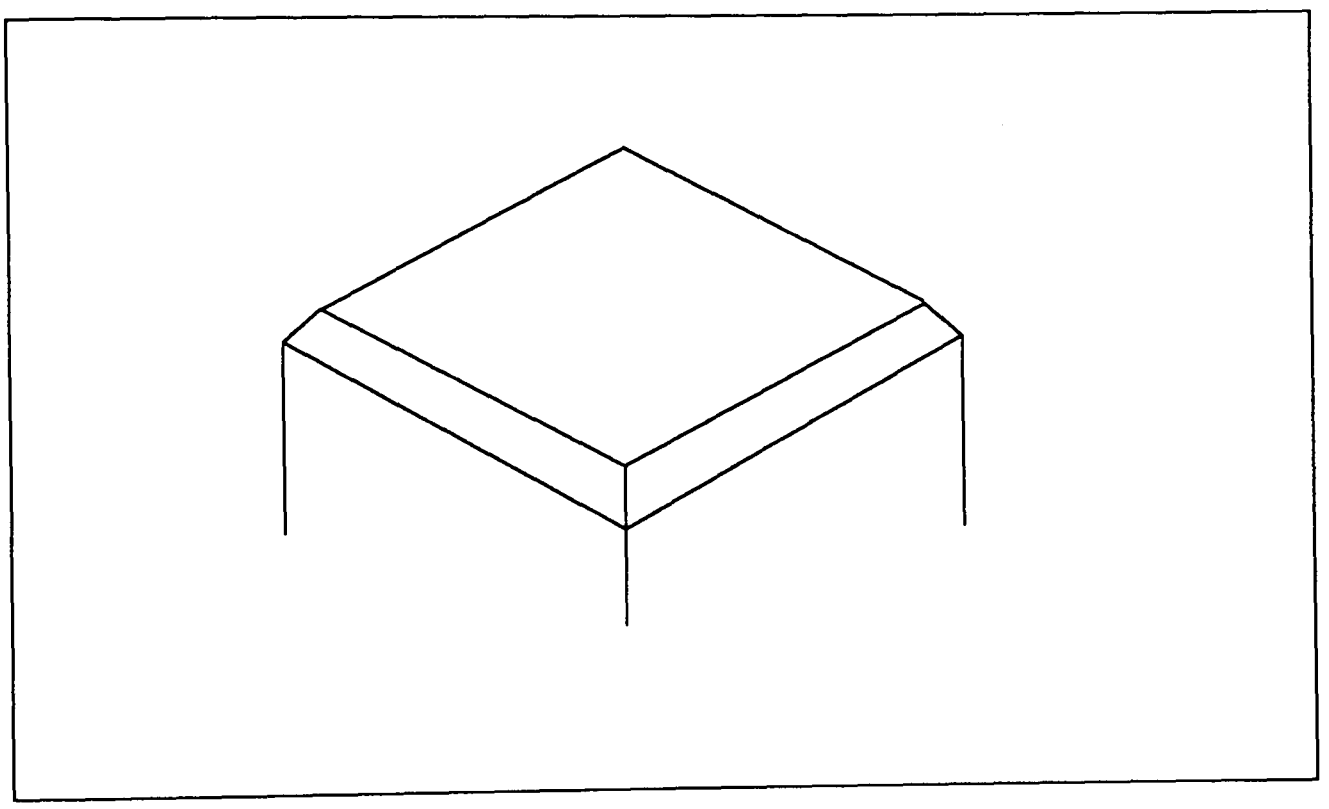

Figure A-3 Chamfered roof edges

Tieleman et al[1992] showed that rounding the roof edges could produce a similarly dramatic reduction in roof edge suctions to those achieved by chamfers. This was true for both mean and peak pressure coefficients, with the magnitude of pressure coefficients being reduced by a factor of three compared to the square edged model.

Vortex disrupters

Tieleman et al[1992] showed that putting an object in the path of the conical vortex can produce a 50% reduction in roof edge suctions. This reduction in loading was achieved by placing two cylinders of 3mm diameter and 12mm high (at a scale of 1:50) in the vortex path close to the corner of the building.

Cochran et al[1995] used permeable gauze screens (as shown in Fig A-4) to disrupt the vortex structure. This reduced point suctions by up 37%. The area averaged load in the corner region was reduced by 24%.

Although these methods produce less dramatic load reductions than modifying edge profiles, they do have the advantage of being more easily and cheaply applied to existing buildings.

Also, roof cladding loads can be reduced by judicious placement of roof features (water tanks, chimneys, etc.) in new designs.

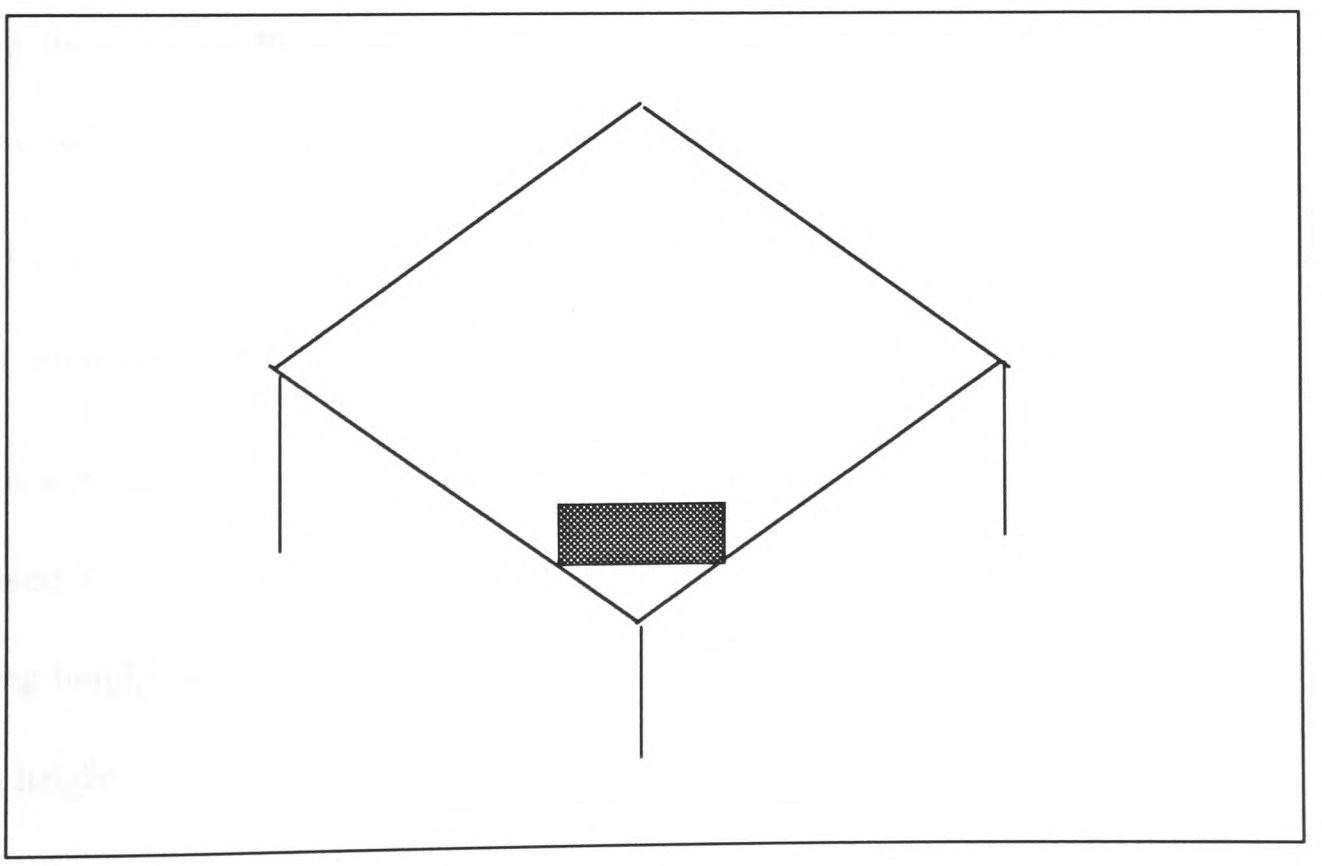

Figure A-4 Permeable vortex fence

Parapets

Roof edge parapets have been shown to reduce roof corner suctions, but only in some cases. Early model studies by Kramer and Gerhardt[1977] and Sockel and Tancher[1981] showed that parapets reduced roof loads. Sockel and Tancher showed that a parapet with a height of 2% of the building height around the perimeter of a roof was sufficient to reduce peak localised suctions by 50%. Both observed reductions in roof loads for all the parapet configurations they tried. However, later work has shown that these benefits come with various caveats.

Lythe and Surry[1983] showed that the ratio parapet height to building height was very important in achieving roof load reductions. The use of parapets on low rise buildings (buildings where height (h) is less than or equal to the typical plan dimension (b)) was shown to be particularly sensitive to parapet height. Lower loads were measured as the parapet height increases. If insufficiently high parapets were placed around the roofs of low rise buildings then the roof suctions increased in comparison to the design without parapets.

Kind[1988] showed that if parapets on low rise buildings were not to increase roof corner suctions then they had to be at least 7% of the building height.

Bienkiewicz and Sun[1992] found that if mean and peak suctions were not to be increased by the addition of parapets, then the parapets had to be at least 4% of building height, and that if a reduction was to be achieved then they had to be at least 8% in height.

Baskaran and Stathopoulos[1988] found a method to alleviate the load increasing effects of low parapets. This method was to discontinue the parapet at the roof corners

as shown in Fig A-5. However, even with these discontinuities, roof loads were still in excess of those where no parapet was in place.

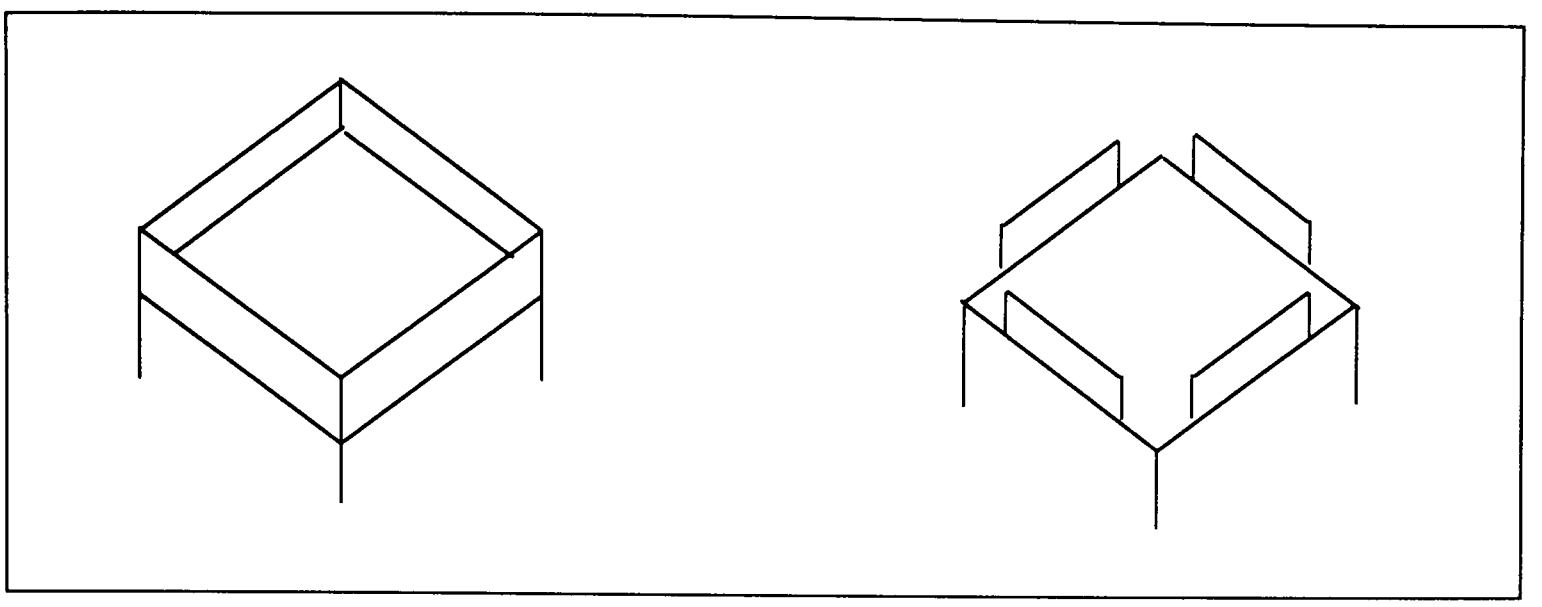

Figure A-5 Full perimeter parapet (left) and modified cornerless parapet (right)

The parapet studies described above have shown that parapets can be very effective in reducing roof corner suctions. However, parapets on low rise buildings must be designed with care, otherwise roof edge loads will be increased.

Permeable roofs

Cheung and Melbourne[1988] showed that a porous roof is subject to less severe wind loads than a similar non-porous roof.

The measurements were made on flat roofed building models. These models had a large number of small holes drilled in the roof panel to allow air to flow into the internal volume of the model. This is shown in Fig A-6.

The porosity was defined as the ratio of the area of the porosity holes to the area of the entire roof. It was shown that a roof porosity of 0.06% was sufficient to produce a reduction of 40% in magnitude of mean roof suctions. This porosity also produced a 15% reduction in peak suctions in roof edge regions.

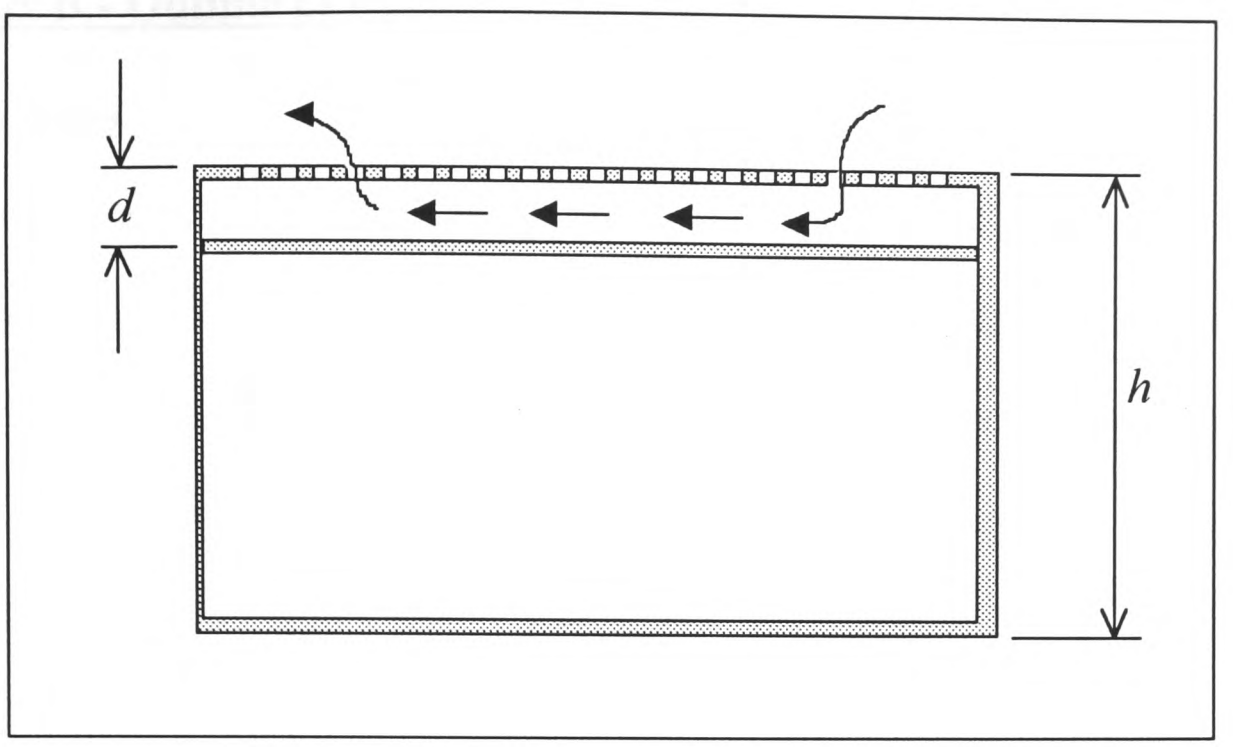

Figure A-6 Porous roof flow

The effect of changing the internal volume of the roof cavity (d / h) was also reported. Overall roof load was shown to decrease with increased internal volume. However, an increase in roof edge suctions was measured.

The effect of internal volume on peak pressures was shown to be negligible.

Appendix B - Outline of Particle Image Velocimetry (PIV)

Basic Principles

Particle image velocimetry (PIV) is a technique to measure fluid flow velocities. Its major benefit over other quantitative measurement techniques is that rather than just measuring data at a single point, it allows data over an entire flow area to be collected in a single measurement. It provides, in effect, a 'snap-shot' of the flow, frozen in time. The basic principle behind PIV is very simple, and closely akin to flow visualisation techniques. The basic steps in making PIV measurements are outlined below.

1. The flow is seeded with particles small enough to follow the flow, but large enough to scatter light (as in LDA measurement).
2. The measurement plane is then illuminated with a sheet of laser light.
3. Either a series of pictures, or one multi-exposed picture is taken of the illuminated particles, one image at time t_1, and then other exposures at short intervals afterwards, t_2, t_3... etc.
4. The position (x_1, y_1) of a particle at t_1 and the position of the same particle at t_2 (x_2, y_2) is then determined from the pictures, or the single multi-exposed picture.
5. Velocity vectors can then be determined for each particle since:

$$u = \lim_{t_2 \to t_1} \left(\frac{x_2 - x_1}{t_2 - t_1} \right) \tag{B.1}$$

$$v = \lim_{t_2 \to t_1} \left(\frac{y_2 - y_1}{t_2 - t_1} \right) \tag{B.2}$$

A schematic of the components in a PIV system is shown in Fig B-1. Fig B-2 shows the principle behind particle imaging.

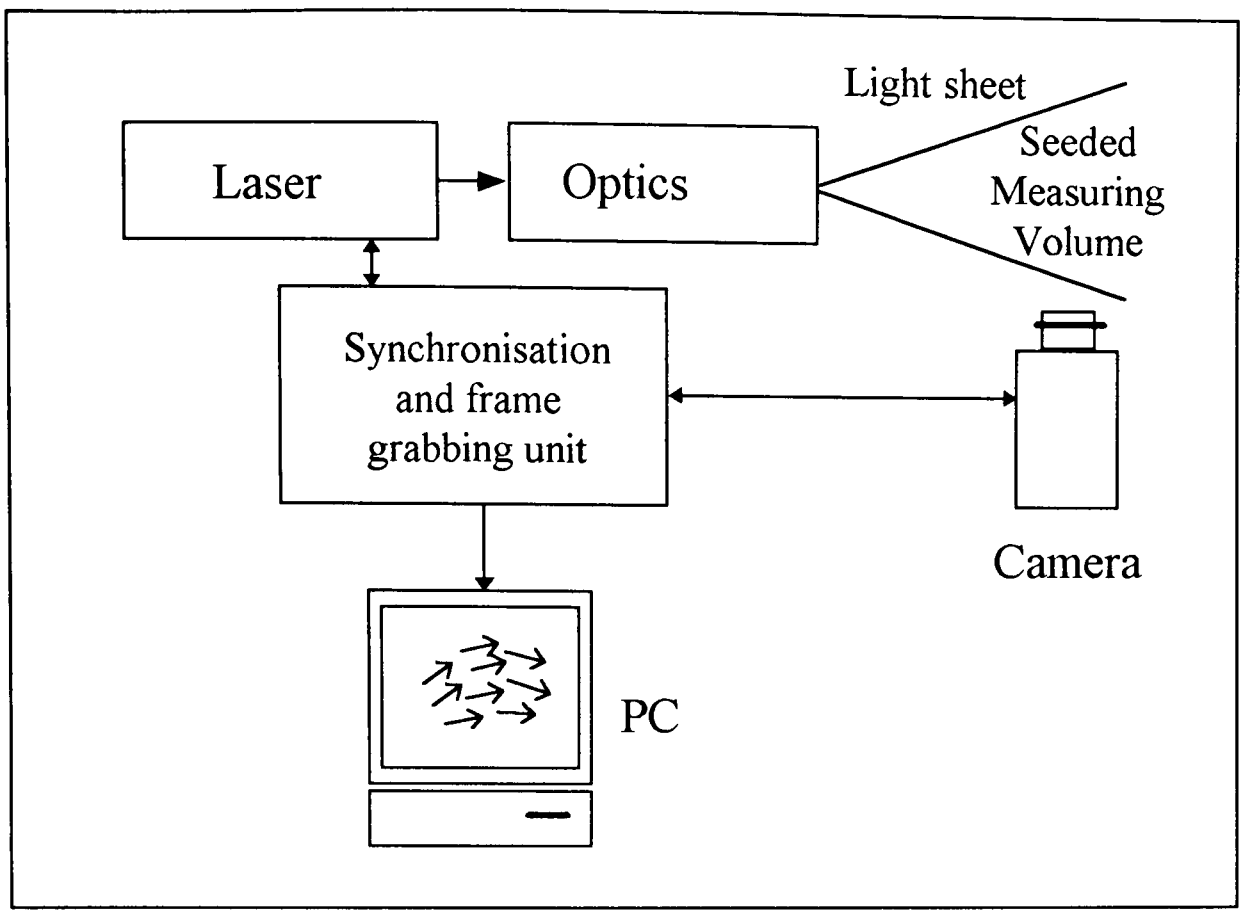

Figure B-1 Schematic of PIV system components

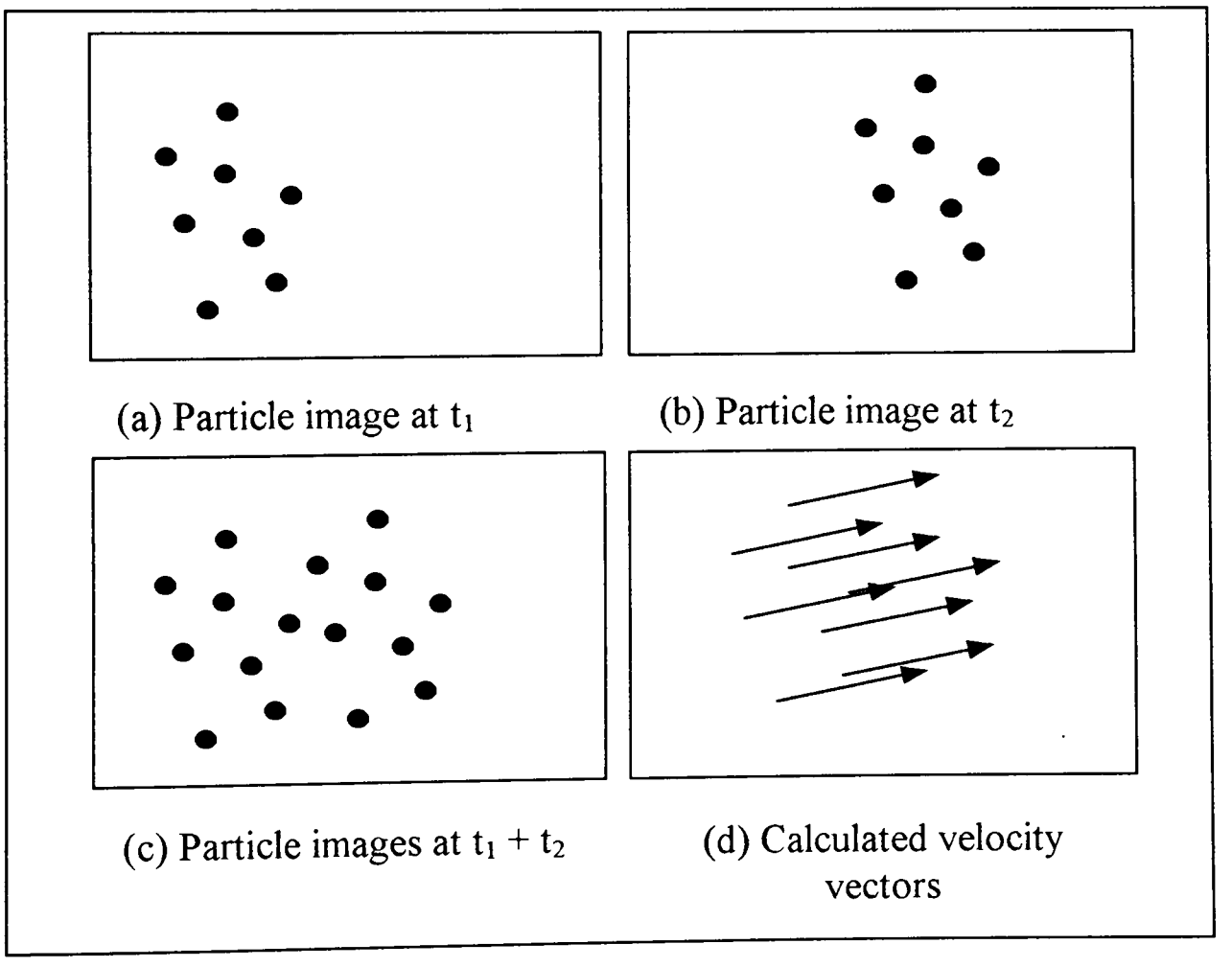

Figure B-2 Particle images and calculated vectors

Although taking PIV images is relatively simple, the processing of the flow maps and the validation of the results is very complex.

Rather than try to summarise here what is a very extensive topic, readers are directed to Adrian[1986] which presents an excellent introduction to PIV techniques and image processing.

Can PIV work in Wind Engineering?

Put simply, the answer to this question is 'Yes'. However, as yet, there is no such thing as a turn-key PIV system and so the measurement system would have to be carefully tailored and developed to the specific application if useful data was to be obtained.

To overcome the measurement problems that would be encountered in the Oxford wind tunnel (such as seeding density in an open circuit wind tunnel, seeding wake or vortex regions and positioning of system components so as not to interfere with the flow being measured) could form a substantial part of a D.Phil. thesis, just as simultaneous pressure-velocity measurement did in this thesis, or the use of LDA did in Minson[1994].

PIV has a very important role in the future of flow measurement and so wind engineering should take it on board as soon as it is practicable, just as LDA technology was employed to supersede hot wire anemometry.

References

Adrian R.J.[1986]; "Multi-point optical measurements of simultaneous vectors in unsteady flow - a review"; International Journal of Heat and Fluid Flow, Volume 7, pp127-145.

Bailey A. and Vincent N. D. G.[1943]; "Wind pressures on buildings, including effects of adjacent buildings"; Journal of the Institution of Civil Engineers, Volume 20, pp243-275.

Baskaran A. and Stathopoulous T.[1988]; "Roof corner wind loads and parapet configurations"; Journal of Wind Engineering and Industrial Aerodynamics, Volume 29, pp79-88.

Bienkiewicz B. and Sun Y.[1992a]; "Wind tunnel testing of wind loading on loose laid roofing systems"; Journal of Wind Engineering and Industrial Aerodynamics, Volume 43, pp1817-1828.

Bienkiewicz B. and Sun Y.[1992b]; "Local wind loading on the roof of a low rise building"; Journal of Wind Engineering and Industrial Aerodynamics, Volume 45, pp11-24.

Blackmore P.A.[1988]; "Load reduction on flat roofs - effect of edge profile"; Journal of Wind Engineering and Industrial Aerodynamics, Volume 29, pp89-98.

Blessman J.[1982]; "The boundary layer TV-2 wind tunnel of the UFRGS"; Journal of Wind Engineering and Industrial Aerodynamics, Volume 10, pp231-248.

Cheung J.C.K. and Melbourne W.H.[1988]; "Wind loads on porous roofs"; Journal of Wind Engineering and Industrial Aerodynamics, Volume 29, pp19-28.

Cochran L.S. and Cermak J.E.[1992]; "Full and model scale cladding pressures on the Texas Tech University experimental building"; Journal of Wind Engineering and Industrial Aerodynamics, Volume 43, pp1589-1600.

Cook N.J.[1985]: Designers guide to wind loading of building structures - Parts 1&2: Butterworths; London.

Cook N.J.[1975]; "A boundary layer wind tunnel for building aerodynamics"; Journal of Wind Engineering and Industrial Aerodynamics, Volume 1, pp3-12.

Cook N.J.[1986]; "Jensen number, a proposal"; Journal of Wind Engineering and Industrial Aerodynamics, Volume 22, pp95-96.

Dalley S. and Richardson G.[1992]; "Reference static pressure measurements in wind tunnels"; Journal of Wind Engineering and Industrial Aerodynamics, Volume 42, pp909-920.

Durst F., Melling A. and Whitelaw J.H.[1976]; "Principles and practice of laser Doppler anemometry"; Academic Press; London.

Engineering Science Data Unit: Item 82026[1990]; "Strong winds in the Atmospheric Boundary layer, Part I - Mean hourly wind speeds."

Engineering Science Data Unit: Item 83045[1984]; "Strong winds in the Atmospheric Boundary layer, Part II - Discrete Gust Speeds."

Engineering Science Data Unit: Item 84011[1990]; "Wind Speed profiles over terrain with Roughness Changes for Flat or Hilly Sites."

Engineering Science Data Unit: Item 85020[1990]; "Characteristics of atmospheric turbulence near the ground - Part II Single point data for strong winds (neutral atmosphere)."

Gerhardt H.J. and Kramer C.[1992]; "Effect of Building Geometry on Roof Wind loading"; Journal of Wind Engineering and Industrial Aerodynamics, Volume 43, pp1765-1774.

Ginger J.D. and Letchford C.W.[1992]; "Peak wind loads under delta wing vortices on canopy roofs"; Journal of Wind Engineering and Industrial Aerodynamics, Volume 43, pp1739-1750.

Ginger J.D. and Letchford C.W.[1993]; "Characteristics of large pressures in regions of flow separation"; Journal of Wind Engineering and Industrial Aerodynamics, Volume 49, pp301-310.

Greenwell D.I. and Wood N.J.[1992]; "Determination of vortex burst location on delta wings from surface pressure measurements"; AIAA Journal, Volume 30, No.11, pp2736-2739.

Gumley S.J.[1981]; "Tubing systems for the measurement of fluctuating pressures in wind engineering"; OUEL Report 1370/1981.

Gumley S.J.[1982]; "A detailed design method for pneumatic tubing systems"; OUEL Report 1407/1982.

Hansen S.O. and Sorensen E.G.[1985]; "A new boundary layer wind tunnel at the Danish Maritime Institute"; Journal of Wind Engineering and Industrial Aerodynamics, Volume 18, pp213-224.

Hertig J-A.[1984]; "A stratified boundary layer wind tunnel designed for wind engineering and diffusion studies"; Journal of Wind Engineering and Industrial Aerodynamics, Volume 16, pp265-278.

Irwin H.P.A., Cooper K.R. and Girard R.[1979]; "Correction of distortion effects caused by tubing systems in measurements of fluctuating pressures"; Journal of Wind Engineering and Industrial Aerodynamics, Volume 5, pp93-107.

Jensen M.[1954]; "The model law for phenomena in natural wind"; Ingenioren, Volume 2 pp4.

Kareem A. and Lu J.-X.[1992]; "Pressure fluctuations on flat roofs with parapets"; Journal of Wind Engineering and Industrial Aerodynamics, Volume 43, pp1775-1786.

Kawai H., and Nishimura G.[1994]; "Flow field around and suction on a flat roof"; Proc. of the 2nd UK conference on Wind Engineering, Warwick.

Kawai H.[1995]; Private communication on effect of upstream gusts.

Kawai H., Nishimura G. and Kusayanagi T.[1995]; "Characteristics of conical vortices on a flat roof in oblique flow"; Paper presented to Japan Wind Engineering Society.

Kind R.J.[1986]; "Worst suctions near edges of flat top roofs on low rise buildings"; Journal of Wind Engineering and Industrial Aerodynamics, Volume 25, pp31-48.

Kind R.J.[1988]; "Worst suctions near edges of flat roof tops with parapets"; Journal of Wind Engineering and Industrial Aerodynamics, Volume 31, pp251-263.

Kramer C. and Gerhardt H.J.[1990]: "Wind effects on roofs and roofing systems"; Journal of Wind Engineering and Industrial Aerodynamics, Volume 36, pp301-308.

Kramer C. and Gerhardt H.J.[1991]: "Wind pressures on roofs of very low and very large industrial buildings"; Journal of Wind Engineering and Industrial Aerodynamics, Volume 38, pp285-296.

Kramer C., Gerhardt H.J. and Regenscheit B.[1984]; "Wind tunnels for industrial aerodynamics"; Journal of Wind Engineering and Industrial Aerodynamics, Volume 16, pp225-264.

Kramer C., Gerhardt H.J. and Scherer S.[1979]: "Wind pressures on block type buildings"; Journal of Wind Engineering and Industrial Aerodynamics, Volume 4, pp229-242.

Laurence D. and Mattei J.D.[1993]; "Current state of computational bluff body aerodynamics"; Journal of Wind Engineering and Industrial Aerodynamics, Volume 49, pp23-44.

Letchford C.W.[1987]; "Pneumatic averaging and its application in wind engineering"; DPhil thesis, University of Oxford.

Letchford C.W.[1995]; "Simultaneous flow visualisation and pressure measurement on the Texas Tech Building"; Submitted to Journal of Wind Engineering and Industrial Aerodynamics.

Letchford C.W. and Marwood R.[1995]; "On the influence of W-component turbulence on roof pressures beneath conical vortices"; Abstract accepted for 3rd Bluff Body Aerodynamics and Application Colloquium, Virginia, USA.

Letchford C.W., Marwood R. and Wood C.J.[1996]; "Simultaneous pressure and velocity measurements in the vicinity of a cuboid wind tunnel model"; 5th National AWES Workshop, Tanunda, South Australia.

Lythe G. and Surry D.[1983]; "Wind loading of roofs with and without parapets"; Journal of Wind Engineering and Industrial Aerodynamics, Volume 11, pp75-94.

Marshall R.D. and Cermak J.E.[1966]; "Wind studies of the Bank of America world Headquarters Building, Pt 2"; FDDL Report No. 66-67-19, Colarado State University.

Marwood R., Belcher R.E., Minson A.J. and Wood C.J.[1994]; "Flow structures associated with extreme suctions on flat roofs"; Proc. of the 2nd UK conference on Wind Engineering, Warwick.

Marwood R., Belcher R.E., Minson A.J. and Wood C.J.[1995]; "Conditional sampling analysis of simultaneous velocity-pressure time series"; Abstract accepted for 3rd Bluff Body Aerodynamics and Applications Colloquium, Virginia, USA.

Melbourne W.H.[1993]; "Turbulence and the leading edge phenomenon"; Journal of Wind Engineering and Industrial Aerodynamics, Volume 49, pp45-64.

Milford R.V., Goliger A.M. and Waldeck J.L.[1992]; "Jan Smuts experiment: Comparison of full scale and wind tunnel results"; Journal of Wind Engineering and Industrial Aerodynamics, Volume 43, pp1705-1716.

Minson A.J.[1994]; "Use of laser Doppler anemometer measurements near model buildings to determine wind loading on building attachments"; Thesis at the University of Oxford.

Minson A.J. and Wood C.J.[1992]; "Investigation of separation bubbles and inclined edge vortices above model buildings using laser Doppler anemometry"; Proc. of the 11th Australasian Fluid Mechanics Conference, Hobart, Australia, pp877-880.

Mochida A., Murakami S., Shoji M. and Ishida Y[1993]; "Numerical simulation of flow field around Texas Tech building by large eddy simulation"; Journal of Wind Engineering and Industrial Aerodynamics, Volume 46-47, pp455-460.

Murakami S.[1993]; "Computational Wind Engineering"; Journal of Wind Engineering and Industrial Aerodynamics, Volume 36, pp517-538.

Okabe M.[1991]; "Wind tunnel tests to determine the wind force on roof blocks for existing buildings": Journal of Wind Engineering and Industrial Aerodynamics, Volume 38, pp393-404.

Okada H. and Ha Y.C.[1992]; "Comparisons of wind tunnel and full scale pressure measurement tests on the Texas Tech building"; Journal of Wind Engineering and Industrial Aerodynamics, Volume 43, pp1601-1612.

Ostrowski J.S.[1960]; "The properties of flow past swept back wings at high incidence"; Archivum budowy Maszyn, Tom VII, Zessyt 4.

Ostrowski J.S. and Golebiewski C.Z.[1958]; "Wind study of the model of the gymnasium at Zakopane"; Report of the chair of aerodynamics, Technological University of Warsaw.

Parkinson G.V.[1984]; "A tolerant wind tunnel for industrial aerodynamics"; Journal of Wind Engineering and Industrial Aerodynamics, Volume 16, pp293-300.

Paterson D.A. and Holmes J.D.[1992]; "Computation of wind pressures on low rise structures": Journal of Wind Engineering and Industrial Aerodynamics, Volume 43, pp1629-1640.

Payne F.M., Ng T.T. and Nelson R.C.[1989]; "Seven hole probe measurement of leading edge vortex flows"; Experiments in Fluids, Volume 7, pp1-8.

Payne F.M., Ng T.T., Nelson R.C. and Schiff L.B.[1988]; "Visualization and wake surveys of vortical flow over a delta wing"; AIAA Journal, Volume 26, No.2, pp137-143.

Rathbun J. C.[1940]; "Wind forces on a tall building"; Transactions of the American Society of Civil Engineers, Volume 105, Paper No 2056.

Rediniotis O.K., Hoang N.T. and Telionis D.P.[1991]; "Multi-sensor investigations of delta wing high alpha aerodynamics"; AIAA Paper No.91-0735, Reno, Nevada.

Richards P.J., Hoxey R.P. and Wanigaratne B.S.[1995]; "The effect of directional variations on the observed mean and rms pressure coefficients"; Journal of Wind Engineering and Industrial Aerodynamics, Volume 54/55, pp359-367.

Richards P.J. and Hoxey R.P.[1992]; "Computational and wind tunnel modelling of mean wind loads on the Silsoe structures building": Journal of Wind Engineering and Industrial Aerodynamics, Volume 46-47, pp1641-1652.

Richardson G.M. and Surry D.[1991]; "Comparisons of wind tunnel and full scale surface pressure measurements on low rise pitched roof buildings"; Journal of Wind Engineering and Industrial Aerodynamics, Volume 38, pp249-256.

Robertson A.P.[1991]; "Effect of eaves detail on wind pressures over an industrial building"; Journal of Wind Engineering and Industrial Aerodynamics, Volume 38, pp325-334.

Roy M.[1957]; "Sur la theorie de l'aile en delta, tourbillons d'appex et nappes en cornet"; La Recherche Aeronautique, No.56.

Saathoff P.J. and Melbourne W.H.[1989]; "Generation of peak pressures in separated/reattaching flows"; Journal of Wind Engineering and Industrial Aerodynamics, Volume 32, pp121-134.

Salter C.[1958]; "Wind effects on flat roofed buildings"; Engineering, pp 508-510.

Selvam R.P. and Konduru P.B.[1993]; "Computational and experimental roof corner pressures on the Texas Tech building": Journal of Wind Engineering and Industrial Aerodynamics, Volume 46-47, pp449-454.

Sockel H. and Taucher R.[1981]: "The influence of a parapet on local pressure fluctuations"; Journal of Wind Engineering and Industrial Aerodynamics, Volume 8, pp31-38.

Stathopoulous T.[1984]; "Design and fabrication of a wind tunnel for building aerodynamics"; Journal of Wind Engineering and Industrial Aerodynamics, Volume 16, pp361-376.

Stathopoulous T. and Zhou Y.S.[1993]; "Numerical simulation of wind induced pressures on buildings of various geometries"; Journal of Wind Engineering and Industrial Aerodynamics, Volume 46-47, pp419-430.

Stathopoulous T., Surry D. and Davenport A.G. [1978a]; "Some general characteristics of turbulent wind effects on low-rise structures"; Proc. of 3rd Colloq. on Industrial Aerodynamics, Aachen.

Stathopoulous T., Surry D. and Davenport A.G. [1978b]; "The assessment of effective wind loads acting on flat roofs"; Proc. of 3rd Colloq. on Industrial Aerodynamics, Aachen.

Stathopoulous T., Surry D. and Davenport A.G. [1980]; "A simplified model of wind pressure coefficients for low-rise buildings"; Proc. of 4th Colloq. on Industrial Aerodynamics, Aachen.

Surry D.[1991]; "Pressure measurements on the Texas Tech building: Wind tunnel measurements and comparison with full scale"; Journal of Wind Engineering and Industrial Aerodynamics, Volume 38, pp235-248.

Surry D. and Stathopoulos T.[1977]; "An experimental approach to the economical measurement of spatially averaged wind loads"; Journal of Wind Engineering and Industrial Aerodynamics, Volume 2, pp385-397.

Sykes D.M.[1977]; "A new wind tunnel for industrial aerodynamics"; Journal of Wind Engineering and Industrial Aerodynamics, Volume 2, pp65-78.

Tieleman H.W.[1993]; "Pressures on surface-mounted prisms: the effects of incident turbulence"; Journal of Wind Engineering and Industrial Aerodynamics, Volume 49, pp289-300.

Tieleman H.W., Surry D. and Lin J.-X.[1992]; "Characteristics of mean and fluctuating pressure coefficients under delta wing vortices"; Proc. of Wind Engineering Society Conference, Cambridge.

Visser K.D. and Nelson R.C.[1993]; "Measurements of Circulation and Vorticity in the Leading edge Vortex of a Delta wing"; AIAA Journal, Volume 31, No.1, pp104-111

Werle H.[1953]; "Sur le tunnel hydrodynamique a visualisation"; La Recherche Aeronautique, No.33.

Williams C.W. and Baker C.J.[1992]; "Developing models for the prediction of wind loading on roofs"; Proc. of 1st UK Wind Engineering Conference, Cambridge.

Williams C.W.[1995]; "The development of a semi-empirical model for the prediction of wind loading on building roofs"; PhD thesis, University of Nottingham.

Wood C.J.[1977]; "The Oxford University 4m x 2m industrial aerodynamics wind tunnel"; OUEL Report No. 1188/77.